Multisite phosphorylation in T cell receptor proximal signalling

Himadri Mukhopadhyay
Christ Church
University of Oxford

A thesis submitted for the degree of
Doctor of Philosophy
Trinity 2015

Acknowledgements

For Mummy and Baba - with love, respect and gratitude - this belongs to You!

To Nanu and Didiya - goodwill and love always!

To all family and friends - research is our collective endeavour!

To all my teachers and professors over the years - thank you!

To the Systems Biology Doctoral Training Centre, the School of Pathology, the University of Oxford and Christ Church - it has been an honour and a privilege to study and pursue research in this enchanting town!

For Oxford - the ideals of Frideswide Devi live on! - we belong to each other forever!

To Omer, Anton and Philip - this belongs to you - you taught, you made us reflect and you inspired - words cannot express my gratitude to you, and for you!

To Ben, Jesse and Shaun - it was your guidance that helped us realize our dream of experimental biology - thank you!

A humble offering at Your Divine Lotus Feet oh Swami - all unto You! shob Tomaie MA THAKUR MA aamar!

This is SAI Kripa!

Abstract

T cell receptor proximal signalling represents a specific instance of a multisite phosphorylation system. Receptor phosphorylation is regulated by the opposing actions of the kinase LCK, and phosphatases such as CD45 and CD148. Particular phosphoforms recruit the kinase ZAP-70, which once bound, propagates downstream signalling. In this thesis we investigate the functional consequences of multiple phosphorylation sites on the dose-response profiles of receptor phosphorylation. We combine mathematical modelling with cellular reconstitution to assess the effect of multiple modification sites on the potency and sensitivity of receptor phosphorylation. We find that multiple sites enhance the potency of receptor phosphorylation, but do not alter the sensitivity of dose-response profiles. This correlation between the number of sites and response potency is consistent with a mechanism whereby phosphorylation mediates an enhancement in the enzymatic efficiencies of modification.

Contents

Abbreviations and definitions

APC: antigen presenting cell. T cells recognize the presence of infections through interactions between the TCR and peptide-MHC molecules located on APCs.

BRR: basic residue rich motifs. BRRs are defined by clusters of positively charged amino acid residues.

CARs: chimeric antigen receptors that fuse the antigen binding domain of an antibody to a signalling subunit such as the TCR ζ-chain.

CD45 and CD148: transmembrane tyrosine phosphatases that dephosphorylate TCR ζ ITAMs.

ITAM: immunoreceptor tyrosine-based activation motif. ITAMs are defined by the amino acid sequence ..YXX[L/I]X69YXX[L/I].., where Y corresponds to tyrosine, L is leucine, I is isoleucine and X represents any amino acid.

ITIM: immunoreceptor tyrosine-based inhibition motif. The consensus amino acid sequence of ITIMs is ..[I/V]XYXX[L/I].., where I is isoleucine, V is valine, Y corresponds to tyrosine, L is leucine and X represents any amino acid.

ITSM: immunoreceptor tyrosine-based switch motif. The amino acid sequence ..TXYXX[V/I].. defines ITSMs, where T is threonine, Y corresponds to tyrosine, V is valine, I is isoleucine and X represents any amino acid.

LAT: linker for activation of T cells. Scaffold protein that is comprised of multiple phosphorylation sites. The phosphorylation of these residues creates binding sites for multiple downstream signalling molecules.

LCK: lymphocyte-specific protein tyrosine kinase. The SRC-family kinase that phosphorylates TCR ζ ITAMs.

MHC: major histocompatibility complex. Peptide fragments are loaded onto MHC molecules, and the cell surface localized peptide-MHC molecules interact with the T cell receptor.

SH2 domain: SRC homology 2 (SH2) domain. The SH2 domain binds phosphorylated tyrosine residues, and is a ubiquitous structure in cellular signal transduction.

SH3 domain: SRC homology 2 (SH3) domain. The SH3 domain binds proline-rich regions.

SLP-76: SRC homology 2 (SH2)-domain-containing leukocyte protein of 76 kDa. An adaptor protein in TCR signalling that is comprised of multiple phosphorylation sites.

TCR ζ: T cell receptor ζ-chain. Signalling subunit that associates with the T cell receptor. Phosphorylation of TCR ζ-chain ITAMs is a functional output of TCR proximal signalling.

ZAP-70: ζ-chain associated protein kinase of 70 kDa. The cytoplasmic tyrosine kinase that is recruited to fully phosphorylated ITAMs. ZAP-70 mediates signal transduction distal to the TCR complex by phosphorylating multiple downstream molecules.

Chapter 1

Introduction and literature review

The regulation of cellular signalling represents a fundamental theme in biology. The molecular interactions that underlie signalling networks give rise to virtually all aspects of cell physiology. Thus elucidating the design principles of biological circuits is an important step towards understanding the emergence of biological form and function.

A specific instance of cell signalling arises in the context of the T cell response. T lymphocytes detect the presence of infections through interactions between clonotypic T cell receptors (TCRs) and peptide-major histocompatibility complex (MHC) molecules located on antigen presenting cells (APCs). Upon stimulation by agonist peptide-MHC molecules, T cells enter a program of proliferation and differentiation into effector cells - a process referred to as T cell activation. The appropriate regulation of T cell signalling is crucial in eliminating infections, while aberrant signalling processes can lead to autoimmune disorders ((1), (2)).

The TCR complex is comprised of an antigen binding subunit that non-covalently associates with signal transducing subunits (Fig 1.1A). The ligand-binding TCR$\alpha\beta$ heterodimer associates with two heterodimeric CD3 chains, along with a homodimer of ζ chains. The CD3 heterodimers and the ζ homodimer represent the signalling components of the TCR complex. Located in the intracellular regions of the CD3 and ζ chains are immunoreceptor tyrosine-based activation motifs (ITAMs), which are characterized by the canonical sequence ..YXX[L/I]X_{6-9}YXX[L/I].., where Y corresponds to tyrosine, L is leucine, I is isoleucine, and X represents any amino acid. While each CD3 chain contains one ITAM, each ζ chain contains three ITAMs. Therefore, the TCR complex is comprised of a total of twenty tyrosine residues (3).

Upon stimulation by agonist peptide-MHC molecules, the tyrosine residues of the TCR complex become phosphorylated by the plasma membrane anchored SRC-family kinase, LCK (lymphocyte-specific protein tyrosine kinase). This event of ITAM phosphorylation due to peptide-MHC stimulation is referred to as *TCR triggering*. The phosphorylation of both tyrosine residues within ITAMs creates binding sites for the cytoplasmic protein kinase ZAP-70 ($\zeta-$chain-associated protein kinase of 70 kDa). The binding of ZAP-70 to a fully phosphorylated ITAM, along with the phosphorylation of ZAP-70 itself, activates the kinase activity of ZAP-70. Moreover, phosphorylation of ZAP-70 is mediated by LCK, or through trans-autophosphorylation. The activation of ZAP-70 represents a crucial step in T cell activation, for ZAP-70

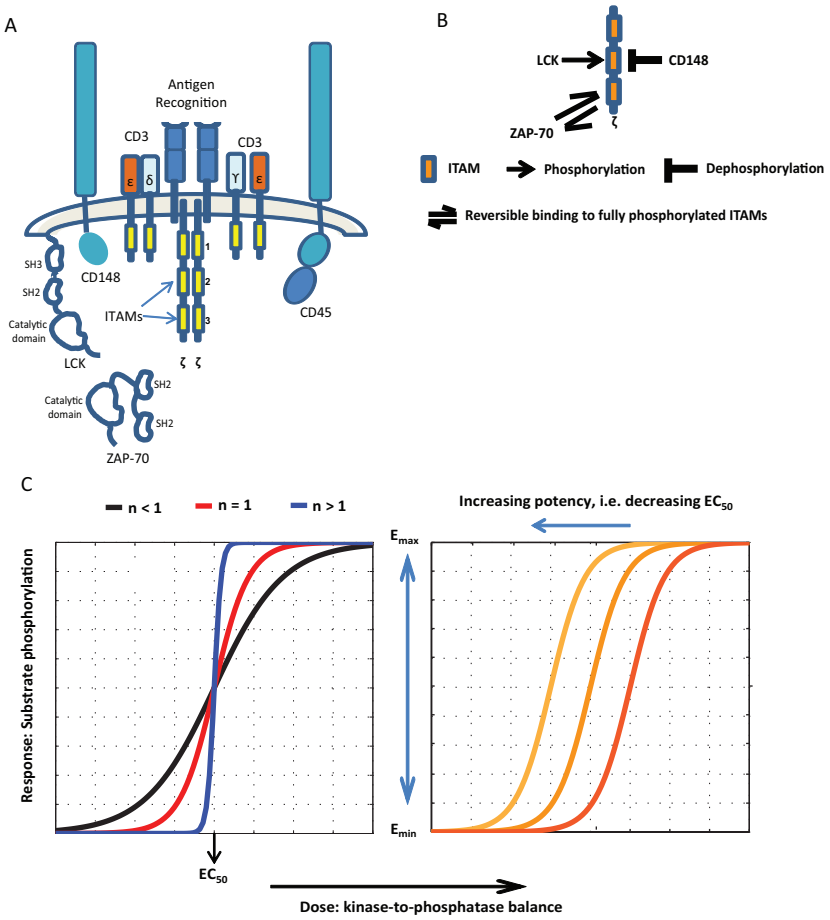

Fig 1.1: The TCR proximal signalling network and the quantification of functional properties through dose-response profiles. (A) The TCR complex is comprised of an antigen-binding heterodimer that non-covalently associates with the signal transducing CD3 and ζ chains. The membrane proximal TCR ζ ITAM is referred to as ITAM 1, while the membrane distal ITAM corresponds to ITAM 3. (B) The TCR proximal signalling network. TCR ITAMs are phosphorylated by the kinase LCK, and dephosphorylated by phosphatases such as CD45 and CD148, while ZAP-70 binds fully phosphorylated ITAMs. (C) Dose-response profiles and Hill function metrics. The magnitude of the response is quantified by the difference between E_{max} and E_{min}. Response sensitivities are quantified by the Hill number n. Ultrasensitive, or switch-like, responses are characterized by Hill numbers greater than unity (left panel). Response potency is quantified by the EC_{50}, or the level of input that gives rise to the half-maximal response. Decreasing EC_{50}s correspond to increasing response potencies (right panel).

phosphorylates the scaffold protein LAT (linker for activation of T cells), as well as the adaptor protein SLP-76 (SRC homology 2 (SH2)-domain-containing leukocyte protein of 76 kDa), on numerous tyrosine residues. Phosphorylated sites on LAT and SLP-76 recruit multiple molecules, which collectively mediate the process of T cell activation. The activation of ZAP-70 ensures that the membrane proximal event of TCR triggering is propagated distal to the TCR complex, and thus ZAP-70 ensures the connectivity of the TCR complex with the downstream molecules that mediate T cell activation (4). The phosphorylation of ITAMs, and the recruitment of ZAP-70 to phosphorylated ITAMs, represent biochemical events that

give rise to processes that ultimately culminate in T cell activation. Such activating processes are complemented by the presence of inhibitory regulatory pathways ((5), (6), (7)). The most membrane proximal form of regulation that opposes TCR triggering occurs through the actions of the transmembrane protein tyrosine phosphatases CD45 and CD148, which dephosphorylate ITAMs. Furthermore, the presence of ITAMs is complemented by immunoreceptor tyrosine-based inhibition motifs (ITIMs) and immunoreceptor tyrosine-based switch motifs (ITSMs), which are defined by the consensus sequences [I/V]XYXX[L/I] and TXYXX[V/I], respectively (1). Examples of inhibitory receptors that contain an ITIM/ITSM in their cytoplasmic domains are PD-1 (programmed death-1) and BTLA (B and T lymphocyte attenuator). The phosphorylation of the tyrosine residue within ITIMs and ITSMs recruits various cytoplasmic phosphatases, including SHP-1 (SH2-containing phosphatase). These phosphatases bind phosphorylated tyrosines through their SH2 domains and, once bound, they can dephosphorylate a wide variety of substrates.

Therefore, TCR signalling represents an intricate process that integrates multiple signalling pathways to give rise to diverse physiological phenomena. However, TCR proximal signalling is characterized by certain recurring themes which manifest themselves throughout many different forms of immune cell signalling and, indeed, throughout biology itself. For instance, the regulation of ITAM phosphorylation represents a paradigm in multisite substrate phosphorylation, where the phosphorylation of a signalling protein is controlled by the opposing actions of protein kinases and phosphatases. Particular substrate phosphoforms result in the creation of binding sites for effector molecules, which propagate further downstream signalling. In this thesis we aim to understand the regulation of TCR proximal signalling, and how mathematical frameworks may be applied to analyze the characteristics of signalling networks.

In this introductory chapter we first consider the molecular components that comprise the TCR proximal signalling network, and we review the current knowledge regarding each molecule. Subsequently, we delve into the mathematical modelling of multisite substrate phosphorylation systems.

T cell receptor proximal signalling

In this section we discuss the individual molecules that comprise the TCR proximal signalling network. We shall use the term *proximal signalling* to refer to the molecular interactions that are localized to the TCR complex. Thus the proximal signalling network is comprised of molecules that directly modify, and/or associate with, the TCR complex. We shall specifically focus on the TCR ζ chain, the modifying enzymes LCK and CD148, and the cytoplasmic kinase ZAP-70.

The TCR ζ chain

There exists a remarkable degree of conservation in the amino acid sequences of TCR ζ chains across multiple species (Fig 1.2(A)). This conservation is evinced through the presence of multiple ITAMs, the amino acid sequences of each of these ITAMs, and the relative locations of these ITAMs in relation to one

another. Furthermore, clusters of positively charged amino acid residues are interspersed between the three TCR ζ ITAMs. We refer to these clusters as *basic residue rich* (BRR) motifs (8). We consider each of these characteristics of the TCR ζ chain in turn, and speculate on the possible functional implications of the overall conservation of amino acid sequences across species.

ITAM conservation

A sequence alignment of the TCR ζ chain across species reveals that individual ITAM sequences are highly conserved (Fig 1.2(A)). On the other hand, ζ-chain ITAMs within the same species are different from each other (Fig 1.2(B)). This suggests that individual ITAMs exhibit important functional differences.

BRR motifs

The conservation of TCR ζ ITAMs is complemented by the presence of BRR motifs interspersed between these ITAMs (Fig 1.2(A)). These BRR clusters are defined by the presence of three or more positively charged amino acid residues, which in this instance correspond to either lysine (K), or arginine (R) residues (8). The location of these BRR motifs relative to the three ITAMs is conserved across species, such that the membrane proximal BRRs 1 and 2 are located between ITAMs 1 and 2, while the membrane distal BRR 3 is located between ITAMs 2 and 3.

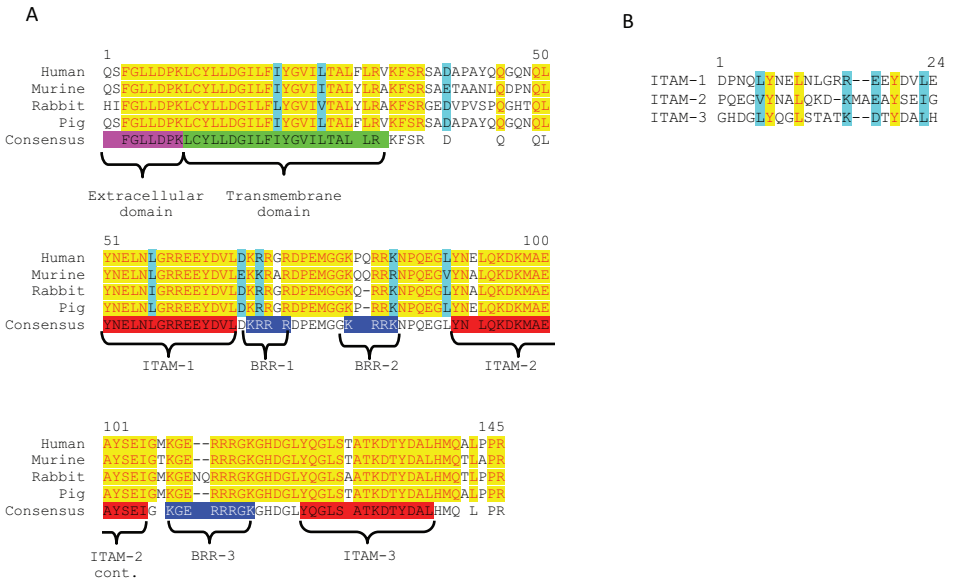

Fig 1.2: Sequence alignment of TCR ζ-chain. (A) Specific ITAM sequences are largely conserved across species, as are the locations of BRR motifs between ITAMs. (B) ITAM sequences in humans. The amino acid sequence of each TCR ζ ITAM in any given species differs from each other. Sequence alignment was performed using Clustal X (http://www.clustal.org/clustal2/).

TCR ζ phosphorylation

Early studies performed on the TCR ζ chain commonly identified two different forms of the protein, with apparent molecular masses of 21- and 23-kD (9). Further investigations that combined mutagenesis, immunoblotting, and mass spectrometry experiments, revealed that these different forms of the TCR ζ chain are generated due to the phosphorylation of specific ITAMs (10). The 23-kD form is observed due to the phosphorylation of all three TCR ζ ITAMs, while the phosphorylation of the two membrane distal ITAMs gives rise to the 21-kD species.

Further FRET-based studies suggested that under resting conditions, the cytoplasmic domain of the TCR ζ-chain associates with the cell membrane (8). Mutations that altered the positively charged lysine and arginine residues within the BRR motifs to alanine were found to abrogate this membrane association. Anti-CD3 stimulation also led to a dissociation of the $zeta$-chain from the membrane, and this was disrupted by an ITAM tyrosine to phenylalanine mutation. This suggests that ITAM phosphorylation leads to a dissociation of the TCR ζ-chain from the membrane.

These investigations led to the following model. Under resting conditions only the membrane distal ITAM is exposed, and thus available for enzymatic modification. The phosphorylation of the membrane distal ITAM counters the electrostatic effect of the membrane distal BRR, and makes ITAM 2 available for phosphorylation. Phosphorylation of the membrane distal ITAMs is posited to counter the effect of the membrane proximal BRR motifs, and to make the membrane proximal ITAM available for phosphorylation.

The notion that membrane association gives rise to a sequential mechanism of TCR ζ-chain phosphorylation is yet to be definitively established. However, myriad *in vitro* studies have suggested that the lipid composition of biological membranes could regulate the structural conformations that a membrane-tethered signalling molecule, such as the TCR ζ-chain, assumes ((11), (12), (13)). Similar to the TCR ζ-chain, FRET-based studies have demonstrated the association of the CD3ϵ subunit with the cell membrane due to electrostatic interactions between positively charged basic amino acid residues, and acidic phospholipids in the inner leaflet of the cell membrane (14). A further study shows that the dual ITIM-containing receptor, PECAM-1, undergoes a sequential mechanism of ITIM phosphorylation in the presence of lipid vesicles that mimic the cell membrane (15). These studies collectively suggest that a combination of electrostatic interactions and receptor triggering can regulate the underlying structure of substrate phosphorylation.

LCK

TCR signalling is initiated through ITAM phosphorylation, and this phosphorylation is mediated by the SRC-family protein tyrosine kinase LCK. Three related features characterize LCK, namely: (i) its membrane localization, (ii) the enzyme's molecular structure, and (iii) regulatory amino acid residues, whose phosphorylation status regulates the conformation and activity of LCK.

LCK localization

The localization and anchorage of LCK to the cell membrane is mediated through the myristoylation of an N-terminus glycine residue, along with the palmitoylation of two N-terminus cysteine residues ((16), (17)). A second, more C-terminal pair, of cysteine residues mediate the tethering of LCK to the cytoplasmic domain of the CD4/CD8 co-receptor ((18), (19)). This membrane localization of LCK is required for the enzyme to be appropriately regulated ((4), (20)).

LCK phosphoforms

The regulation of LCK activity is best understood through considering the enzyme's structure. Much like other SRC-family kinases, LCK is comprised of a SRC homology 3 (SH3) domain, a SH2 domain, and a catalytic kinase subunit (16). Furthermore, the enzyme contains two regulatory tyrosine residues, and the phosphorylation state of these residues regulates the conformations adopted by the enzyme. The first of these (Tyr394) is located in the enzyme's catalytic domain, and the second (Tyr505) is situated close to the carboxy terminus of the protein.

LCK activity

The presence of SH3 and SH2 domains, as well as multiple residues that can be phosphorylated, suggests that LCK can exist in multiple conformations and have numerous substrates and binding partners. A model for the regulation of LCK activity has emerged over the last decades, where particular profiles of the enzyme's phosphorylation status results in LCK adopting particular conformations (21). These different conformations determine the catalytic activity of LCK.

When LCK is not phosphorylated on any regulatory amino acid residue, the enzyme exists in a *primed* conformation (4). The subsequent phosphorylation of Tyr505 results in the enzyme's SH2 domain binding to the phospho-tyrosine, thus inhibiting the catalytic activity of the kinase domain. Further interactions between the SH3 domain and a proline-rich region that links the SH2 and kinase domains stabilizes this inhibited conformation. The dephosphorylation of this tyrosine residue results in LCK reverting to the primed configuration.

From the primed state, the phosphorylation of Tyr394 results in the catalytic activation of the enzyme. The enzyme has also been shown to exist in a doubly phosphorylated state, where both tyrosine residues, Tyr394 and Tyr505, are phosphorylated (22). *In vitro* studies have revealed that this doubly phosphorylated form of LCK is catalytically active as well.

A quantification of the relative abundance of each LCK phosphoform has revealed that a substantial amount of active LCK exists in unstimulated, resting T cells, and this does not change substantially upon TCR engagement ((22), (23)). This is in contrast to myriad other signalling systems, where receptor ligation results in enzyme activation. The existence of a high basal level of active LCK suggests that TCR proximal signalling, and TCR ζ chain phosphorylation, is regulated by a mechanism other than LCK activation.

Pervanadate treatment and TCR triggering

The stimulation of resting T cells with the tyrosine phosphatase inhibitor pervanadate induces TCR phosphorylation ((24), (25), (26)), indicating that TCR proximal signalling is regulated by tyrosine phosphatases. The dominant transmembrane phosphatase is CD45, and CD148 is expressed in some T cells. We next review the pertinent features of these transmembrane phosphatases.

CD45 and CD148

The LCK-mediated phosphorylation of the TCR ζ-chain is opposed by the transmembrane protein tyrosine phosphatase CD45 and, in some T cells, CD148. These phosphatases dephosphorylate the TCR ζ-chain, and thus prevent spurious T cell activation.

The most striking feature of CD45 and CD148 is their large extracellular domains, and the multiple sites of glycosylation that exist on these domains (5). The CD45 ectodomain is comprised of three fibronectin domains and a cysteine-rich globular domain that are both enriched in potential sites for N-linked glycosylation. Similarly, the CD148 extracellular domain is comprised of eight to nine fibronectin domains, which also contain sites of N-linked glycosylation (5).

The extracellular domain of CD45 exists in multiple alternatively spliced isoforms, which contain numerous sites for O-linked glycosylation (5). Thus different alternative spliced isoforms are characterized by different glycosylation states, and these various forms are unique to hematopoietic cell type, stage of differentiation, and state of activation (27). Currently there is no evidence that CD148 also exists in multiple isoforms.

Both phosphatases contain a transmembrane region, followed by intracellular tyrosine phosphatase domains. Two phosphatase domains are found in the intracellular region of CD45, but only the membrane proximal D1 domain possesses enzymatic activity. However, both phosphatase domains are necessary for optimal phosphatase activity *in vivo* (28). On the other hand, CD148 contains a single phosphatase domain.

A final point of interest concerns the relative abundance of transmembrane phosphatases on the T cell surface. CD45 is one of the most abundant cell surface molecules (27), raising the question of the functional significance of having a large excess of phosphatase relative to the amount of kinase. One possible answer lies in the design architecture of the TCR proximal signalling network, and the inherent asymmetries that characterize TCR proximal signalling. We delve into this notion further by considering the cytosplasmic kinase ZAP-70.

ZAP-70

The phosphorylation of both tyrosine residues within an ITAM creates binding sites for the cytosolic kinase ZAP-70 (ζ chain-associated tyrosine phosphoprotein of 70 kDa). The recruitment of ZAP-70 to phosphorylated ITAMs represents a crucial step in T cell activation, for ZAP-70 mediates further downstream

signalling events that occur distal to the TCR complex. The structure of ZAP-70 is characteristic of other Syk-family kinases, and the regulation of ZAP-70 activity is reminiscent of many SH2 domain containing enzymes ((29), (30)).

ZAP-70 contains two SH2 domains, which are separated by an interdomain linker region (31). A further linker region connects the C-terminal SH2 domain to the enzyme's kinase domain. Interactions between the linker regions, and the SH2 and kinase domains, give rise to an extensive hyrogen bonding network that enables the enzyme to assume a conformation that inhibits its kinase activity. However, the binding of the SH2 domains to phosphorylated tyrosine residues disrupts this inhibited conformation ((32), (33)).

Along with abrogating intramolecular inhibition, the binding of ZAP-70 to fully phosphorylated ITAMs also exposes tyrosine residues within the enzyme that can be further phosphorylated. For instance, the phosphorylation of Tyr493 in the enzyme's kinase domain results in the catalytic activation of ZAP-70. Several other tyrosine residues have also been identified within the enzyme that could potentially interact with other molecules upon being phosphorylated (31). The multiple substrates and binding partners with which ZAP-70 interacts together ensure the connectivity of the TCR signalling machinery (4). Thus the initial event of TCR triggering recruits ZAP-70 to the TCR complex, and the activation of ZAP-70 elicits many of the downstream pathways that lead to T cell activation.

TCR triggering

The exact mechanisms through which the extracellular event of TCR-peptide-MHC binding is transduced to elicit intracellular biochemical responses are currently unknown. Several mechanisms have been proposed, including kinetic-segregation, conformational changes of the TCR complex, receptor clustering, mechanical effects and changes in the lipid environment of the TCR (reviewed in (23)). One common theme that unites most of these models is that the binding of the TCR to peptide-MHC molecules acts upon the local kinase-phosphatase balance that regulates the phosphorylation of the TCR complex. Therefore, TCR ligation with agonist peptide-MHC molecules leads to ITAM phosphorylation, the recruitment of ZAP-70, and the downstream events that mediate T cell activation. On the other hand, stimulation of the TCR with self-peptides does not elicit TCR triggering.

TCR proximal signalling as a multisite substrate phosphorylation system

As mentioned previously, the TCR ζ-chain is comprised of three ITAMs, and each ITAM contains two tyrosine residues. These tyrosine residues are phosphorylated by LCK, and dephosphorylated by CD45 and CD148. Therefore the TCR ζ-chain is a multisite substrate, whose phosphorylation profile is regulated through the opposing actions of LCK and CD45/CD148. The phosphorylation of both tyrosine residues within an ITAM creates binding sites for ZAP-70. Since ZAP-70 mediates further downstream signalling,

the functional outputs of the TCR proximal signalling network correspond to: (i) total TCR ζ phosphorylation, and (ii) the amount of ZAP-70 that is bound to the TCR ζ chain. We next consider how mathematical models of multisite phosphorylation can be applied to characterize TCR proximal signalling.

Mathematical models of multisite phosphorylation

Phosphorylation represents a fundamental mechanism of cellular signalling, and diverse biological phenomena, such as the control of gene expression ((34), (35)), transitions between different stages of the cell cycle (36), and the determination of cell fate (37), are mediated through protein phosphorylation. T cell receptor (TCR) signalling also represents a paradigm in multisite phosphorylation, and in this section we consider the theoretical literature on post-translational modification systems.

A recurring question in cellular biology concerns the number of phosphorylation residues that a molecule is comprised of, and the additional functionality that an increasing number of modification sites can impart. In the context of TCR proximal signalling, why is the TCR complex comprised of twenty phosphorylation sites distributed across ten ITAMs? Moreover, what are the implications of the binding of an effector molecule, such as ZAP-70, to phosphorylated residues located on TCR ITAMs? We pose these questions in the light of TCR proximal signalling, however, the reversible modification of a multisite substrate, and the binding of downstream molecules to particular substrate phosphoforms, is reminiscent of myriad biological processes, and represents a central theme in cellular signalling ((38), (39)).

The application of theoretical frameworks to analyze the properties of biochemical reaction networks has a long tradition in mathematical biology. We now briefly review the mathematical literature that has been inspired by reversible covalent modification systems. We adopt a largely historical approach to the subject, and consider theoretical frameworks of increasing complexity. Our initial discussion will focus on the modification of a single site substrate; we shall subsequently extend the mathematical models of interest to consider multisite substrate phosphorylation. Through all the frameworks of substrate phosphorylation that we consider, our objective will be to evaluate the functional properties of the system of interest. A common method to quantify the functional properties of a system is to use the Hill function. Therefore, in the next section, we review the general properties of a Hill function, and subsequently delve into mathematical frameworks of substrate modification systems.

The Hill function

A generic method to characterize the nature of a response is to consider it in terms of a Hill function, which is of the form:

$$y = \frac{\mathrm{E_{max}} x^n}{(\mathrm{EC_{50}})^n + x^n} \tag{1.1}$$

where y corresponds to the output of the Hill function, and x refers to the input. Moreover, *n* is referred to as the Hill coefficent, E_{max} is the maximum value of the Hill function, and EC_{50} refers to the value of x where the output is half the maximal value (Fig 1.1C). While the Hill coefficent quantifies the sensitivity of a response, the EC_{50} provides a measure of response potency. When $n = 1$ the response is referred to as being a *hyperbolic* or *Michaelian response*. Alternatively, an *ultrasensitive* or *switch-like* response is characterized by $n > 1$, while a *subsensitive* response corresponds to the case where $n < 1$.

The Hill function is a generic means to quantify the properties of myriad forms of biological data. We shall consider how the Hill function can provide a means to quantify the sensitivity and potency of TCR proximal signalling, and multisite substrate phosphorylation in general.

An important consideration in applying a Hill function is to define the relevant input and output of interest. In the context of multisite phosphorylation, the input is usually assumed to be the kinase-phosphatase balance in the system. Similarly, the functionally relevant output corresponds to some measure of substrate phosphorylation. We discuss these notions further below.

Single site enzymatic catalysis

One of the simplest forms of a biochemical reaction mechanism is the enzymatic modification of a molecule on a single site. Here we review early mathematical models that considered single site substrate modification. We first consider the modification of a single site substrate by a single enzyme. Subsequently, we consider the reversible modification of a single site substrate.

Substrate modification by a single enzyme

An early instance of a mathematical model of a biochemical reaction mechanism was the enzymatic modification of a single site substrate ((40), (41)):

$$E + S \underset{k_{\text{off}}}{\overset{k_{\text{on}}}{\rightleftharpoons}} ES \overset{k_{\text{cat}}}{\rightarrow} E + P \tag{1.2}$$

where *S* corresponds to the substrate, and *E* corresponds to the modifying enzyme. Enzymatic catalysis proceeds through a two-step mechanism, where the enzyme binds to the substrate to form a complex *ES*, and catalyzes a reaction to form the product *P* (42). The parameters of the model are the rate constants of enzyme-substrate binding (k_{on}) and unbinding (k_{off}), and the catalytic rate constant (k_{cat}).

The traditional approach to analyzing model (1.2) is to assume mass action kinetics, where the rate of a reaction is assumed to be proportional to the product of the concentrations of the reactants (41). The energetic requirements of enzyme catalysis have not been explicitly specified, and thus are assumed to be incorporated into the model parameters. Also, the rates of synthesis and degradation of the enzyme and substrate are assumed to occur on a much longer timescale than those of binding and catalysis. Upon

applying mass action kinetics, the resulting system of differential equations describes the time evolution of each chemical species in model (1.2). This general scheme provides a historical foundation for subsequent frameworks of substrate modification that we consider in the remainder of this chapter.

Reversible covalent modifications

The natural extension to model (1.2) is to consider the scenario where a single site substrate is reversibly modified by two complementary enzymes. In our case, we assume that the particular modifications correspond to phosphorylation and dephosphorylation reactions, which are mediated by a kinase and phosphatase, respectively. A generic model to characterize such a reversible modification process is given by the following:

$$\begin{aligned} E + S &\underset{ek_{\text{off}}}{\overset{ek_{\text{on}}}{\rightleftharpoons}} ES \overset{ek_{\text{cat}}}{\rightarrow} E + S_P \\ F + S_P &\underset{fk_{\text{off}}}{\overset{fk_{\text{on}}}{\rightleftharpoons}} FS_P \overset{fk_{\text{cat}}}{\rightarrow} F + S \end{aligned} \tag{1.3}$$

where *S* corresponds to the unmodified, or dephosphorylated substrate, while S_P represents the phosphorylated form of the substrate. The concentration of free kinase in the system is denoted by *E*, while *F* refers to the concentration of free phosphatase. Finally, the enzyme-substrate complexes are denoted by *ES* and FS_P.

Similar to our discussion in the previous subsection, the usual approach to mathematically represent these reactions is to derive a system of differential equations that describe the time evolution of each molecular species specified in model (1.3). We solve these equations and compute the steady state properties of model (1.3). An important consideration is the definition of model inputs and outputs, and the means through which the input is perturbed. We consider these further in the following subsection.

Inputs, outputs, and perturbations

The phosphorylation status of the substrate in model (1.3) is determined by the opposing actions of the modifying kinase and phosphatase. Therefore, an appropriate input to the system is the ratio of total enzyme concentrations. On the other hand, the functional output of interest corresponds to the proportion of substrate that is phosphorylated at steady state. Thus as the ratio of total enzyme concentrations is varied, the objective is to derive the steady state profile of substrate phosphorylation. Traditionally, this is referred to as a *dose-response*, where the *dose*, or input, is the kinase-phosphatase balance in the system, and the *response* corresponds to the concentration of phosphorylated substrate at steady state. Finally, the varying of relative enzyme concentrations corresponds to the means of perturbing the system, which can be achieved

by varying the amount of either enzyme, while maintaining the concentration of the second enzyme constant. The essential objective in defining inputs, outputs, and perturbations, is to consider the dose-response characteristics of model (1.3) under various conditions and parameter regimes.

Zero order ultrasensitivity

A specific parameter regime of interest is when the total amount of substrate is much greater than the amount of the modifying enzymes. In this limit of enzyme saturation, the dose-response profile of substrate phosphorylation exhibits a switch-like, or ultrasensitive response (43). This concentration dependent form of ultrasensitivity has traditionally been referred to as *zero order ultrasensitivity* (43).

An intuitive explanation for zero-order ultrasensitivity is that since the enzymes are saturated by the amount of substrate, a small perturbation around a threshold value of the kinase-to-phosphatase balance elicits a large change in the amount of phosphorylated substrate. In this parameter regime, the intermediate enzyme-substrate complexes in model (1.3) are negligible. Moreover, the ratio of the Michaelis-Menten constant to the total amount of substrate is much lower than unity. In this limit, the dose-response profile of the phosphorylated substrate exhibits an ultrasensitive, or switch-like response.

Zero order ultrasensitivity is unlikely to apply in TCR proximal signalling, since the modifying enzymes are present in excess of the TCR ζ-chain (44), and thus we do not pursue this theme any further. We now consider mathematical models of multisite phosphorylation, and the functional properties of such systems.

Multisite substrate phosphorylation

Multisite protein phosphorylation represents a ubiquitous regulatory mechanism in cellular signalling. Specific profiles of protein phosphorylation can regulate cellular localization, protein function, and the interactions between proteins. An existing paradigm of cell signalling suggests that the phosphorylation state of proteins and other macromolecules is regulated by the balance of regulatory kinases and phosphatases. The canonical mathematical model that characterizes this reversible process of substrate phosphorylation is:

$$\begin{aligned} E + S_j &\underset{ek_{\text{off}}}{\overset{ek_{\text{on}}}{\rightleftharpoons}} ES_j \overset{ek_{\text{cat}}}{\rightarrow} E + S_{j+1} \\ F + S_{j+1} &\underset{fk_{\text{off}}}{\overset{fk_{\text{on}}}{\rightleftharpoons}} FS_{j+1} \overset{fk_{\text{cat}}}{\rightarrow} F + S_j \end{aligned} \tag{1.4}$$

where E denotes the concentration of free kinase in the system, and F represents the concentration of free phosphatase. The substrate is represented as S_j where j corresponds to the number of sites on which the substrate is phosphorylated. The substrate is assumed to have a total of N phosphorylation sites. Thus we have that $0 \leq j \leq N$.

The binding parameter ek_{on} denotes the rate of binding between the kinase and the substrate, while fk_{on} is the binding rate between the substrate and phosphatase. Similarly, ek_{off} is the rate of unbinding of the kinase-substrate complex ES_j, while fk_{off} is the unbinding rate of the substrate-phosphatase complex FS_{j+1}. Moreover, ek_{cat} is the rate constant of kinase-mediated phosphorylation, while fk_{cat} denotes the rate of phosphatase-mediated catalysis. An implicit assumption in model (1.4) is that each site is identical. Thus the ek_{on} is the same for each site, and the same fk_{on} applies for all sites as well. Similarly, the rates of unbinding for the kinase are the same for each site, and the same holds true for the phosphatase unbinding rates. Finally, the kinase rates of catalysis are also identical for each site, and the same is true for phosphatase catalytic rates. Finally, the rate constants of binding and catalysis in model (1.4) do not depend on the phosphorylation state of the substrate.

As with our discussion in the previous subsections, the conventional approach is to derive a system of differential equations to describe the time evolution of each molecular species in model (1.4). We solve these equations and compute the steady state properties of the system.

Inputs, outputs, and perturbations

The choice of inputs and outputs in model (1.4) is dependent on the biological context in which the multisite phosphorylation system operates. A common approach is to define the system input as the ratio of total kinase and phosphatase concentrations. Alternatively, several studies define the input as being the ratio of free enzyme concentrations ((45), (46)). We must also decide upon a way to perturb the system. This perturbation usually varies the relative enzymatic concentrations, by either perturbing the amount of kinase or phosphatase in the system.

As the input to the system (the dose) is varied, the dose-response profile describes how the functionally relevant output (the response) of the system changes. For instance, if the biological context under study involves the phosphorylation of a multisite protein, which undergoes an allosteric transition once phosphorylated on all modification sites, then the appropriate output to consider is the maximally phosphorylated phosphoform. Alternatively, if a protein activates further downstream pathways once phosphorylated on a subset, k, of the total number of modification sites, N, then the functionally relevant output corresponds to the proportion of substrate phosphorylated on a minimum of k sites, where $0 \leq k \leq N$.

Furthermore, the reversible phosphorylation of the T cell receptor creates potential binding sites for ZAP-70. Thus an appropriate functional output of TCR proximal signalling corresponds to total substrate phosphorylation, which quantifies the total number of phosphate groups attached to the TCR signalling chains.

Underlying structures of phosphorylation: random and sequential mechanisms

An important consideration in analyzing model (1.4) concerns the underlying structure of phosphorylation (47). This is relevant for TCR proximal signalling because previous studies have suggested that ζ-chain

phosphorylation follows a particular sequence, whereby the membrane distal ITAM is phosphorylated before the membrane proximal ITAM ((10), (8)).

A random mechanism of phosphorylation entails that the modification of individual sites is independent. In contrast, a sequential mechanism of phosphorylation requires particular sites to be modified before subsequent sites are available for modification. In Chapter 3 we will show that random and sequential mechanisms give rise to different types of dose-response profiles, and we will quantify these differences in the context of TCR proximal signalling. We now consider theoretical studies of multisite substrate phosphorylation systems, the inputs and outputs that these studies assumed, and the general conclusions that emerged.

Thresholds and switches

One possible functional output to consider in model (1.4) is the amount of substrate that is phosphorylated on all possible modification sites at steady state. This particular substrate phosphoform is referred to as the maximally phosphorylated substrate. A physiological instance where a molecule must be phosphorylated on all modification sites to be active arises in the MAP-kinase cascade. In this instance, the dual phosphorylation of kinases within the cascade activates their catalytic activities (37).

The dose-response profile for such a system is derived by varying the kinase-phosphatase balance in the system (the dose), and by computing the equilibrium concentration of maximally phosphorylated substrate (the response). Thus for each value of the ratio of kinase-to-phosphatase, the maximally phosphorylated substrate concentration is determined. Moreover, the ratio of kinase-to-phosphatase in the system may be varied in two related manners: (i) by varying the ratio of total enzyme concentrations, or, (ii) by perturbing the ratio of free enzymes in the system.

A recently published study (45) considers the dose-response characteristics of the maximally phosphorylated substrate, as the ratio of free kinase to free phosphatase is varied. Using model (1.4) as the starting point, the study assumes (i) a sequential mechanism of substrate phosphorylation, and (ii) similar kinase and phosphatase catalytic efficiencies. The functional output of interest corresponds to the proportion of free substrate that is phosphorylated on all modification sites at steady state. Thus the output of interest is

$$\rho_N = \frac{[S_N]}{[S_0] + [S_1] + ... + [S_N]} \tag{1.5}$$

where $[S_N]$ refers to the concentration of substrate that is phosphorylated on all N sites, and generally, the subscripts refer to the number of sites on which the substrate is phosphorylated.

Under such a scenario, the dose-response profile of the maximally phosphorylated substrate exhibits good thresholding properties, but does not exhibit switch-like characteristics (45). The thresholding efficiency of the system is evaluated by the fact that a relatively high magnitude of dose is required to elicit a substantial response. However, the switching efficiency of the system is poor when compared to an ultrasensitive Hill function. The important result here is that multisite substrate phosphorylation does not necessarily exhibit switch-like responses.

The maximally phosphorylated substrate phosphoform is only one possible functionally relevant output of interest. In the subsequent section, we review a further study which considers a slightly different output.

Non-essential sites

An alternative functional output in model (1.4) is the proportion of substrate that is phosphorylated on k sites, where $0 < k \leq N$, and N corresponds to the total number of modification sites. The interpretation of such a framework is that a protein must be phosphorylated on a minimum of k sites to be considered active; thus k is referred to as the *minimal activation number* (46). A physiological instance of such a mechanism arises in the regulation of the cell cycle, and the phosphorylation of a cyclin-dependent kinase inhibitor (36).

At steady state, the fraction of substrate that is phosphorylated on at least k sites is given by

$$\rho_k = \frac{[S_k] + ... + [S_N]}{[S_0] + [S_1] + ... + [S_k] + ... + [S_N]} \tag{1.6}$$

where $[S_i]$ corresponds to the steady state concentration of free substrate phosphorylated on i sites.

Such a model framework was recently analyzed by Wang and colleagues (46). The authors use a sequential mechanism of substrate phosphorylation to characterize model (1.4), and assume that the relative enzymatic catalytic efficiencies are approximately equal to each other. The study considers the dose-response characteristics of the proportion of active substrate, as the ratio of free kinase to free phosphatase is varied in the system. Of specific interest is how the interplay between the minimal activation number and the total number of substrate modification sites enhances the switch-like characteristics of the multisite phosphorylation system.

The main conclusion of this study was that the inclusion of non-essential sites enhances the switch-like characteristics of multisite substrate phosphorylation. Thus if the minimal activation number, k, is fixed, increasing the total number of modification sites (N) improves the ultrasensitivity exhibited by the multisite phosphorylation system. On the other hand, if the total number of phosphorylation sites is fixed, then there exists an optimal minimal activation number for which maximum ultrasensitivity is achieved.

The effects of membrane confinement

The application of a multisite phosphorylation framework to membrane-anchored proteins was recently performed by Dushek and colleagues (44). The authors study a diffusion-limited model where the modifying enzymes and substrate must first form an *encounter complex* before enzymatic catalysis can proceed. Thus the enzyme-substrate complex formation in model (1.4) is preceded by the formation of an encounter complex. The general scheme that the authors analyze is shown below:

$$X + S_j \underset{k_-}{\overset{k_+}{\rightleftharpoons}} X..S_j \underset{k_{\text{off}}}{\overset{\lambda k_{\text{on}}}{\rightleftharpoons}} XS_j \tag{1.7}$$

where X corresponds to either the kinase or phosphatase, and S_j refers to the substrate phosphorylated on j sites. In order to interact, the relevant free enzyme and substrate must come into close proximity to form an intermediate encounter complex ($X..S_j$). Once bound to the substrate, the modifying enzyme may catalyze a reaction and dissociate, or simply dissociate to yield the encounter complex. The authors assume a random mechanism of phosphorylation, thus $\lambda = N - j$ for the kinase, and $\lambda = j$ for the phosphatase. As before, *j* corresponds to the number of sites on which the substrate is phosphorylated, and *N* is the total number of phosphorylation sites. The study also assumes that the modifying enzymes are in excess of the substrate. Under such a scheme, the authors compute the normalized total substrate phosphorylation at equilibrium as a function of the ratio of total enzyme concentrations. Thus the functional output of this model is the normalized total phosphorylation of the substrate, and it is given by

$$< S >= \sum_{j=0}^{N} j(S_j + E..S_j + ES_j + F..S_j + FS_j)/(NS_T) \tag{1.8}$$

where E refers to the kinase, F to the phosphatase and S_T is the total amount of substrate.

When the system is assumed to be reaction-limited, the total substrate phosphorylation exhibits a subsensitive response. However, when the system is diffusion-limited, and when the modifying enzymes undergo a certain refractory period subsequent to catalysis, the total substrate phosphorylation exhibits an ultrasensitive response (44). The refractory period refers to the assumption that subsequent to enzymatic catalysis, the modifying enzyme is briefly inactivated before it can bind and catalyze a further reaction.

The origin of the observed ultrasensitivity is an effective zero-order effect. This is because subsequent to catalysis, the modifying enzymes become unavailable for catalysis. Increasing the number of modification sites gives rise to a regime where the amount of modifiable substrate far exceeds that of the available enzyme, thus eliciting a form of enzyme saturation. Such enzyme saturation enhances ultrasensitivity with increasing numbers of phosphorylation sites.

The dose-response properties of total substrate phosphorylation is an appropriate output of TCR proximal signalling. This is because the addition of phosphate groups to TCR ζ ITAMs creates binding sites for ZAP-70. Moreover, ZAP-70 binding represents a form of substrate sequestration, and we consider this mechanism further in the next section.

Substrate sequestration

A further study by Liu and colleagues (48) demonstrated that a combination of multisite phosphorylation and substrate sequestration can exhibit ultrasensitive responses. The analysis performed by the authors simplifies model (1.4) by ignoring the formation of enzyme substrate complexes. A general scheme that the authors initially study is shown below:

$$
\begin{aligned}
E + S_j &\xrightarrow{k_j} E + S_{j+1} \\
S_{j+1} &\xrightarrow{d_j} S_j \\
S_j + C &\underset{k_j^d}{\overset{k_j^a}{\rightleftharpoons}} S_j C
\end{aligned}
\tag{1.9}
$$

where *E* refers to the concentration of free kinase in the system, and S_j refers to the concentration of substrate phosphorylated on *j* sites. The authors normalize by setting the concentration of phosphatase to unity. The term *C* refers to a sequestering compartment such as the cell membrane or nucleus, with which the substrate *S* associates. The rate coefficents k_j^a and k_j^d characterize the binding and dissociation, respectively, of the substrate from the sequestering compartment. Also, k_j and d_j are the rates of phosphorylation and dephosphorylation, respectively. An alternative scheme that the authors consider modifies the above to allow enzymatic catalysis only when the substrate is bound to the sequestering compartment.

There exist several possible functional outputs of interest in the models that Liu and colleagues study. For instance, along with the amount of maximally phosphorylated substrate, the authors also analyze the proportion of substrate that is bound to the sequestering compartment. As the total kinase concentration in the system is varied, the authors analyze the dose-response characteristics of several functional outputs. The basic conclusion that the authors arrive at is that a combination of multisite phosphorylation and substrate sequestration gives rise to a greater number of parameters, which can be fine-tuned through evolution to generate ultrasensitive responses.

The general phenomenon of substrate sequestration is reminiscent of ZAP-70 binding to fully phosphorylated ITAMs. Thus it will be interesting to consider the consequences of ZAP-70 binding for the possible switch-like characteristics exhibited by the TCR proximal signalling network.

Multistability

There exists a large body of mathematical literature based on the stability of dynamical systems (49). Multistability arises in natural phenomena when a certain process or system transitions between multiple steady states, or equilibria. A steady state is considered linearly stable if small perturbations do not alter the eventual state of the system; similarly, unstable steady states are characterized by large systemic changes due to small perturbations.

A recent study (50) considers the existence of multiple steady states, and the stability properties of these steady states, in the context of multisite substrate phosphorylation systems. A substrate that is comprised of N phosphorylation sites is capable of existing in 2^N possible phosphoform states. Moreover, each substrate phosphoform may exhibit distinct biological properties, and mediate unique cellular processes.

A mathematical analysis of model (1.4) reveals that under certain parameter regimes, multisite substrate phosphorylation systems are capable of exhibiting multiple stable steady states (50). Each steady state

corresponds to particular phosphoform distributions, whereby the amount of modified substrate is comprised of substrate species with different phosphorylation profiles. Thus we can imagine a scenario where different substrate and enzyme concentrations within different intracellular compartments give rise to distinct steady state distributions of substrate phosphoforms throughout the cell.

The experimental detection of multistability in a cellular context is complicated by the fact that modern biochemical approaches usually detect an output of interest across an entire population of cells. Thus it is extremely difficult with current techniques to understand substrate phosphoform distributions within a single cell - let alone within specific intracellular compartments. However, it is important to note that multistability is possible in multisite phosphorylation systems, and the existence of multistability could have important functional implications.

Bistability versus ultrasensitivity

The instance of two linearly stable steady states is referred to as bistability. In the context of multisite phosphorylation, bistability refers to the case where the same kinase-to-phosphatase balance can elicit two different phosphoforms distributions, and thus two different levels of total substrate phosphorylation. The steady-state phosphorylation profile for a given kinase-to-phosphatase ratio depends on system initial conditions. Bistability is different from ultrasensitivity, since ultrasensitive responses elicit a unique level of substrate phosphorylation for any given kinase-to-phosphatase balance (Fig 1.3). However, bistable systems can also exhibit switch-like characteristics.

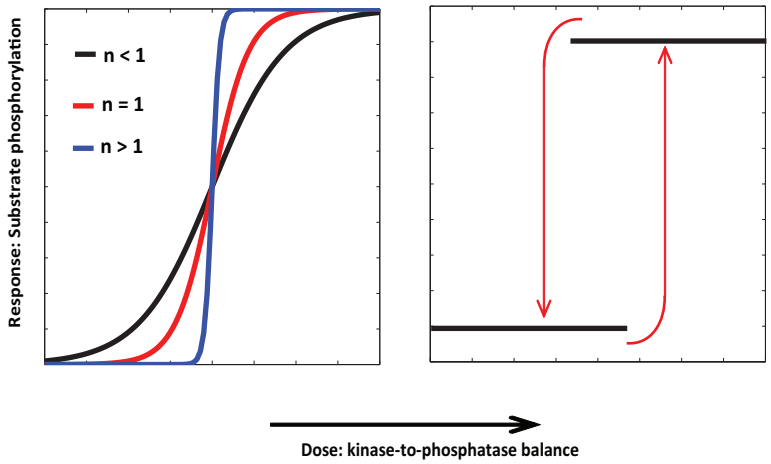

Fig 1.3: A comparison of sensitivity and bistability. Ultrasensitive responses (left panel, n>1) elicit a unique level of phosphorylation for a given kinase-to-phosphatase balance. A unique input-output response also holds true for subsensitive (n<1) and hyperbolic responses (n=1). In contrast, bistable systems can exhibit different levels of phosphorylation for the same input (right panel).

Bistable systems often exhibit a memory-like characteristic, whereby the current state depends on its previous temporal history. This memory-like feature of is referred to as hysteresis ((49), (41)). The detection of hysteresis relies on first varying the input in one direction and quantifying the system output.

Subsequently, the input is varied in the opposite direction, and the system response is again quantified. If the transition in the system output in either direction occurs at different levels of input, the system exhibits hysteresis.

In the context of multisite phosphorylation, bistability and hysteresis can be detected with the following experimental design. First the kinase-to-phosphatase balance would be increased, and the steady-state substrate phosphorylation would be quantified. Subsequently, the kinase-to-phosphatase ratio would be decreased, and substrate phosphorylation would again be quantified. If the transitions in system output are found to occur at different kinase-to-phosphatase ratios, then the system is bistable and exhibits hysteresis.

It is difficult to experimentally detect hysteresis in multisite phosphorylation systems with current biochemical techniques, because it is challenging to perturb the kinase-to-phosphatase balance in opposite directions in the same experiment. One possible strategy is to use two different pharmacological reagents such as pervanadate and PP2. Pervanadate increases the kinase-to-phosphatase ratio by inhibiting the phosphatase, while PP2 is a kinase inhibitor and thus decreases the ratio. However we do not pursue such two-inhibitor experiments due to the many unforeseen effects that this could have.

Objectives and motivations of research

The regulation of multisite substrate phosphorylation represents an important paradigm in cell signalling, and there perhaps exist multiple functional implications of substrates comprised of numerous modification sites. As is evident through our discussion, multisite substrate phosphorylation can modulate the sensitivity and potency of biological phenomena, and thus effectively regulate cellular responses to different forms of stimuli.

The question that arises concerns the additional functionality that multiple ITAMs confer upon the signalling capabilities of the TCR complex. The regulation of ITAM phosphorylation, along with the binding of ZAP-70 to fully phosphorylated ITAMs, represents an intriguing design architecture, that could exhibit subtle characteristics such as ultrasensitivity.

The elementary interactions that characterize the TCR proximal signalling network is deeply reminiscent of myriad processes throughout biology. These interactions include the modification of a multisite substrate by extrinsic enzymes, along with the binding of effector molecules to particular substrate phosphoforms. Thus the mathematical and experimental analysis of TCR proximal signalling represents an elegant paradigm in striving to understand the general design principles of cellular signalling. Subsequent to our Materials and Methods chapter, we apply mathematical frameworks of multisite phosphorylation to characterize TCR proximal signalling. Mathematical modelling reveals the design principles that give rise to ultrasensitive response profiles of TCR ζ phosphorylation. We complement our theoretical frameworks with cellular reconstitution of the TCR proximal signalling network, and we present the results of these experimental studies in the following chapter. Our objective was to combine mathematical modelling with

experimental studies to gain insights into the regulation of TCR ζ phosphorylation. Thus in the final results chapter we reconcile our theoretical frameworks of TCR proximal signalling with the experimental results obtained through our cellular reconstitution system. We conclude the thesis with a discussion of our pertinent findings, and the implications of our work towards advancing the human condition!

Chapter 2

Materials and Methods

Mathematical and computational methods

The biochemical reaction networks that underlie T cell receptor (TCR) proximal signalling were defined in BioNetGen (52). The BioNetGen language (BNGL) is a rule-based programming environment, whereby individual sites on proteins can be explicitly defined. Thus BNGL enables us to specify site-specific modifications and binding interactions.

The BNGL provides a tractable method of defining multisite modification systems such as TCR proximal signalling. Our approach was to characterize the signalling network through systems of ordinary differential equations (ODEs), and to assess the steady-state properties of these systems. Multisite phosphorylation gives rise to many species and equations, and BNGL provides a means to generate these large systems.

Systems of ODEs were generated from BioNetGen program code. These ODEs were solved to reach steady state in MATLAB (Mathworks, MA). The steady state concentrations of chemical species were used to compute total TCR ζ phosphorylation for different amounts of total phosphatase. These yielded dose-response profiles of TCR ζ-chain phosphorylation. These response profiles were fit to logarithmic Hill functions to quantify response magnitudes, potencies and sensitivities. The specific methods associated with Chapters 3 and 5 are described at the end of those Chapters.

Experimental procedures

Constructs used for transfection

The TCR ζ-chain variants were cloned into a pcDNA3.1 vector. Each variant was a recombinant protein of rat CD2 fused to mouse TCR ζ, and each ITAM mutation changed ITAM tyrosine residues to phenylalanine.

Mouse LCK was cloned into a pEF3 vector. Wild type LCK had a Y505F point mutation to mimic a constitutively active form of the enzyme, while LCK ΔSH2 was a R158K mutant.

The intracellular domain of mouse CD148 was cloned into a pcDNA3.1 vector. A FLAG tag was introduced for detection with flow cytometry. Finally mouse ZAP-70 was cloned into a pcDNA3 vector.

Cellular reconstitution

HEK 293T cells were grown in T175 cell culture flasks to reach 60-70 % confluence levels at 37°C 10 % CO_2, and the medium was replaced with 45 ml plain DMEM. Transfection stocks were prepared depending on the signalling network reconstituted. In our experiments with LCK, CD148 and TCR ζ-chain variants, we created transfection stocks containing 25 μg/ml of branched polyethylenimine (PEI) (Aldrich) and 25 μg/ml of plasmid DNA in 900 μl of plain DMEM. Experiments with ZAP-70 involved introducing an additional 25 μg of ZAP-70 DNA to the transfection stock, and we thus doubled the amount of PEI that we used. This transfection stock was pipetted onto the DMEM under which the cells were submerged. The cells were incubated at 37°C 10 % CO_2 for four hours, after which the DMEM was replaced with fresh cell culture medium. Cells were grown for twenty four hours and treated the following day.

Preparation of sodium pervanadate

The following mixture was created: (i) 100 μl of 100 mM sodium orthovanadate (New England Biolabs), (ii) 880 μl of H_2O and (iii) 20 μl of 30 % H_2O_2. This was incubated at room temperature for ten minutes, upon which it was added to 9 ml of DMEM. A serial dilution was performed with this stock to yield varying concentrations of sodium pervanadate.

Sodium pervanadate treatment

Transfected cells were harvested and resuspended in medium, and 60 μl containing 300,000 cells were placed in each well of a 96-well plate. Cells in each well were subjected to 60 μl of sodium pervanadate (New England Biolabs) concentrations ranging from 1 mM to no treatment. Cells were treated for half an hour at 37°C 10 % CO_2, and were then lysed with 120 ul 2 % Nonidet P-40 substitute (Roche). The lysis buffer contained 1 % (v/v) of a mammalian Protease Inhibitor Cocktail (Sigma) as well as 0.25 % (v/v) 100 mM sodium orthovanadate (New England Biolabs). The lysis was incubated for twenty minutes at 4°C, upon which the cells were centrifuged at 3000 RPM for a minute. 200 μl of the lysate was transferred onto an immunosorbent capture plate (see below), and this was incubated overnight at 4°C.

Immunosorbent capture plate preparation

An anti-rat CD2 (AbD Serotec MCA154G) antibody was used to capture the different TCR ζ variants. 100 μl of 0.7 μg/ml of this capture antibody, made in carbonate-bicarbonate buffer (Sigma), was placed on clear NUNC maxisorp immunosorbent plates (ThermoScientific) and this was incubated at 4°C overnight. Before transfer of lysate onto this capture plate, the plate was blocked with 1 % BSA for an hour at room temperature.

Quantification of TCR ζ phosphorylation

The capture plate containing lysate was washed six times with 0.05 % Tween-20. 100 μl of 1 μg/ml of a biotinylated anti-phosphotyrosine antibody, clone pY20 (BioLegend), was placed in each well. This was incubated for an hour at room temperature, and then washed three times with 0.05 % Tween-20. 100 μl of 0.1 μg/ml IRDye 800 CW streptavidin (LICOR Biosciences) was then placed in each well, and this was again incubated for an hour at room temperature. Finally the plate was washed thrice with 0.05 % Tween-20, dried, and scanned using a LICOR infrared 800 CW scanner (LICOR Biosciences).

Curve fitting

Phosphorylation profiles were fitted in GraphPad Prism to four parameter Hill functions, and the maxima, minima, EC_{50}s and Hill numbers for each dose-response profile were obtained.

Flow cytometry

Relative expression levels of transfected molecules were observed and analyzed using flow cytometry. Transfected cells were washed with PBS and lysed in 0.1 % saponin buffer for ten minutes at room temperature. Cells were resuspended in 100 ul of a mixture containing the following detection antibodies: (i) anti-mouse LCK (Alexa Fluor 488 BD Biosciences), (ii) anti-FLAG for CD148 staining (M2 FITC Sigma-Aldrich), (iii) anti-rat CD2 for TCR ζ-chain detection (AbD Serotec MCA154PE) and (iv) anti-mouse ZAP-70 (Invitrogen MHZAP7028). Cells were incubated for an hour at room temperature, upon which they were washed thrice. Flow cytometry was performed using a CYTEK detection system.

Chapter 3

Mathematical modelling of T cell receptor proximal signalling reveals emergent ultrasensitivity

Introduction

T cells patrol the body in search of infection and cancer derived antigens ((2), (53)). They are activated to respond by interactions between T cell antigen receptors (TCRs) on their surface and antigens, in the form of peptides bound to major histocompatibility complexes (pMHCs), on the surfaces of antigen presenting cells (APCs). When activated, T cells can lyse infected cells, secrete cytokines, and perform other effector functions that collectively allow T cells to initiate and regulate adaptive immune responses (2).

The importance of the TCR in initiating and regulating adaptive immune responses has meant that TCR proximal proteins have been extensively studied. The TCR itself is a multi-subunit receptor that contains subunits for ligand binding ($\alpha\beta$ heterodimer) and signal transduction (CD3$\epsilon\delta$and CD3$\epsilon\gamma$ heterodimers, and $\zeta\zeta$ homodimer). Collectively, the signal transducing subunits contain 20 tyrosine residues distributed on 10 immunoreceptor tyrosine based activation motifs (ITAMs) (3). These ITAMs are phosphorylated by the SRC-family tyrosine kinase LCK and dephosphorylated by transmembrane tyrosine phosphatases, such as CD45 and CD148. Phosphorylated ITAMs serve as docking sites for the tandem SH2 domain-containing cytosolic kinase ZAP-70, which, upon binding, is able to catalyze additional reactions propagating downstream signalling. Despite the small number of molecules involved, their interactions form the basis of a complex regulation network which is poorly understood (54).

There are many intriguing aspects of this signaling module (54). While each CD3 signal transducing subunit contains a single ITAM, the TCR ζ-chain contains three ITAMs (3) (Fig 3.1). These 3 ITAMs have been shown to be sequentially phosphorylated (membrane-distal to membrane-proximal) by LCK (10) and it has been shown that ZAP-70 binds to these ITAMs with increasing affinities (membrane-distal to membrane-proximal) ((55), (56), (57), (58), (59)). In addition, CD45, a phosphatase that dephosphorylates these ITAMs, is thought to be among the most abundant molecules on T cells (27). The purpose of multiple

ITAMs, their sequential phosphorylation, the differential binding affinities of ZAP-70, and the abundance of CD45, remain unknown.

The binding of pMHC to the TCR is thought to change the kinase-phosphatase ratio leading to phosphorylation of TCR ITAMs and the initiation of an intracellular signalling cascade that leads to T cell activation, which, if inappropriate, can result in autoimmune disorders (23). Therefore TCR ITAM phosphorylation is thought to be tightly regulated. Given that LCK and CD45 are constitutively active in resting T cells ((25), (22)), spontaneous (stochastic) pMHC-independent fluctuations in the local LCK or CD45 concentrations can lead to ITAM phosphorylation. These fluctuations may also allow for ITAM phosphorylation in response to endogenous pMHC. On the other hand, maximal ITAM phosphorylation should proceed for antigenic pMHC. Switch-like responses at the scale of individual TCRs provide thresholds, so that phosphorylation is prevented over a wide range of enzyme concentrations below the threshold, and all-or-none responses, so that maximal ITAM phosphorylation proceeds beyond the threshold. However, it is presently unknown whether the TCR proximal signalling architecture supports a switch-like response at the scale of individual TCRs.

In recent years, therapies have been developed to exploit T cells by re-directing them towards infected or cancerous cells (53). Several research groups have developed therapies based on chimeric antigen receptors (CARs), whereby the variable domains of a monoclonal antibody recognizing pathogen or cancer derived antigens is fused to a signalling chain, most commonly the TCR ζ-chain (60). These CARs are transfected into T cells that are then adoptively transferred into patients, generating a pathogen/cancer specific T cell population. However, the antigenic targets of CARs, although highly expressed on cancerous cells, are not exclusively expressed on these cells. This observation, coupled with the fact that the extracellular domains of CARs often exhibit very high affinity to their target antigens, means that off-target cell killing can be frequent (60). Therefore, optimal CARs should exhibit low potency, so that T cells only respond to cells that highly express target antigens, and CARs should also exhibit a high maximum response to ensure complete target cell killing when responding. Although CARs are routinely modified in order to achieve these desired properties, there is presently no mechanistic model to guide the rational development of the signalling domains of CARs to obtain optimal properties.

We begin this chapter by contrasting random and sequential mechanisms of phosphorylation. We subsequently construct a systems model of TCR proximal signalling that includes the 3 ζ-chain ITAMs, their sequential modification by LCK and CD45/CD148, and the binding of ZAP-70 to these ITAMs with affinities increasing in the direction of phosphorylation. We find that this signalling architecture produces a novel mechanism of ultrasensitivity (switch-like response) at the scale of individual TCRs. Furthermore, we find that all three factors are critical for generating a switch-like response, so that removal of ITAMs, sequential phosphorylation, or differential ZAP-70 binding affinities abolishes the switch and therefore this switch can be thought of as an emergent property of the TCR proximal signalling architecture. Our results provide a

rationale for the intriguing architecture of TCR proximal signalling, as well as a mechanistic framework for the design of novel CARs with desired properties.

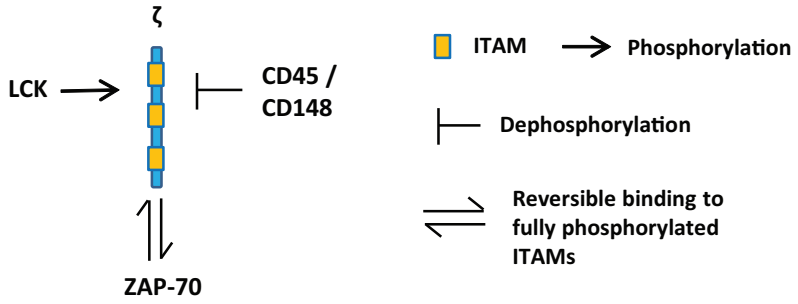

Fig 3.1: **The TCR proximal signalling network.** Phosphorylation of ITAMs is mediated by LCK, while dephosphorylation is mediated by CD45/CD148. Fully phosphorylated ITAMs create binding sites for ZAP-70 (see text for full details).

Random and sequential mechanisms of phosphorylation

A central feature of multisite phosphorylation is the underlying structure of substrate modification. Two extreme scenarios are represented by random and sequential mechanisms of phosphorylation (3.2). Random phosphorylation corresponds to a completely unstructured mechanism, whereby transitions between the completely dephosphorylated to the fully phosphorylated state may proceed through any path (3.2A). On the other hand, sequential mechanisms represent scenarios where substrate modifications occur through a specified pathway (3.2B).

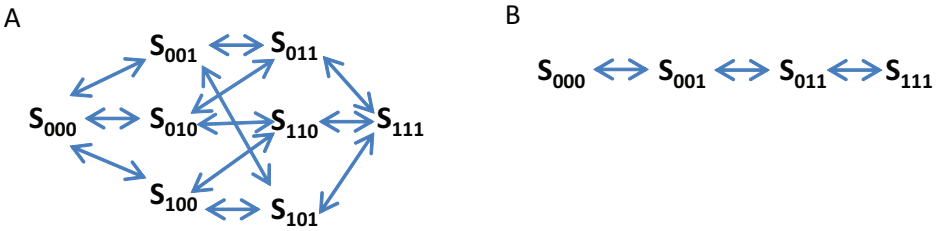

Fig 3.2: **Random and sequential mechanisms of substrate phosphorylation.** Schematic of different underlying structures of multisite phosphorylation for a substrate with three sites. A phosphorylated site is represented as 1 while an unphosphorylated site is denoted 0. (A) Random mechanism of phosphorylation. Starting from the completely dephosphorylated state S_{000}, the substrate can traverse any path to reach the fully phosphorylated state S_{111}. (B) Sequential mechanism of phosphorylation. Substrate traverses a specific sequence of phosphorylation from the completely unphosphorylated to the fully phosphorylated states.

An important question concerns the functional properties of multisite phosphorylation under these different schemes of substrate modification. In Fig 3.3 we depict the consequences of increasing the number of modification sites on the dose-response profiles of substrate phosphorylation. As is expected, increasing the number of modification sites increases the maximal response under both sequential and random mechanisms

of phosphorylation (Fig 3.3A-D). Moreover, the potency of phosphorylation also stays the same under both mechanisms (Fig 3.3E,F). However we notice that the shapes of the dose-response profiles under sequential and random mechanisms are different, and this is quantified by the Hill Numbers (Fig 3.3G,H). We note that by increasing the number of modification sites, the sensitivities of the dose-response profiles increase under sequential phosphorylation (Fig 3.3H), but not under random mechanisms of phosphorylation. Thus we conclude that sequential mechanisms of phosphorylation give rise to more ultrasensitive responses, and this ultrasensitivity is enhanced with increasing numbers of modification sites.

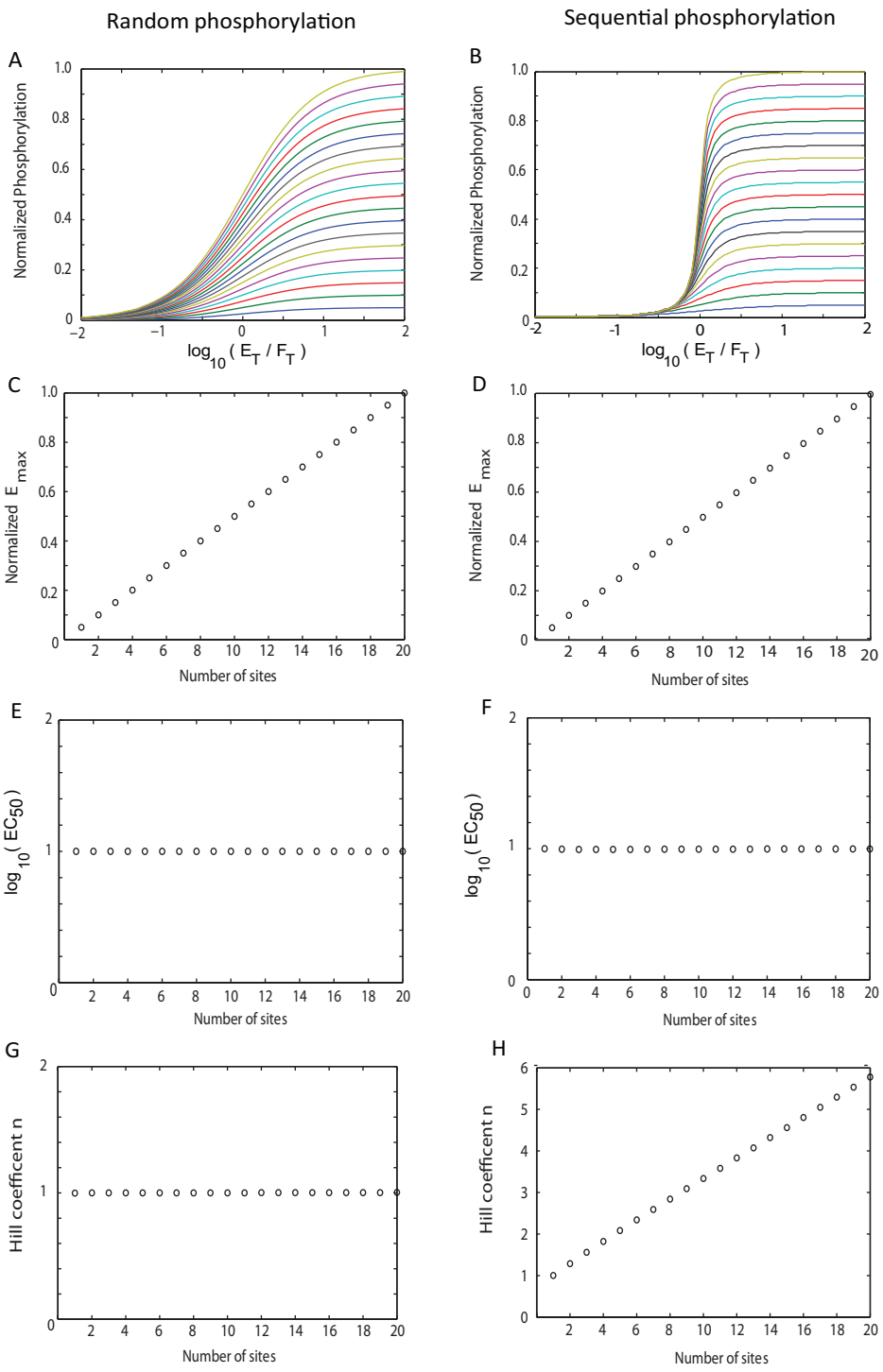

Fig 3.3: **Functional properties of sequential and random mechanisms of phosphorylation with increasing number of phosphorylation sites.** Left column: random phosphorylation; right column: sequential phosphorylation. (A and B) Normalized dose-response profiles for (A) random and (B) sequential phosphorylation as the number of modification sites is increased. The x axis varies the ratio of the total amounts of kinase (E_T) versus phosphatase (F_T), and the y axis denotes the normalized total substrate phosphorylation. Each colour corresponds to a substrate with different numbers of modification sites. The panels show dose-response profiles as the number of substrate modification sites is increased, eliciting profiles with increasing maxima. (C and D) Normalized E_{max} for (C) random and (D) sequential mechanisms. (E and F) Potencies of dose-response profiles for (E) random and (F) sequential mechanisms of phosphorylation. (G and H) Sensitivities of dose-response profiles for (G) random and (H) sequential mechanisms.

Mathematical model of TCR proximal signalling network

We construct a systems model that incorporates the enzymatic kinetics of the tyrosine kinase LCK in sequentially phosphorylating and the dominant phosphatase CD45 in sequentially dephosphorylating TCR ζ ITAMs. In this way, the membrane-distal ITAM ($\zeta 3$) must be doubly phosphorylated before LCK is able to phosphorylate the second ITAM ($\zeta 2$), and so on.

We note that a strictly sequential mechanism is an idealized representation of the underlying biology. In our introductory chapter we discussed several lines of evidence that are suggestive of the membrane distal ITAMs being phosphorylated before the membrane proximal ITAMs. However there is no direct evidence for CD45 also dephosphorylating ITAMs in such a membrane distal-to-proximal manner. Our purpose in assuming sequential ITAM modifications is to gain insights into the effects of the underlying structure of phosphorylation on the dose-response profiles of ζ-chain phosphorylation. Mathematical models in biology are simplified descriptions, and the assumption of a strictly sequential ITAM modification scheme is such a simplification. We shall discuss this assumption further at the end of this chapter.

The model incorporates ZAP-70 by allowing it to bind each ITAM when it is doubly phosphorylated, independent of reactions taking place by LCK or CD45 on other ITAMs. The affinity between ZAP-70 and $\zeta 1$ is taken to be 10-fold higher than $\zeta 2$, which we take to have an affinity 10-fold higher than $\zeta 3$. The exact affinity values for ZAP-70 binding for each ITAM differ between studies and therefore we vary these parameters. All enzymatic reactions are modelled in full without any simplifications. The system of ordinary-differential-equations (ODEs) is generated in BioNetGen, a rule-based framework for generating biochemical reaction networks, and produced 53 chemical species and 168 reactions. The number of chemical species and reactions is large despite only including 4 distinct molecules because the systems model accurately captures all possible molecular complexes that can form.

Multiple TCR ζ ITAMs produce signal amplification, high potency and ultrasensitivity

To study how this signaling architecture regulates the activity of ZAP-70, total TCR ζ phosphorylation was calculated as a function of the relative concentrations of the kinase (E_T) LCK, and phosphatase (F_T) CD45 (Fig 3.4A). In the case of the wild type TCR ζ-chain ($\zeta 123$), we unexpectedly observed an ultrasensitive or switch-like response, whereby small perturbations to LCK or CD45 produced large changes in the TCR ζ phosphorylation. We quantified this observation by fitting a Hill function to the kinase-phosphatase curve to extract estimates of the maximum (E_{max}, Fig 3.4B), the potency (EC_{50}, Fig 3.4C), and the sensitivity (Hill number, Fig 3.4D). We found a Hill number of 5.2, which is greater than 1, indicating a switch-like response. Since the concentrations of the modifying enzymes (LCK, CD45) are comparable or in excess of the substrate (TCR ζ), the observed ultrasensitivity is not a result of the classic zero-order mechanism.

We next investigated the contribution of multiple ITAMs. We repeated the calculations when removing the first ITAM (ζX23) or both the first and second ITAMs (ζXX3) (Fig 3.4A). As expected, we observed a

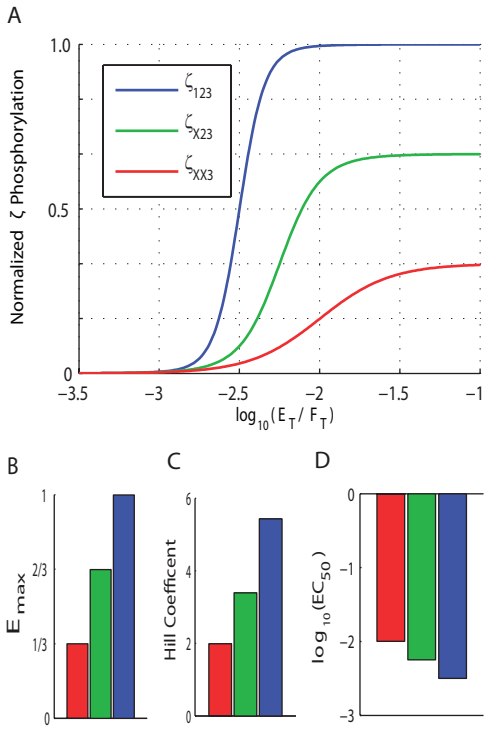

Fig 3.4: **Multiple TCR ζ ITAMs not only mediate signal amplification, but also increase potency and sensitivity.** (A) TCR ζ phosphorylation as a function of the relative kinase (E_T) to phosphatase (F_T) concentration. Results are shown for the wild-type ζ-chain (ζ123), and for ITAM mutants ζX23 and ζXX3, where the first and second ITAMs are removed, respectively. Each curve is fitted to a Hill function to extract estimates of (B) the maximum (E_{max}), (C) the potency (EC_{50}), and (D) the sensitivity (Hill number). Model and parameter values can be found in the Methods section at the end of this Chapter.

reduction in the maximal level of TCR ζ phosphorylation (Fig 3.4B), reflecting the signal amplification characteristic of multiple ITAMs. However, removal of ITAMs also decreased potency (Fig 3.4C) and sensitivity (Fig 3.4D). These effects were not mediated by substrate concentration, as increasing the concentration of ζXX3 by a factor of 3 did not restore ultrasensitivity or potency (not shown). Therefore multiple ITAMs on a single ζ-chain are predicted to mediate not only signal amplification, but also potency and sensitivity.

ZAP-70 binding modulates potency and ultrasensitivity

We next investigated the contribution of ZAP-70 binding to potency and sensitivity. To do this, we calculated the total concentration of phosphorylated ζ-chain, as may be detected by an anti-phosphotyrosine antibody, as a function of the ratio of active enzymes in, respectively, the absence and presence of ZAP-70 (Fig 3.5A, blue and green curves). A marked increase in potency and ultrasensitivity is observed in the presence of ZAP-70 (Fig 3.5B,C).

The increase in potency (decrease in EC_{50}) in the presence of ZAP-70 occurs because ITAMs bound by ZAP-70 become inaccessible to phosphatases. Therefore, the absolute ZAP-70 affinity for ITAMs is

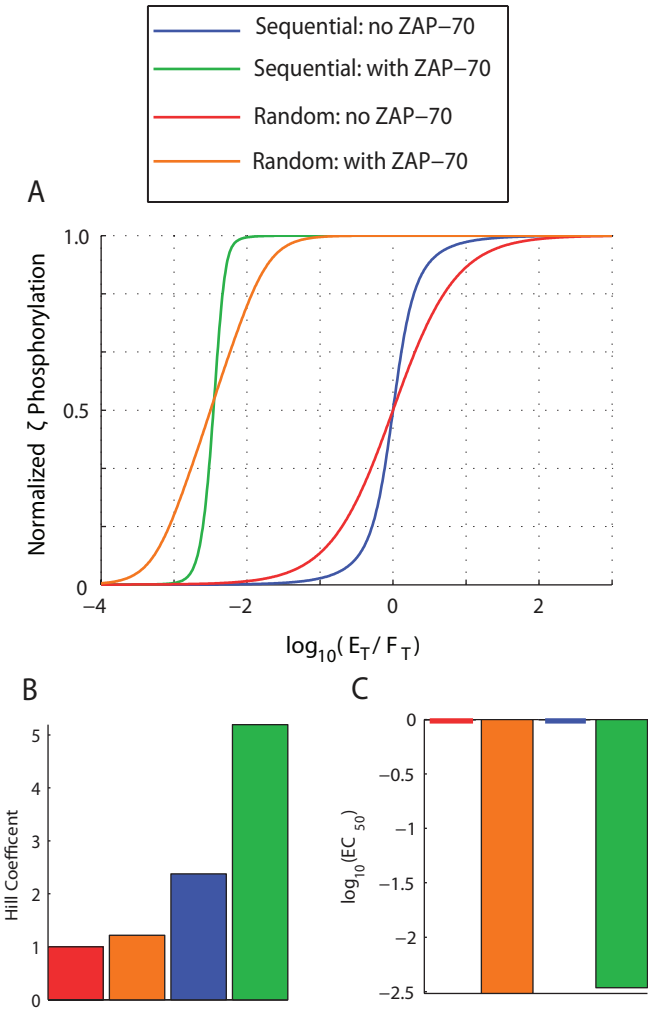

Fig 3.5: **ZAP-70 binding to phosphorylated ITAMs enhances both ultrasensitivity and potency.** (A) The concentration of total ζ-chain phosphorylation as a function of the relative concentration of kinase (E_T) to phosphatase (F_T). Results are shown for sequential phosphorylation (blue, green) and random phosphorylation (red, orange) in the absence (blue, red) and presence (green, orange) of ZAP-70. (B) Hill numbers and (C) EC_{50} for all four curves reveal that ZAP-70 binding dramatically increases both ultrasensitivity and potency when phosphorylation is sequential but not random.

expected to determine potency. Comparisons between the wild-type ζ-chain (ζ123) and domain duplication constructs that contain three copies of the high affinity ITAM (ζ111), intermediate affinity ITAM (ζ222), and low affinity ITAM (ζ333) reveal that increased potency can be achieved by increasing the ZAP-70 affinity (Fig 3.6A,C). The high potency (low EC_{50}) observed in the presence of ZAP-70 provides a plausible explanation for the abundance of CD45 on T cells. In order to keep the TCR unphosphorylated, an excess of phosphatase is required to balance the constitutive activity of LCK and the binding of ZAP-70.

We observed reduced sensitivity for ζ-chains containing identical ITAMs (Fig 3.6) and therefore surmised that the differential ZAP-70 affinities produce ultrasensitivity. In Fig 3.7A we compare the wild-type

ζ-chain (ζ123) to a construct containing identical ITAMs (ζ222) and to a construct where ITAM 1 and 3 have switched positions (ζ321). We observe that ultrasensitivity relies not only on differential ZAP-70 affinities but also on differential affinities that increase in the direction of phosphorylation, i.e. membrane-distal to membrane-proximal (Fig 3.7B). This is comprehensively illustrated in Fig 3.7C, which shows a heat map of Hill numbers as a function of the ZAP-70 unbinding rate for ITAM 1 (x-axis) and ITAM 3 (y-axis) when the unbinding rate for ITAM 2 is fixed at 1 s^{-1}. Ultrasensitivity is observed when the unbinding rate is small for ITAM 1 and large for ITAM 3.

In summary, the absolute ZAP-70 affinity for TCR ζ ITAMs modulates potency while the differential ZAP-70 affinity gives rise to ultrasensitivity.

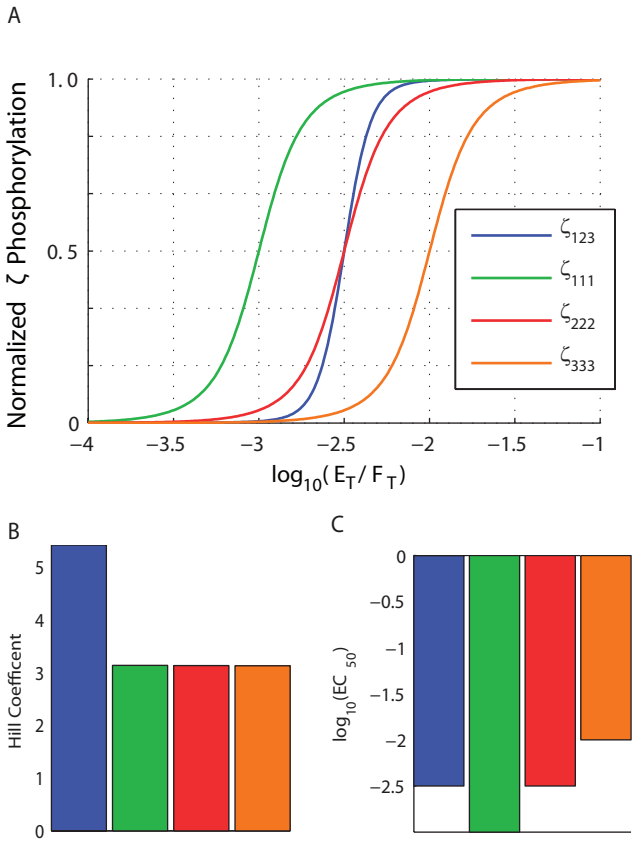

Fig 3.6: **The absolute ZAP-70 affinity for ζ-chain ITAMs modulates potency.** (A) TCR ζ phosphorylation as a function of the concentration of active kinase (E_T) to phosphatase (F_T). Results are shown for the wild-type ζ-chain (ζ123) and for three additional ζ-chains that contain all high affinity ITAM 1 (ζ111), intermediate affinity ITAM 2 (ζ222), or low affinity ITAM 3 (ζ333). Comparison of these ζ-chains reveals that (B) sensitivity is unchanged whilst (C) potency is modulated.

Sequential phosphorylation is required for ultrasensitivity

The observation that ultrasensitivity relies on ZAP-70 affinities increasing in the direction of sequential phosphorylation (Fig 3.7A, ζ123 vs ζ321), suggests that sequential phosphorylation may contribute to ultrasensitivity. We contrasted sequential phosphorylation to random phosphorylation, whereby each ITAM can be independently phosphorylated or dephosphorylated. We found that removal of sequential phosphorylation abolished ultrasensitivity in total TCR ζ-chain phosphorylation (Fig 3.5A, ζ123 Random; and Fig 3.7A, ζ123 Random).

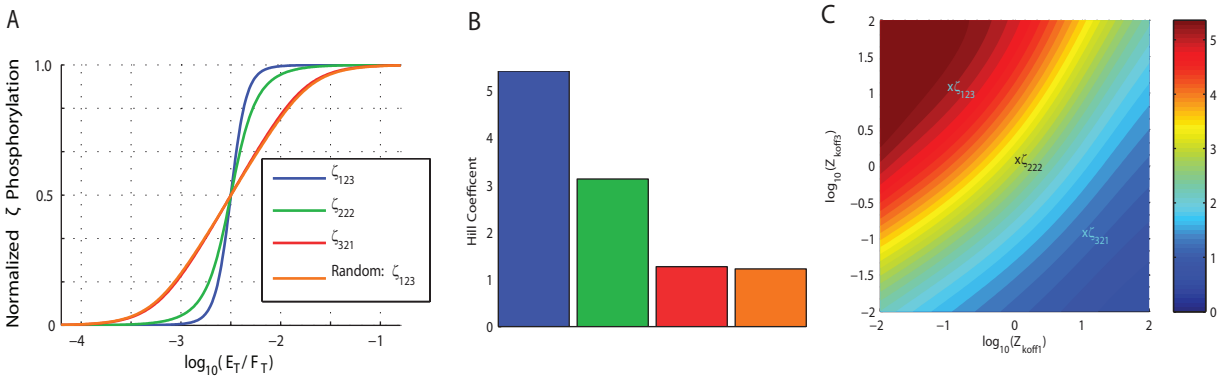

Fig 3.7: **Differential ZAP-70 affinity and sequential phosphorylation produces ultrasensitivity.** (A) TCR ζ phosphorylation as a function of the relative concentration of active kinase (E_T) to phosphatase (F_T). Shown are the wild-type ζ-chain (ζ123), and additional constructs where all ITAMs are identical (ζ222), switched (ζ321), or where phosphorylation is no longer sequential (ζ123 Random). (B) The Hill numbers reveal that ultrasensitivity is decreased if ZAP-70 does not exhibit differential affinity (ζ222), if the affinity decreases as the ζ-chain is sequentially phosphorylated (ζ321), or if phosphorylation is no longer sequential. (C) Heat map of Hill numbers as a function of the ZAP-70 unbinding rate for ITAM 1 (Z_{koff1}) and ITAM 3 (Z_{koff3}), where the unbinding rate for ITAM 2 is fixed at 1 s^{-1}. The calculation is performed under sequential phosphorylation. Maximum sensitivity is found in the top left of the heat map, where ZAP-70 binds with the largest affinity to ITAM 1 and with lowest affinity to ITAM 3.

Ultrasensitivity is an emergent property of the TCR proximal signalling architecture, relying on multiple ITAMs, sequential phosphorylation, and differential ZAP-70 affinity

We have shown the contribution of multiple ITAMs, sequential phosphorylation, and differential ZAP-70 affinity to producing ultrasensitivity. Importantly, ultrasensitivity critically relies on each of these factors so that removal of multiple ITAMs (Fig 3.4A, ζXX3), removal of sequential phosphorylation (Fig 3.7A, Random ζ123), or differential ZAP-70 affinity (Fig 3.7B) can markedly reduce or abolish ultrasensitivity.

The origin of the proposed emergent ultrasensitivity is in the effective cooperative binding of ZAP-70 and it can be compared to classical ultrasensitivity observed in allosteric models of Haemoglobin. In these models, as the total ligand concentration increases the concentration of bound ligand exhibits an ultrasensitive response (with large Hill numbers) because ligand binding induces an allosteric conformational

change in the receptor that increases the effective binding affinity of subsequent ligand binding. Similarly, increasing the concentration of LCK increases the phosphorylation of the TCR which sequentially produces docking sites for ZAP-70 of increasing affinity. In both cases if the affinity does not increase as molecules bind to the receptor ultrasensitivity is reduced. In the case of the TCR, increases in affinity critically rely on the binding sites being sequentially phosphorylated and ZAP-70 having different affinities for these sites, implicitly implying a requirement for multiple ITAMs.

Design of novel chimeric antigen receptors

As described in the Introduction of this Chapter, chimeric antigen receptors (CARs) are routinely developed without predictive mechanistic models of signalling. We therefore applied the present mechanistic model to understand existing CARs and to design novel CARs. The growing consensus in the community is that optimal CARs should exhibit high affinity to target antigens, low antigen potency, and large maximum responses. Early studies compared CARs containing the TCR ζ-chain and the FcϵRIγ-chain ((61), (62)). These studies showed improved cytotoxic responses from ζ-chain fused CARs compared to FcϵRI-γ-chain fused CARs. The key differences between these two signalling chains are ITAM multiplicity and ZAP-70 affinity; whereas the ζ-chain contains 3 ITAMs that bind ZAP-70 with various affinities, the FcϵRI-γ-chain contains only a single low affinity ITAM. The FcϵRI-γ ITAM has an affinity comparable to the low-affinity ζ3 ITAM (59).

In Fig 3.8 we compare six different CAR designs. CARs containing a single ITAM taken from ζ1, FcϵRI-γ, and FcϵRI-β exhibit successively lower ZAP-70 affinity, with 10-fold decreased affinity between ζ1 and FcϵRI-γ and a further 10-fold decrease in affinity between FcϵRI-γ and FcϵRI-β (59). Using these ITAMs, we construct single or triple ITAM CARs and find that low potency and maximum responses are best achieved by a triple low affinity ITAM signalling chain based on the ITAM from FcϵRI-β. In summary, although the commonly used TCR ζ-chain exhibits a larger maximum compared to the single ITAM-containing FcϵRI-γ, it has an undesirably large potency (small EC_{50}). We predict that improved CARs, with reduced off-target cell killing, can be generated by using three (or more) low affinity ITAMs, such as the FcϵRI-γ or FcϵRI-β ITAM. Experimental assays to evaluate these novel CARs are discussed below.

Discussion

We have used a systems model to reveal that multiple ITAMs, sequential phosphorylation, and differential ZAP-70 binding produces emergent switch-like responses at the scale of individual TCRs. This provides a rationale for understanding the functional significance of these previously described aspects of the TCR proximal signaling architecture.

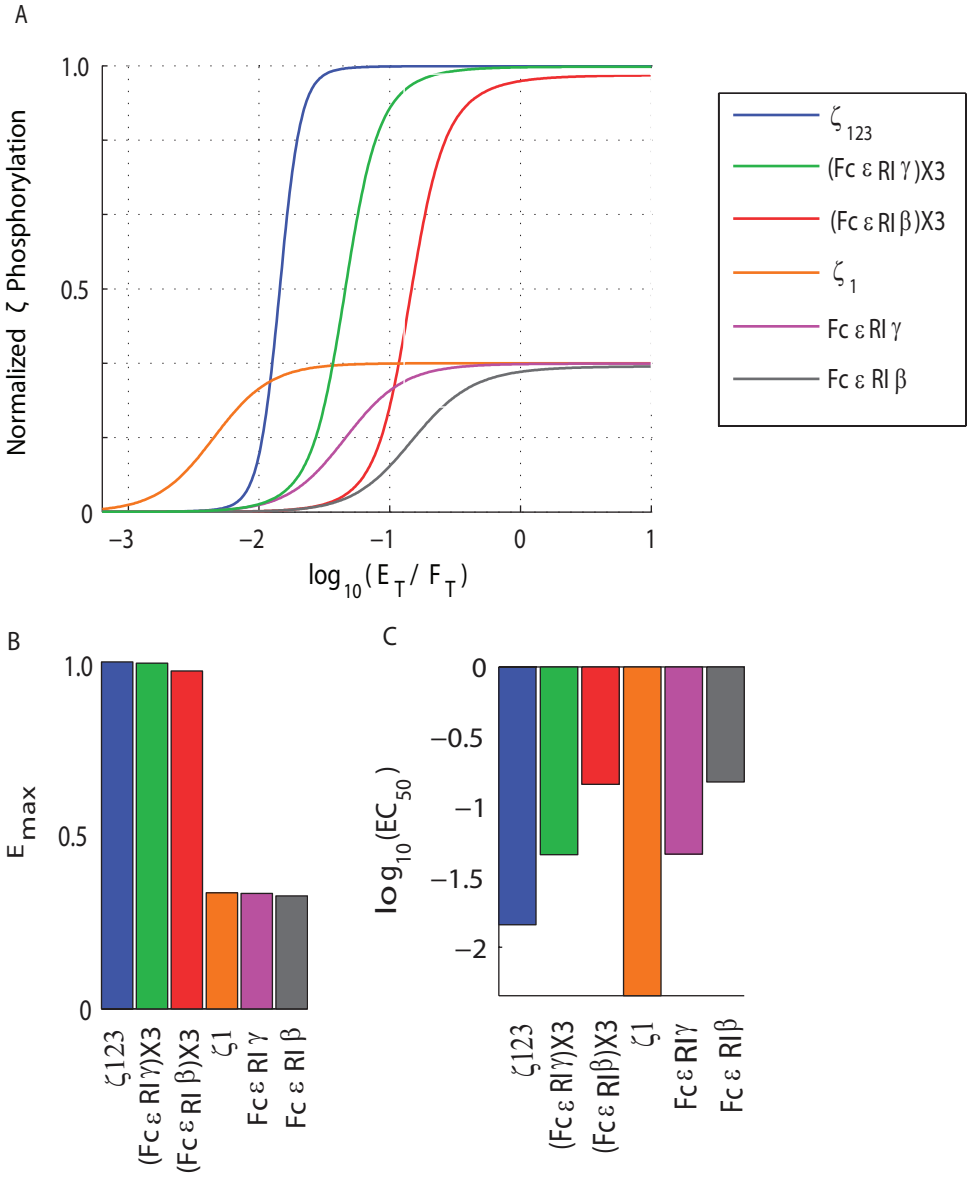

Fig 3.8: **The mathematical model predicts novel chimeric antigen receptors (CARs) design.** (A) TCR ζ phosphorylation as a function of the relative concentration of active kinase (E_T) to phosphatase (F_T) for six cytoplasmic CAR domains. These domains include the wild type ζ-chain (blue), chains containing 3 copies of the low affinity ITAM from FcϵRI-γ (green) and FcϵRI-β (red), a single high affinity ζ-chain ITAM (orange), and chains containing a single copy of the low affinity ITAM from FcϵRI-γ (magenta) and FcϵRI-β (grey). Panels (B) and (C) illustrate the E_{max} and EC_{50} for all CARs shown in panel (A). Most CARs are developed based on the wild type ζ-chain but this construct, although having a large E_{max} has an undesirably large potency (low EC_{50}). Novel CARs containing multiple low affinity ITAMs (e.g. (FcϵRIγ)x3, (FcϵRIβ)x3) have the desirably low potency (large EC_{50}) while maintaining the desirably large E_{max}.

Differential binding affinity

Evidence for differential ZAP-70 binding affinities comes from competition experiments performed at low temperatures with the SH2 domains of ZAP-70 ((55), (56), (57), (58), (63)). Future work is required to

directly measure the affinity of full ZAP-70 at 37°C.

Sequential phosphorylation

We have assumed that phosphorylation of the TCR ζ-chain proceeds sequentially from the membrane-distal to the membrane-proximal ITAM (10). However, earlier work suggested an alternate and more complex sequence of phosphorylation whereby individual tyrosines across ITAMs are phosphorylated first, possibly before any individual ITAM is fully phosphorylated (64). This alternate sequence is compatible with our model provided that fully phosphorylated ITAMs appear in sequence from membranedistal to membrane-proximal. The mechanism underlying sequential phosphorylation of the TCR ζ-chain is unknown (54). Recently, it has been proposed that lipid-binding segments of the cytoplasmic domain of PECAM-1 mediate sequential tyrosine phosphorylation (15). Given that lipid-binding basic residue rich stretch (BRS) are present in the TCR signaling subunits and have been shown to associate with the plasma membrane ((14), (11), (8)), it may be that their interactions mediate sequential phosphorylation.

Significance of high levels of phosphatase

Our detailed model has revealed that an excess of CD45 over LCK is required to keep the TCR ζ-chain dephosphorylated because although LCK and CD45 may have similar enzymatic rates, the binding of the ZAP-70 SH2 domains to phosphorylated ITAMs protects them from dephosphorylation. Previous work has demonstrated that SH2 domains protect tyrosines from dephosphorylation by phosphatases (65). This asymmetry in signalling, whereby molecules bind and protect phosphorylated but not dephosphorylated tyrosines, may apply to other ITAM, ITIM, and ITSM mediated signalling and may explain the need for abundant phosphatases on immune cells. Mathematical models have previously highlighted the need for high phosphatase activity in order to explain the rapid dephosphorylation of tyrosine phosphorylated receptors ((66), (67)).

Relation to existing mathematical models

We have studied the regulation of the TCR ζ-chain using a systems model that includes LCK, CD45, the TCR ζ-chain, and ZAP-70. Despite including only four molecules, the interaction network that we have generated is very large because of the combinatorial complexity that emerges from including a high level of molecular detail. Previous studies have included these molecules and many others ((68), (69)) but at the cost of removing molecular detail.

The activity of LCK has been proposed to be regulated by CD45 and several other molecules. A previous mathematical model has predicted that this regulation may produce bistability in the activity of LCK (70) but, to our knowledge, bistability in LCK has not been experimentally observed. Moreover, experimental work has shown that the concentration of LCK in its various phosphorylation states remains largely unchanged upon T cell activation (22). We have omitted this in the present work because it would dramatically increase the complexity and uncertainty of the model. We note that the precise mechanism by which antigen binding

to the T cell receptor alters the kinase-phosphatase balance leading to receptor phosphorylation, a process termed receptor triggering, remains controversial (23). A complete understanding of receptor triggering will provide insights into how antigens of varying affinity alter TCR proximal signalling.

The TCR ζ-chain contains 6 phosphorylation sites and is therefore considered a multisite substrate. There is a growing body of literature investigating the purpose of multisite phosphorylation (47). Previously, it was proposed that membrane-anchored, but not cytosolic, multisite substrates can produce ultrasensitivity (44). However, to achieve Hill numbers of greater than 5, membrane-anchored substrates require around 20 phosphorylation sites whereas the TCR ζ-chain is predicted to achieve this cooperativity with only 6 sites. This level of cooperativity is achieved by both ZAP-70 binding and sequential phosphorylation. The binding of ZAP-70 is a form of product inhibition, which has previously been proposed to increase cooperativity (48) and sequential phosphorylation has also been implicated in switch-like responses (46). Although multiple mechanisms of ultrasensitivity have been previously proposed, the TCR ζ-chain utilizes mechanisms that cooperate so that large ultrasensitivity is achieved with only 6 phosphorylation sites. We note that the ultrasensitivity we have reported is distinct from multi-stability, which has been previously proposed to be taking place on multisite substrates ((50), (51)).

Implications for other receptors

In addition to the TCR, other immune receptors (e.g. FcγRIII, IGSF4 (71), NKp30, NKp46) associate with the ζ-chain and therefore the predictions made here may be applicable to these receptors. There are many other receptors, termed Non-catalytic Tyrosine-Phosphorylated Receptors (NTRs) (72), with multiple phosphorylation sites that are regulated by extrinsic enzymes and like the TCR, spurious activation of these receptors may be avoided by switch-like responses that contain strong thresholds. The mathematical model used in the present study can be used to study the regulation of NTR phosphorylation.

Implications for CARs

CARs are a class of therapeutic receptors that contain variable domains of a monoclonal antibody that recognizes pathogen or cancer derived antigens fused to the TCR ζ-chain ((53), (60)). The majority of CARs rely on the TCR ζ-chain, or variants thereof, because early studies showed that CARs containing the TCR ζ-chain exhibited higher target cell killing efficiencies compared to other signalling chains, such as the FcϵRIγ (62). In contrast to the ζ-chain, the FcϵRIγ contains only a single ITAM that binds ZAP- 70 with low affinity, comparable to the low affinity interaction between ZAP-70 and ζ3 (59). This improved killing efficiency is likely due to ITAM multiplicity on the ζ-chain (Fig 3.8, ζ123 vs FcϵRIγ). However, the ζ-chain containing CAR also has the unfavourable property of increased potency. As shown in Fig 3.8, novel CAR designs that maintain low potency and high maximum are possible by using three copies of low affinity ITAMs taken from either FcϵRIγ or FcϵRIβ.

We propose that in vitro target cell killing assays can be used to determine optimal CARs. However, these assays need to be performed using titration of antigens on the target cells (with a fixed number of target cells) not the more commonly performed assay that involves titrating the number of target cells (with a fixed antigen concentration). Optimal CARs should exhibit low potency (large EC_{50}), only killing cells that highly express specific antigens, and large maximum (large E_{max}), killing many cells that highly express specific antigens. An alternative assay is to use measures of cellular activation (e.g. expression of CD107a) in response to titrations of immobilized antigen. In the present work we predict that CARs fused to wild type ζ-chain or signaling chains that contain three copies of low affinity ITAMs, such as the FcϵRIγ or FcϵRIβ ITAMs, will exhibit similar maxima. However, only the signalling chains containing three copies of the low affinity ITAMs will exhibit the desired low potency (large EC_{50}).

Methods

Systems model

The model includes the TCR ζ-chain with 6 phosphorylation sites (distributed on 3 ITAMs) that are sequentially phosphorylated by LCK (membrane-distal to membrane-proximal) and sequentially dephosphorylated by CD45. We assume that LCK and CD45 cannot simultaneously bind the TCR ζ-chain. We take k_{on}, k_{off}, and k_{cat} to be identical for both enzymes. Doubly phosphorylated ITAMs serve as binding sites for ZAP-70 (provided that CD45 is not bound to the ITAM) and therefore a maximum of three ZAP-70 molecules can bind per TCR ζ-chain. Binding of ZAP-70 to an ITAM occurs independently of reactions on other ITAMs and while bound, ZAP-70 protects the ITAM from dephosphorylation by CD45. Note that ZAP-70 binding only relies on doubly phosphorylated ITAMs. Differential ZAP-70 affinity is implemented by decreasing the k_{off} for ITAM binding by a factor of 10 between each ITAM (membrane-distal to membrane-proximal) while keeping k_{on} identical between ITAMs.

The system of ODEs representing the biochemical reaction network based on the above scheme was generated in BioNetGen (52) and integrated in Matlab (Mathworks, MA). The BioNetGen program code is provided in the appendix section of the thesis. The parameter values used for concentrations and reaction rates are estimated based on known values. However, we stress that our main results are not sensitive to the precise values of the parameters. The concentration of ITAM-bound ZAP-70 or total ζ-chain phosphorylation was calculated at steady-state by varying the concentration of phosphatase (identical results can be obtained by varying the concentration of the kinase). Total ζ-chain phosphorylation is the multiplicative product of 1) the concentration of a particular TCR ζ isoform (regardless of whether it is bound to an enzyme) and 2) the number of phosphate groups attached to the isoform.

In addition to the wild-type signaling architecture, several modified architectures were investigated. We compared sequential to random phosphorylation by allowing LCK and CD45 to catalyze reactions at

ITAMs independent of the phosphorylation state of the ζ-chain. This random or unstructured phosphorylation scheme generated 2688 reactions and over 500 chemical species compared to 168 reactions and 53 chemical species generated for the sequential scheme. Note that a mixed scheme, whereby phosphorylation is sequential but dephosphorylation is random cannot be implemented without an excessive number of additional assumptions (e.g. if dephosphorylation takes place on ITAM 3 whilst ITAM 2 is fully phosphorylated, it is unclear if sequential phosphorylation requires re-phosphorylation of ITAM 3 before phosphorylation on ITAM 1 can take place). The various ζ-chain constructs were implemented by changing k_{off} between ZAP-70 and each ITAM. For example, the ζ222 construct is generated by taking $k_{off} = 0.1s^{-1}$ between ZAP-70 and all 3 ITAMs. In each modified architecture, we preserve all remaining properties of the wild type architecture.

Curve fitting

The profiles of total TCR ζ-chain phosphorylation are fit to logarithmic Hill functions using lsqcurvefit in Matlab (Mathworks, MA),

$$y = E_{min} + \frac{E_{max} - E_{min}}{1 + 10^{(\log(EC_{50} - x))n}}$$

where y corresponds to total TCR ζ-chain phosphorylation and x is the kinase-to-phosphatase ratio on a logarithmic (base 10) scale. The fitted parameter values include: E_{min} and E_{max}, which correspond to the minimum and maximum values, respectively; $\log(EC_{50})$, which is the logarithmic value of the kinase-to-phosphatase ratio that yields half of the maximal response (otherwise known as potency), and n, which is the Hill number that determines the steepness of the response (otherwise known as the sensitivity).

Our theoretical dose-response profiles were all fit in MATLAB, while in the subsequent chapter, we shall use GraphPad Prism software to fit our experimental data. The reason for these different fitting methods is that we needed to quantify the experimental variations in our experimental data, and GraphPad Prism has many sophisticated in-built methods for doing so. We note that similar results are obtained with both software packages.

Chapter 4

Cellular reconstitution of T cell receptor proximal signalling: multiple TCR ζ ITAMs enhance the potency of phosphorylation

Introduction

A central question in cellular signal transduction is: what are the mechanisms through which molecular interactions give rise to physiological function? Signalling through the T cell receptor (TCR) mediates cellular activation, and thus the appropriate regulation of TCR signalling has important consequences in health and pathology (2). In this chapter we describe our experimental investigations of TCR proximal signalling, and we relate our findings to the mathematical models that we presented in the previous chapter.

Phosphorylation of TCR ζ ITAMs is mediated by the kinase LCK, and dephosphorylation is catalyzed by transmembrane phosphatases such as CD148. Fully phosphorylated ITAMs recruit the cytosolic kinase ZAP-70, and together these molecules form the TCR proximal signalling network (Fig 4.1A). In the previous chapter we presented a systems model of TCR proximal signalling that incorporated several previously published results. These include a sequential mechanism of TCR ζ ITAM phosphorylation ((10), (8)) and binding of ZAP-70 to phosphorylated ITAMs with affinities increasing in the direction of phosphorylation (55). Under these model assumptions, we predicted that multiple TCR ζ ITAMs enhance the potency and sensitivity of receptor phoshorylation. In this chapter we experimentally evaluate our model assumptions and predictions.

TCR signalling is comprised of multiple signalling modules intertwined over several spatial and temporal scales. This means that studying TCR proximal signalling is difficult to pursue in primary cells or cell lines, because many molecules interact with the proximal signalling network. One alternative is *in vitro* reconstitution ((73), (74)) but this method lacks an underlying cellular context. A compromise is to reconstitute signalling in heterologous cells which lack the T cell signalling machinery, but preserve background cellular processes. Such a strategy was recently pursued by James and Vale (75), whereby the authours reconstituted the TCR complex in HEK cells.

In this chapter we discuss the reconstitution of TCR proximal signalling in HEK cells (Fig 4.1B). The HEK cell line lacks the T cell signalling machinery, thus enabling us to study the functional properties of TCR proximal signalling in isolation. Our objective is to obtain experimental dose-response profiles of TCR ζ phosphorylation as the number of ITAMs is varied (Fig 4.1C). We will compare the maxima, potencies and sensitivities of dose-responses to the model predictions from the previous chapter, and we shall consider how the model assumptions must be refined to explain our experimental data.

We obtain dose-response profiles of TCR ζ phosphorylation by perturbing the relative balance of the modifying enzymes LCK and CD148. We achieve this with pervanadate, a pharmacological inhibitor of tyrosine phosphatases. Treatment of reconstituted cells with different concentrations of pervanadate results in differential TCR ζ phosphorylation, thus yielding dose-response profiles of ζ-chain phosphorylation.

In this chapter we show that multiple ITAMs mediate signal amplification and an enhancement in the potency of ζ-chain phosphorylation. We find that ZAP-70 further enhances the potency of ζ-chain phosphorylation, but this enhancement is independent of the number of ITAMs present. We do not find any significant differences in the sensitivities of phosphorylation as the number of ITAMs is varied. In the following chapter we reconcile these experimental results with mathematical models of TCR proximal signalling.

Optimization of cellular reconstitution system

Our experimental strategy was comprised of two main procedures. The first of these was transfection of HEK cells to express the molecules that mediate TCR proximal signalling (see Materials and Methods for constructs used). We reconstituted CD148 instead of CD45, even though CD148 is expressed only in some T cells. This is because CD45 is difficult to express, and the two phosphatases are functionally equivalent (76).

The second procedure treated reconstituted cells with varying concentrations of the tyrosine phosphatase inhibitor pervanadate, and quantified the level of total ζ-chain phosphorylation corresponding to each treatment dose (Fig 4.1B). Through this section we discuss the optimization of these two methods in turn.

Protein expression in HEK cells

We first sought to understand relative expression levels of molecules, and how expression patterns vary over time post-transfection. We reasoned that the optimal time to treat reconstituted cells is when relative expression levels are maximally correlated, since it is the relative amounts of molecules that determine biochemical reaction kinetics. Thus we reconstituted HEK cells to express LCK, CD148 and wild type TCR ζ, and we detected the expression level of each molecule over a three day period using flow cytometry (Fig 4.2).

In the panels labelled (i) in Fig 4.2, we depict three-component stains of LCK, CD148 and TCR ζ. We observed a clear separation between cells that express all three molecules, and cells that do not express any

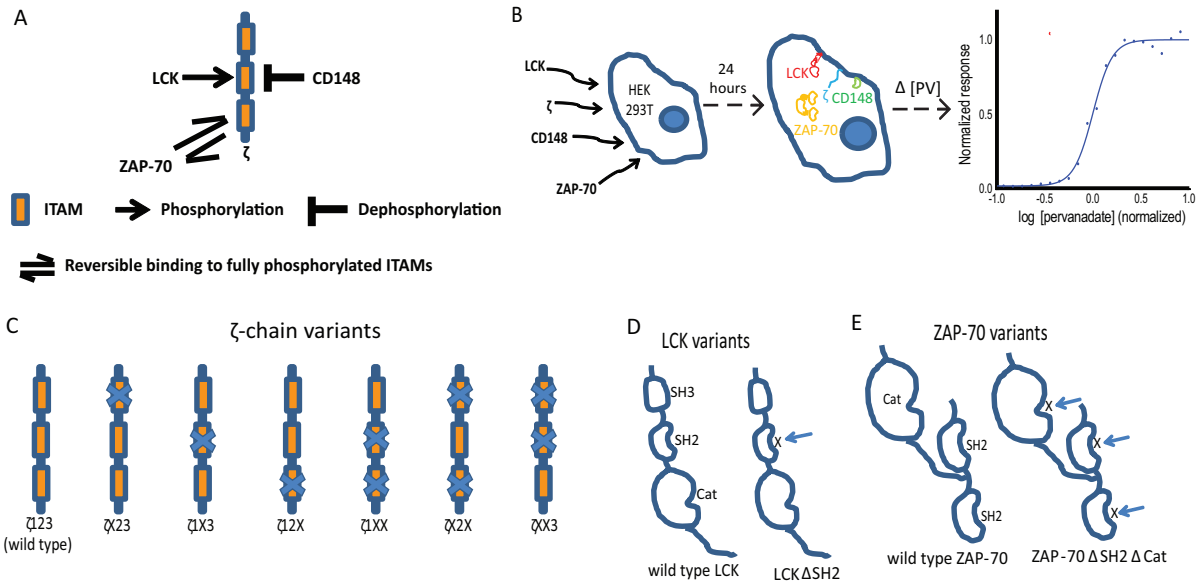

Fig 4.1: **Reconstitution of wild type and mutant TCR proximal signalling modules.** (A) The TCR proximal signalling network. TCR ζ ITAM phosphorylation is mediated by LCK and dephosphorylation is catalyzed by CD148. Phosphorylated ITAMs create binding sites for ZAP-70. (B) Cellular reconstitution of TCR proximal signalling in HEK cells, and quantification of ζ-chain phosphorylation. The molecules that comprise TCR proximal signalling were introduced into HEK cells. Reconstituted cells were treated with varying concentrations of pervanadate (Δ[PV]), and ζ-chain phosphorylation was quantified. (C-E) Molecular variants of TCR ζ, LCK and ZAP-70. (C) TCR ζ variants included the wild type ζ-chain, the single ITAM mutants (ζX23, ζ1X3 and ζ12X), and the double ITAM mutants (ζ1XX, ζX2X and ζXX3). Each variant mutated the ITAM tyrosines to phenylalanines. (D) LCK variants used were the wild type molecule and LCKΔSH2, with a point mutation in the SH2 domain binding site. (E) ZAP-70 variants used were the wild type molecule and ZAP-70ΔSH2ΔCAT with point mutations in the SH2 and catalytic domains.

molecule. We used the k-means clustering algorithm in MATLAB to classify cells that express all molecules (red dots), and cells that do not express any molecule (blue dots). We quantified the proportion of positive cells (Fig 4.2D), and observed peak expression profiles around twenty four hours post-transfection.

Steady-state profiles of substrate phosphorylation are determined by the relative amounts of molecules. We thus sought to determine the time post-transfection when molecular expression levels are maximally correlated. Through panels (ii)-(iv) in Fig 4.2 we show two-dimensional projections of molecular expression profiles post-transfection, and we use these to calculate two-component correlation coefficents (see Materials and Methods). We found maximal correlation between molecules also within twenty four hours after transfection (Fig 4.2E). These temporal expression profiles collectively suggest that the optimal time to perform experiments on the reconstituted cells is about twenty four hours after HEK cell transfection.

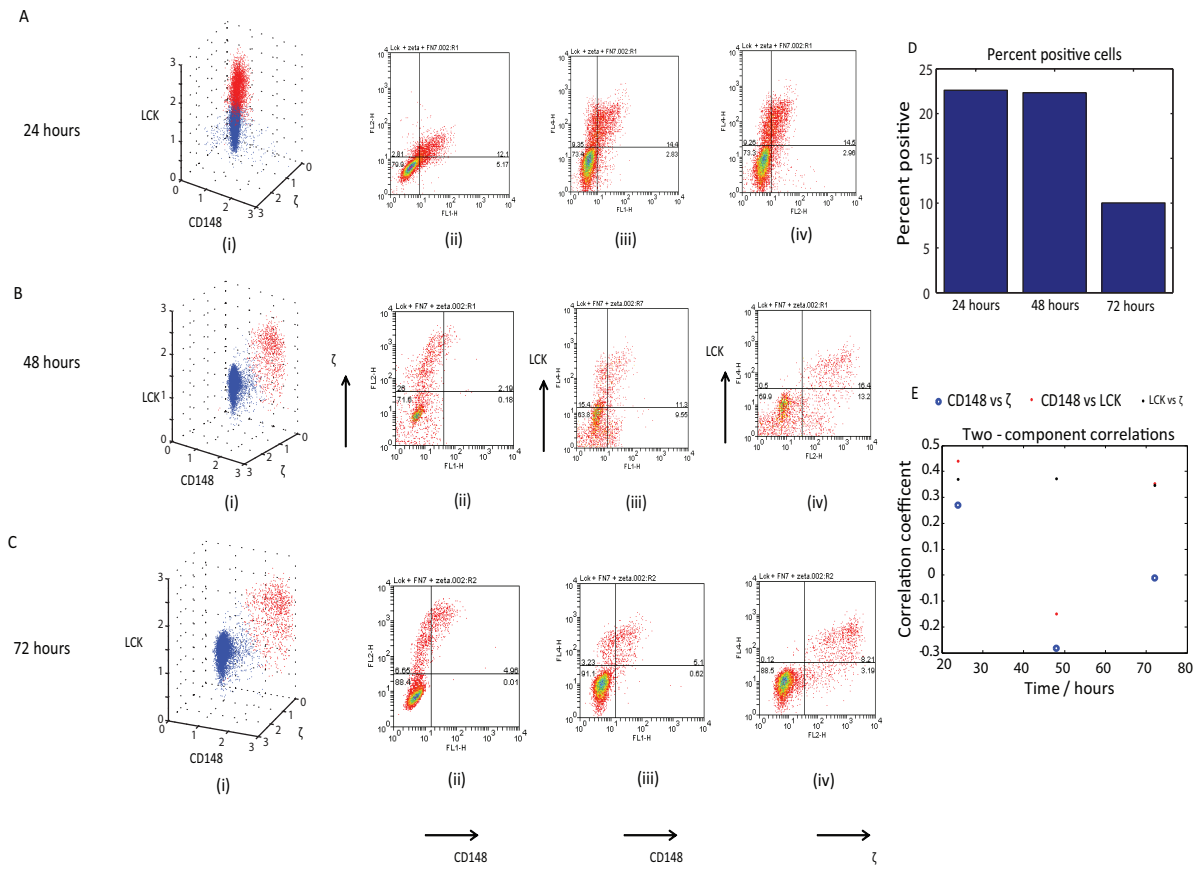

Fig 4.2: **Temporal profiles of molecular expression after HEK cell reconstitution.** HEK cells were transfected to introduce LCK, CD148 and the wild type TCR ζ-chain. Expression profiles of LCK, CD148 and the ζ-chain were detected with flow cytometry (A) 24 hours, (B) 48 hours and (C) 72 hours post-transfection. Panels labelled (i) depict the three component stain of LCK, CD148 and TCR ζ. Red dots correspond to positive cells that express all three molecules, while blue dots represent cells that do not express any molecule. Panels (ii)-(iv) are two-dimensional projections, plotting (ii) CD148 and TCR ζ, (iii) CD148 and LCK and (iv) TCR ζ and LCK. (D) Proportion of cells that express all molecules over time, calculated from panels (i). (E) Two-component correlation coefficents in time, calculated from panels (ii)-(iv).

Equilibration timescale and specificity of TCR ζ phosphorylation

To perturb the relative activities of the kinase LCK and the phosphatase CD148 we treated reconstituted cells with increasing concentrations of pervanadate. In order to determine the timescale at which the system reaches steady state, we performed a time-course of wild type ζ-chain phosphorylation (Fig 4.3A). We found that the system reaches steady state within fifteen minutes of treatment, and the curves equilibrate to similar responses subsequent to that time point (Fig 4.3A). Thus we treated reconstituted cells with different concentrations of pervanadate for half an hour at 37°C.

Given that HEK cells express endogenous tyrosine kinases and phosphatases, it was important to determine their contribution to the phosphorylation of the reconstituted ζ-chain. To do this, we transfected three combinations of proteins: (i) LCK, CD148 and ζ; (ii) LCK and ζ; (iii) CD148 and ζ, and treated

each of these reconstituted systems with increasing concentrations of pervanadate (Fig 4.3B). Given that transfection (ii) lacks an exogenous phosphatase, any dephosphorylation will be mediated by endogenous phosphatases. Similarly, since transfection (iii) lacks an exogenous kinase, any phosphorylation will be mediated by endogenous kinases. In the absence of exogenous CD148 maximal levels of phosphorylation was observed even at very low concentrations of pervanadate (Fig 4.3B red). Similarly, in the absence of LCK phosphorylation was observed only at high concentrations of pervanadate (Fig 4.3B green). This demonstrates that the dose response profile observed under our experimental conditions (Fig 4.3B blue) is primarily mediated by exogenous LCK and CD148.

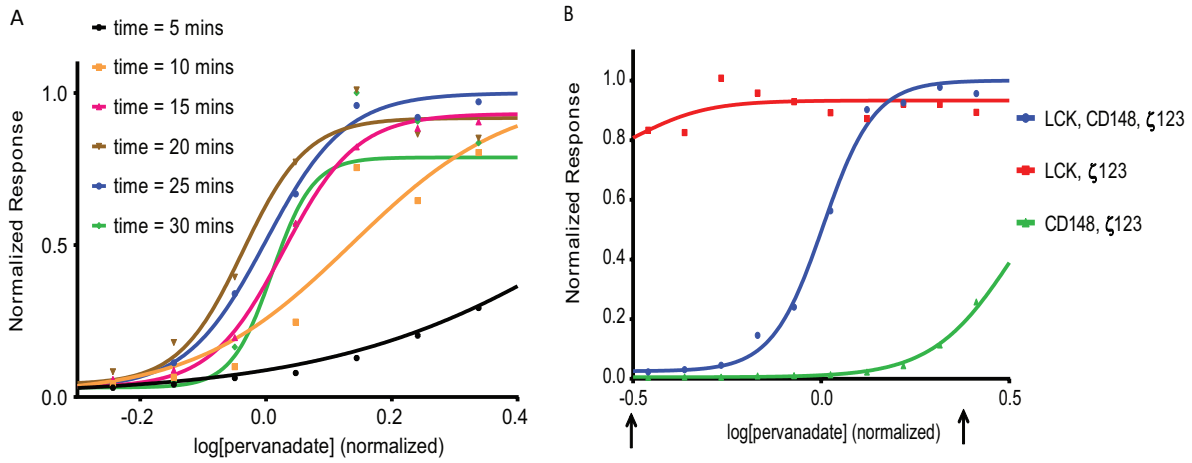

Fig 4.3: **Timescale of equilibration and specificity of ζ-chain modification.** (A) HEK cells were reconstituted to express LCK, CD148 and the wild type TCR ζ-chain. Reconstituted cells were treated with increasing concentrations of pervandate, and the reaction was quenched at the times indicated. (B) HEK cells were transfected to express either (i) LCK, CD148 and ζ (blue) (ii) LCK and ζ (red) or (iii) CD148 and ζ (green). Each reconstituted system was treated with increasing concentrations of pervandate. Response profiles were normalized to the blue curve. Arrows denote concentration range where at most 20% of the response profile is mediated by endogenous enzymes.

Emergent properties of TCR proximal signalling

The TCR proximal signalling network is a multisite phosphorylation system. Through mathematical modelling (Chapter 3) we predicted that multiple TCR ζ ITAMs enhance the potency and sensitivity of receptor phosphorylation. We sought to evaluate our model predictions and assumptions through our experimental system. Thus we generated ζ-chain variants comprised of different numbers of ITAMs (Fig 4.1C), where each mutation substitutes ITAM tyrosine residues to phenylalanine. The ζ-chain variants we generated were the (i) wild type ζ-chain (ζ123), (ii) single ITAM mutants (ζX23, ζ1X3 and ζ12X), and (iii) double ITAM mutants (ζ1XX, ζX2X and ζXX3).

We found the enhancement of potency and sensitivity to be dependent on a sequential mechanism of TCR ζ phosphorylation, and ZAP-70 binding affinities increasing in the direction of phosphorylation. To

evaluate these predictions we first reconstituted HEK cells to express the different TCR ζ-chains with the modifying enzymes LCK and CD148. Through a further set of experiments we introduced ZAP-70 to the core multisite phosphorylation module.

We pursued the same experimental strategy of treating reconstituted cells with varying concentrations of pervanadate, and quantifying total TCR ζ phosphorylation corresponding to each treatment dose. Through this section we first present results of TCR ζ phosphorylation by LCK and CD148. We subsequently consider the effects of ZAP-70 on TCR proximal signalling.

The regulation of TCR ζ phosphorylation by LCK and CD148: multiple ITAMs enhance response potency

We first sought to understand the regulation of TCR ζ phosphorylation by LCK and CD148, and the functional consequences of multiple ζ-chain ITAMs. We depict a representative set of dose-response profiles in Fig 4.4A. As is expected, increasing the number of TCR ζ ITAMs results in increases in the maximal level of phosphorylation, E_{max}.

We obtained phosphorylation profiles for all the double- and single-ITAM mutant ζ-chain constructs, and all these profiles exhibited non-zero maxima. This suggests that a strictly sequential mechanism of ζ-chain phosphorylation does not hold true.

We fit our dose-response profiles to logarithmic Hill functions, and computed the potencies and sensitivities of phosphorylation for each ζ-chain variant (see Materials and Methods). The potency is quantified by the EC_{50}, while the Hill number quantifies the sensitivity of response (Fig 4.4A).

We observed a direct correlation between response potency and the number of ζ-chain ITAMs. The wild type ζ-chain (ζ123) exhibited the most potent response (ie lowest EC_{50}), the single ITAM mutants exhibited an intermediate potency, while the response profiles of the double ITAM mutants were the least potent (ie highest EC_{50}). Therefore multiple ITAMs enhance the potency of TCR ζ phosphorylation, and this enhancement is directly correlated to the number of phosphorylation sites.

There were no significant differences in response potencies within a group of ζ-chain ITAM variants. Thus the single ITAM mutants exhibited similar response potencies, and the same held true for the double ITAM mutants. The similarity of the values of the EC_{50}s across the double ITAM mutants suggests that the relative catalytic efficiency of modification is similar for individual TCR ζ ITAMs, and that the juxtaposition of these ITAMs into the wild type configuration elicits a cooperative effect, giving rise to an enhancement of response potency.

We also sought to quantify the sensitivity of TCR ζ phosphorylation as the number of ITAMs is altered, and this is represented as the Hill numbers in Fig 4.4A. We did not observe any significant differences across the ζ-chain variants, and thus multiple ITAMs do not enhance the sensitivity of phosphorylation.

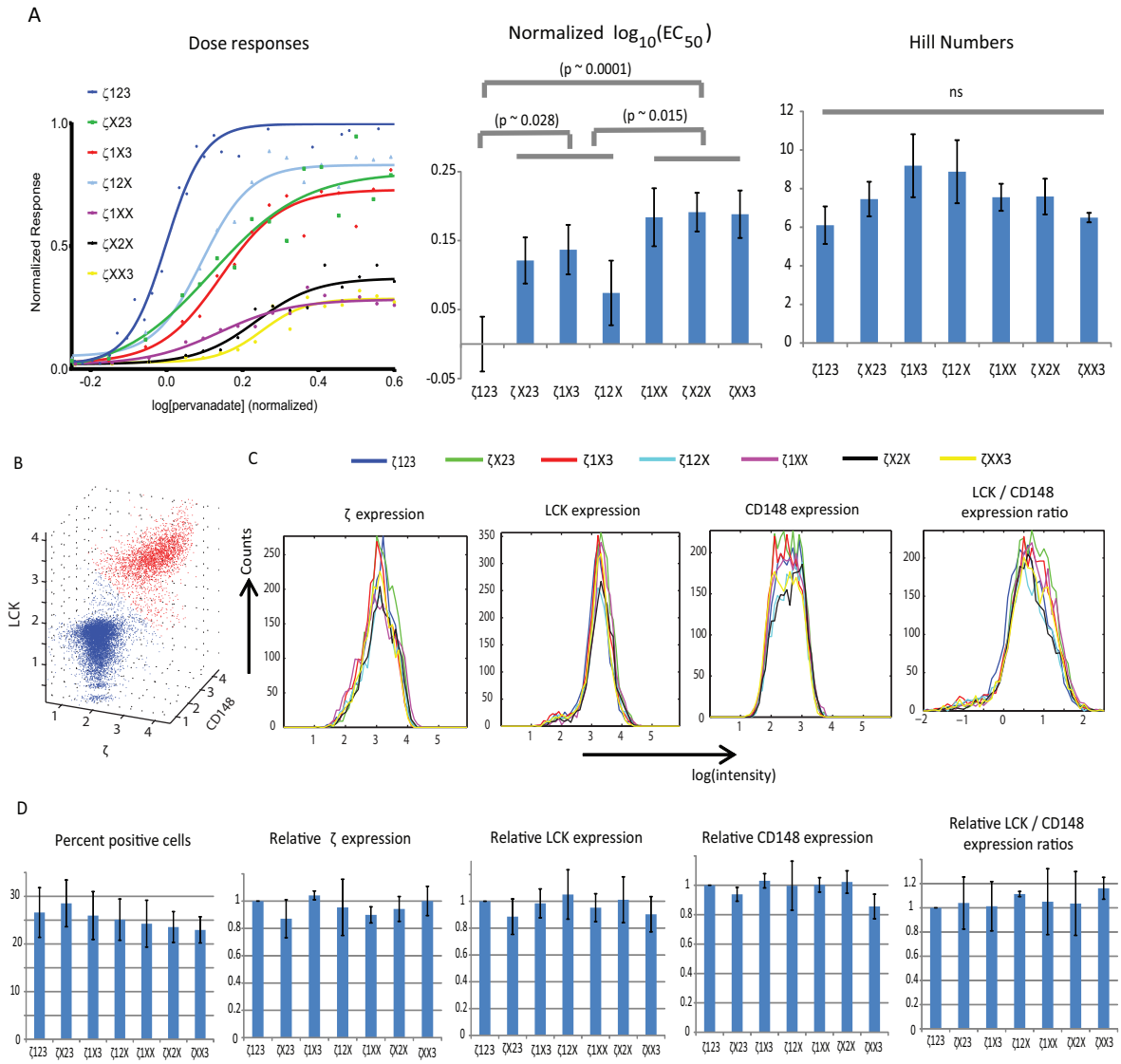

Fig 4.4: **Multiple TCR ζ-chain ITAMs enhance the potency of receptor phosphorylation.** HEK cells were reconstituted to express LCK, CD148 and the TCR ζ-chain variants. Reconstituted cells were treated with increasing concentrations of pervanadate, and ζ-chain phosphorylation corresponding to each pervanadate dose was quantified. Dose-responses were fit to logarithmic Hill functions. (A) Representative dose-response profiles, normalized EC_{50}s ($\log_{10}$ scale) and Hill numbers. Metrics were averaged across nine independent experiments, and are presented as mean ± sem. (B-C) Representative expression profiles of molecules from one experiment. (B) Three-component stain of LCK, CD148 and TCR ζ. Cells were classified as expressing all molecules (red dots), or not expressing any molecule (blue dots) with k-means clustering algorithm in MATLAB. (C) Molecular expression histograms of the ζ-chain variants, LCK, CD148 and the LCK/CD148 expression ratio for all the ITAM mutant signalling modules reconstituted. (D) Averaged expression levels across all experiments of proportion of cells expressing molecules, and relative expression levels of ζ-chain variants, LCK, CD148 and LCK/CD148 expression ratios. Data are presented as mean ± sem across eight independent experiments.

Relative expression of molecules

The differences we observe in the dose-responses of the TCR ζ variants may be due to differential expression levels of molecules. We verified that this is not the case through flow cytometry, and we present these results in Fig 4.4B-D.

In Fig 4.4B we depict a representative three-component stain of LCK, CD148 and TCR ζ. We used the k-means clustering algorithm in MATLAB to classify cells that express all molecules (red molecules), versus cells that do not express any molecule (blue dots). We quantified the proportion of cells that express the transfected molecules, and we consistently found approximately 25% of cells to be positive (Fig 4.4D).

We also sought to quantify the relative expression levels of the different ζ-chain variants, LCK and CD148 (Fig 4.4C,D). We found similar expression levels of all molecules across all signalling modules reconstituted. Finally, we calculated the relative expression ratios of LCK and CD148, and we found similar ratios across all TCR ζ-chain variants (Fig 4.4C,D).

Enhancement of potency is independent of LCK SH2 domain

We reasoned that the enhancement of potency with increasing numbers of TCR ζ ITAMs (Fig 4.4A) could be mediated by the recruitment of LCK to phosphorylated tyrosine residues through its SH2 domain, and an enhancement of catalytic efficiency due to an increase in the local concentration of the enzyme. To further test this possibility we created an LCK variant with a R158K point mutation in the SH2 domain which disrupts phosphotyrosine binding (77), and we refer to this molecule as LCKΔSH2 (Fig 4.1D).

We performed the same set of reconstitution and treatment experiments with LCKΔSH2, CD148 and the TCR ζ variants (Fig 4.5). We found the same correlation between the potency of TCR ζ phosphorylation and the number of ζ-chain ITAMs (Fig 4.5A). Thus we conclude that the enhancement of potency is independent of phosphotyrosine binding by the LCK SH2 domain. Also, the sensitivities of phosphorylation were similar for all TCR ζ-chain variants (Fig 4.5A). Finally, we performed the same set of flow cytometry experiments to confirm that the relative expression levels of molecules was similar across all ITAM variants (Fig 4.5B,C).

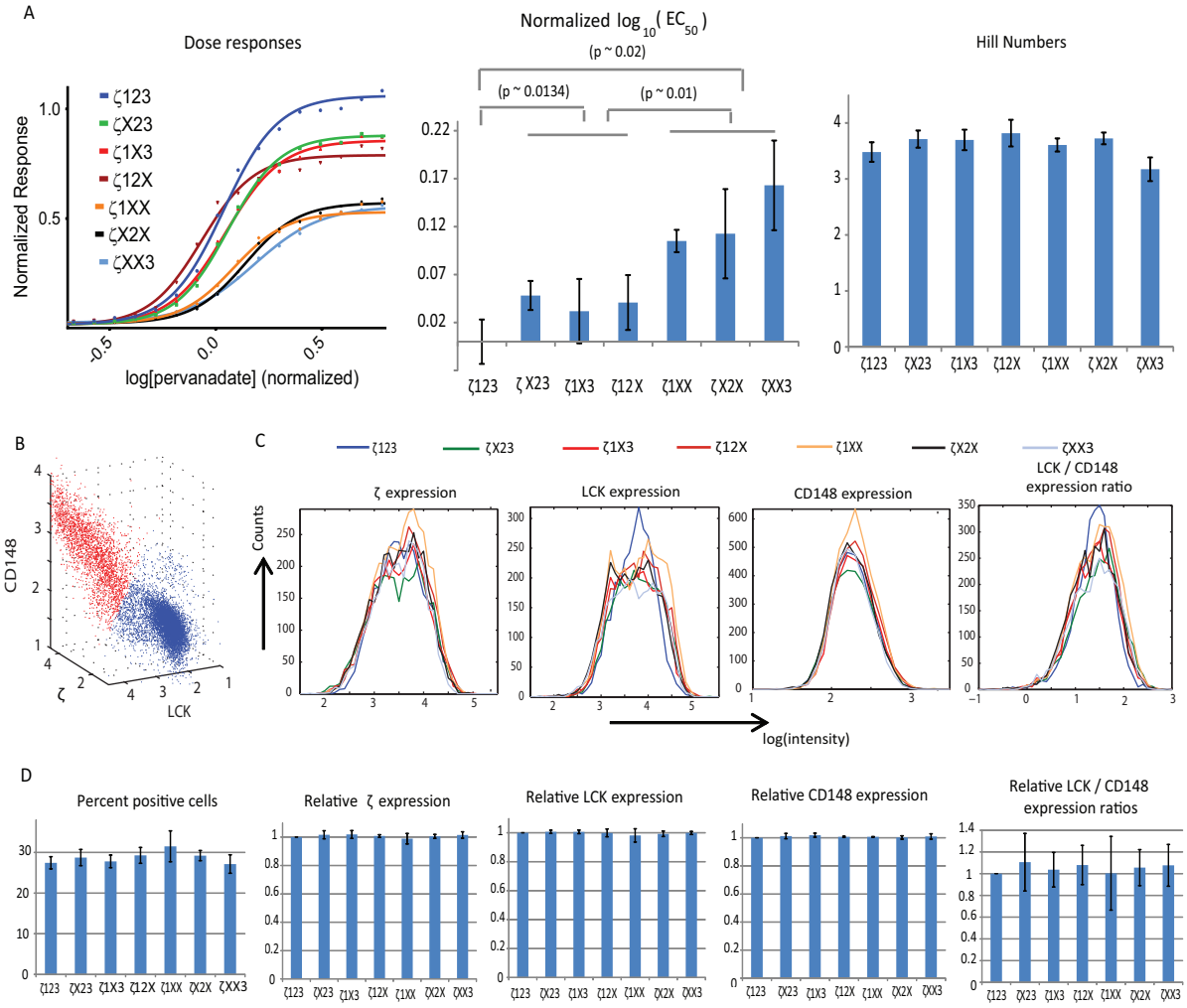

Fig 4.5: **The direct correlation between the number of TCR ζ-chain ITAMs and response potency is independent of the SH2 domain of LCK.** HEK cells were reconstituted to express LCKΔSH2 (denoted LCK in this figure), CD148 and the TCR ζ-chain variants. Reconstituted cells were treated with increasing concentrations of pervanadate, and ζ-chain phosphorylation corresponding to each pervanadate dose was quantified. Dose-responses were fit to logarithmic Hill functions. (A) Representative dose-response profiles, normalized EC_{50}s (log_{10} scale) and Hill numbers. Metrics were averaged across four independent experiments, and are presented as mean ± sem. (B-C) Representative expression profiles of molecules from one experiment. (B) Three-component stain of LCK, CD148 and TCR ζ. Cells were classified as expressing all molecules (red dots), or not expressing any molecule (blue dots) with k-means clustering algorithm in MATLAB. (C) Molecular expression histograms of ζ-chain variants, LCK, CD148 and the LCK/CD148 expression ratio for all the ITAM mutant signalling modules reconstituted. (D) Averaged expression levels across all experiments of proportion of cells expressing molecules, and relative expression levels of ζ-chain variants, LCK, CD148 and LCK/CD148 expression ratios. Data are presented as mean ± sem across four independent experiments.

ZAP-70 further enhances the potency of TCR ζ phosphorylation

Mathematical modelling in the previous chapter predicted that the recruitment of ZAP-70 to phosphorylated ITAMs enhances the potency and sensitivity of TCR ζ phosphorylation. It is also predicted that the enhancement in sensitivity relies on the sequential phosphorylation of TCR ζ ITAMs, and ZAP-70 binding affinities increasing in the direction of phosphorylation. We sought to evaluate these model predictions, and thus we transfected HEK cells to express LCK, CD148, ZAP-70 and the TCR ζ-chain variants. We treated reconstituted cells with varying concentrations of pervanadate, and we quantified total TCR ζ phosphorylation corresponding to each treatment dose.

It was necessary to control for the inclusion of an additional protein in the transfection protocol. Thus we created a ZAP-70 molecule that contained point mutations that are predicted to disrupt the functions of the SH2 domains (R37K and R190K) and the catalytic domain (K368A), and we refer to this molecule as ZAP-70ΔSH2ΔCAT (Fig 4.1E). We first compared the dose-response profiles of (i) wild type TCR ζ without ZAP-70, (ii) wild type TCR ζ with ZAP-70ΔSH2ΔCAT, and (iii) wild type TCR ζ with wild type ZAP-70 (Fig 4.6).

The inclusion of ZAP-70ΔSH2ΔCAT resulted in small changes in the potency and sensitivity of TCR ζ phosphorylation (Fig 4.6A). The reason for this is unclear but it may be the result of the change in the transfection conditions and/or inclusion of an additional protein. Thus we use the dose-response profile of ZAP-70ΔSH2ΔCAT to represent the system without ZAP-70, and we evaluate the effects of wild type ZAP-70 with respect to the ZAP-70ΔSH2ΔCAT curve.

Wild type ZAP-70 enhances the potency of TCR ζ phosphorylation, but does not change the sensitivity of the dose-response profile (Fig 4.6A). Similar to our previous sets of experiments, we verified similar expression levels of all molecules with the different forms of ZAP-70 reconstituted (Fig 4.6B,C).

We subsequently sought to elucidate the effects of ZAP-70 in the context of multisite phosphorylation. Thus we reconstituted HEK cells to express LCK, CD148, ZAP-70 and the different ζ-chain variants. We pursued the same experimental strategy of treating cells with pervanadate and quantifying total ζ-chain phosphorylation. We present the results from this set of experiments in Fig 4.7.

ZAP-70 increases the potency of all the TCR ζ-chain variants in comparison to reconstitution without ZAP-70 (not shown). However ZAP-70 reconstitution maintains a similar difference in potency between the ITAM mutants (Fig 4.7A). Thus the direct correlation between the number of ITAMs and the potency of phosphorylation is observed with and without ZAP-70. We did not observe any significant differences in the Hill numbers between the ζ-chain variants (Fig 4.7A).

Finally, we verified similar relative expression levels of all molecules across all signalling modules reconstituted with ZAP-70. (Fig 4.7B,C). Thus we conclude that the differences in TCR ζ phosphorylation profiles that we observe are not due to differential expression of molecules.

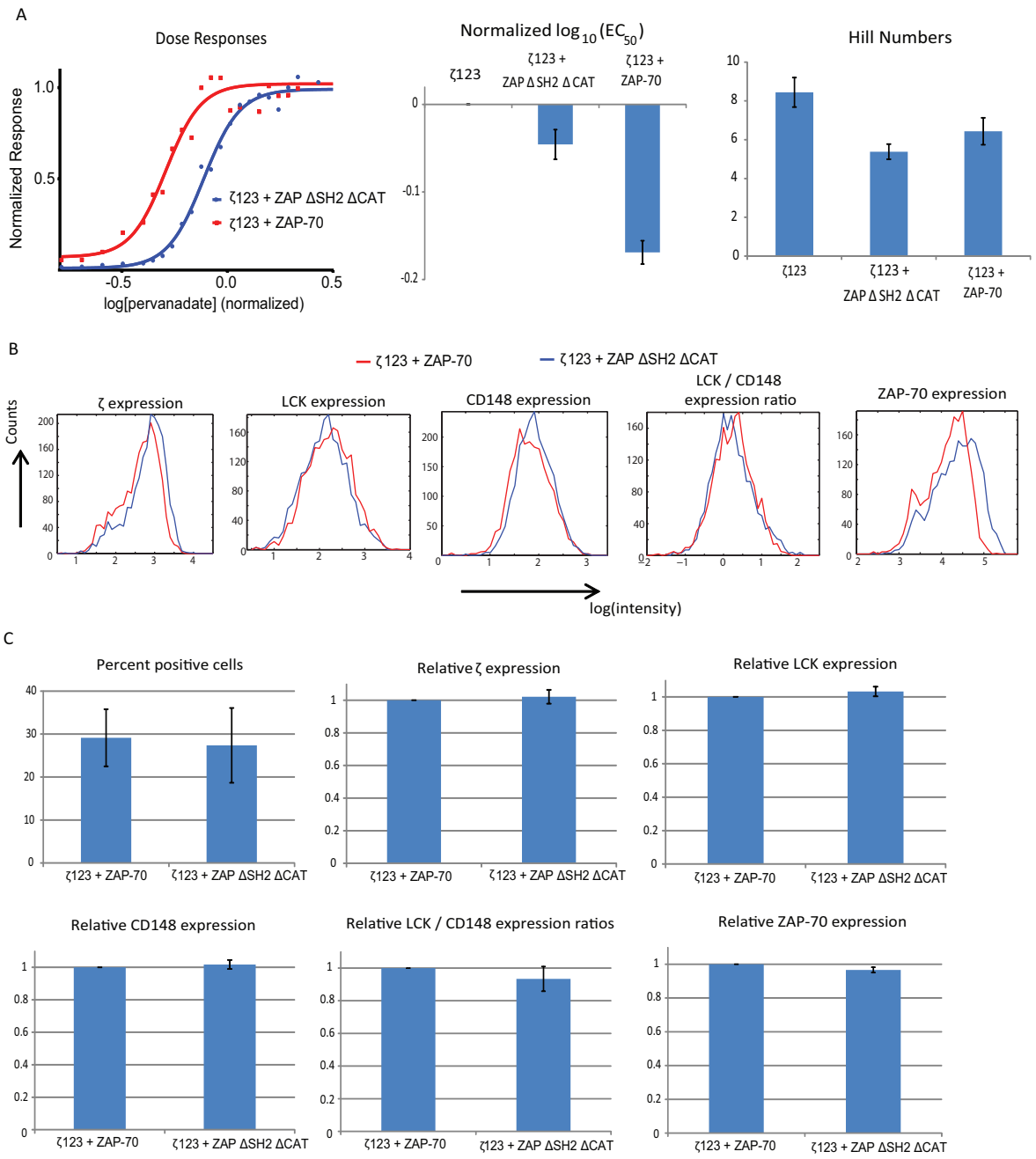

Fig 4.6: **ZAP-70 enhances the potency of TCR ζ phosphorylation.** HEK cells were reconstituted to express LCK, CD148, the wild type TCR ζ-chain and either wild type ZAP-70 or ZAP-70ΔSH2ΔCAT. Reconstituted cells were treated with increasing concentrations of pervanadate, and ζ-chain phosphorylation corresponding to each pervanadate dose was quantified. Dose-responses were fit to logarithmic Hill functions. (A) Representative dose-response profiles, normalized EC_{50}s (log_{10} scale) and Hill numbers. Metrics were averaged across five independent experiments, and are presented as mean ± sem. (B-C) Molecular expression profiles of cells classified as expressing all molecules with k-means clustering algorithm. (B) Expression histograms of ζ-chain, LCK, CD148, the LCK/CD148 expression ratio and ZAP-70 variants. (C) Averaged expression levels across all experiments of proportion of cells expressing molecules, and the relative expression levels of wild type TCR ζ-chain, LCK, CD148 the LCK/CD148 expression ratio and ZAP-70 variants. Data are presented as mean ± sem across five independent experiments.

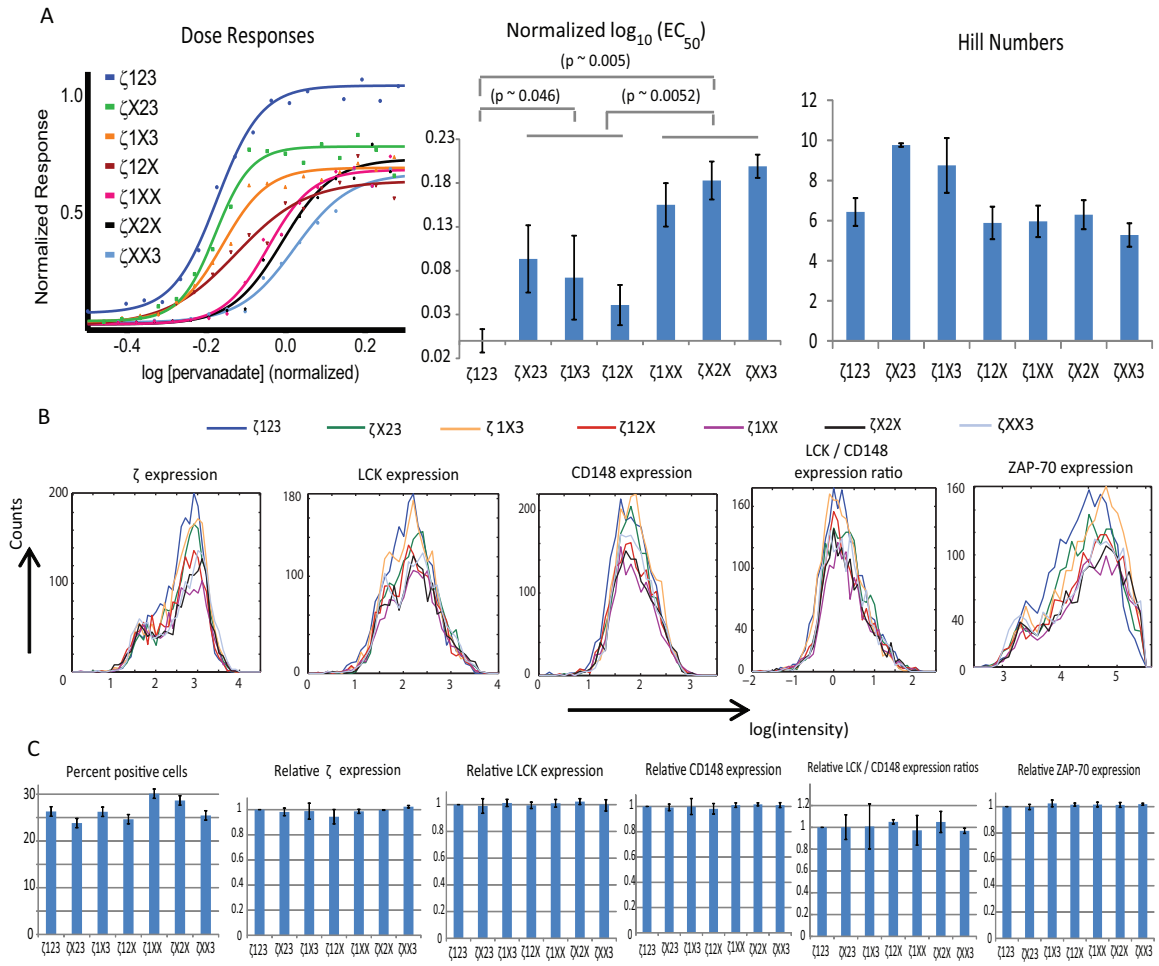

Fig 4.7: **The direct correlation between the number of TCR ζ-chain ITAMs and potency of receptor phosphorylation persists in the presence of ZAP-70.** HEK cells were reconstituted to express LCK, CD148, ZAP-70 and the different TCR ζ-chain variants. Reconstituted cells were treated with increasing concentrations of pervanadate, and ζ-chain phosphorylation corresponding to each pervanadate dose was quantified. Dose-responses were fit to logarithmic Hill functions. (A) Representative dose-response profiles, normalized EC_{50}s (log_{10} scale) and Hill numbers. Metrics were averaged across three independent experiments, and are presented as mean ± sem. (B-C) Molecular expression profiles of cells classified as expressing all molecules with k-means clustering algorithm. (B) Expression histograms of the TCR ζ-chain variants, LCK, CD148, the LCK/CD148 expression ratio and ZAP-70. (C) Averaged expression levels across all experiments of proportion of cells expressing molecules, and the relative expression levels of TCR ζ-chain variants, LCK, CD148 the LCK/CD148 expression ratio and ZAP-70. Data are presented as mean ± sem three five independent experiments.

Trends in dose-response profiles are not due to differential expression levels of molecules

We also performed general analyses across our datasets whereby we compared (i) the maxima of our dose-response profiles to the expression levels of the ζ-chain variants (Fig 4.8A) and (ii) the relative expression levels of LCK and CD148 versus the EC_{50}s of our dose-response profiles (Fig 4.8B). In both cases we did not find any significant correlation between expression levels and dose-response metrics, thus further suggesting that the changes we observe are not due to differential expression levels of molecules.

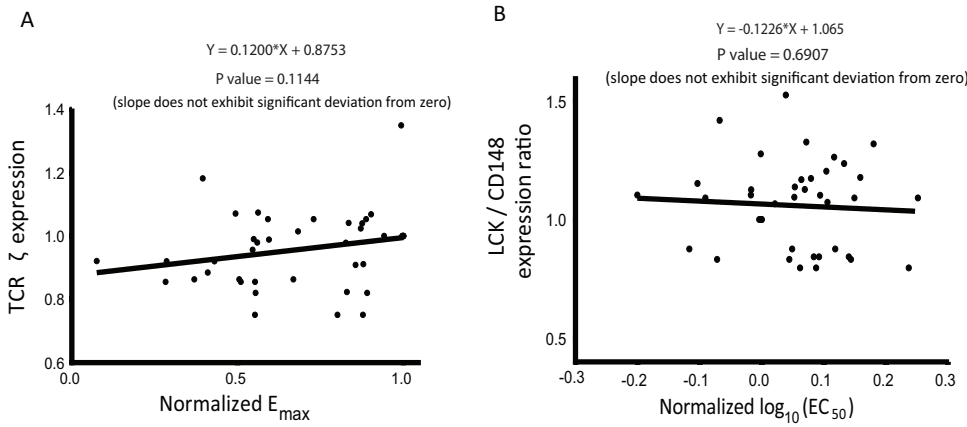

Fig 4.8: **Changes in the functional characteristics of dose-response profiles are not due to differential expression levels of molecules.** Expression profiles of the TCR ζ-chain variants, LCK and CD148 were quantified with flow cytometry. The normalized Emax and EC_{50}s were obtained from the dose-response profiles of TCR ζ phosphorylation. (A) Normalized Emax of dose-response profiles versus normalized fluorescence levels of ζ-chain expression across all experiments. (B) Normalized EC_{50} of dose-responses versus LCK/CD148 fluorescence ratio across all experiments.

Protein expression levels

One possible explanation for the high level of sensitivity observed in our experiments is that the enzymes LCK and CD148 are at much lower concentrations than the TCR ζ-chain, which can result in zero-order ultrasensitivity. In order to investigate this possibility we sought to quantify the absolute numbers of LCK, CD148 and TCR ζ molecules expressed in our reconstitution system. We reasoned that as long as TCR ζ expression does not vastly exceed the expression levels of the modifying enzymes, response profiles will not be impacted by concentration-dependent effects.

We used commercial beads calibrated with defined numbers of anti-IgG molecules, and we incubated our flow cytometry detection antibodies with these beads. In this manner we were able to relate fluorescence levels with numbers of molecules for the TCR ζ-chain (Fig 4.9A), CD148 (Fig 4.9B) and LCK (Fig 4.9C). We detected approximately a million molecules of LCK, CD148 and TCR ζ per cell, with slightly more CD148 and LCK than TCR ζ. These results show that our experiments were not performed in the zero-order regime.

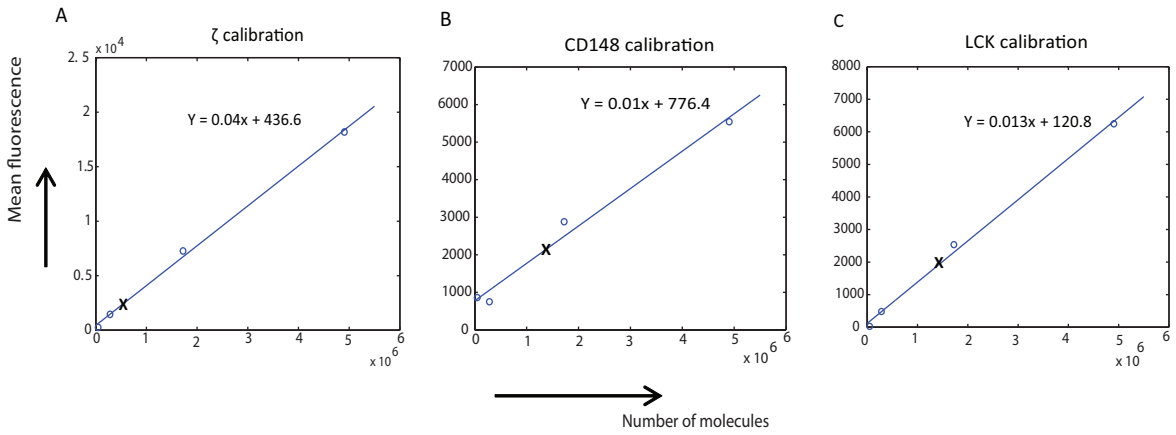

Fig 4.9: **Relating fluorescence levels in flow cytometry with exact numbers of molecules expressed.** Flow cytometry detection antibodies were incubated with beads coated with anti-IgG molecules, and fluorescence levels were related to numbers of molecules. (A-C) Relationships of mean fluorescence levels versus numbers of molecules for (A) TCR ζ, (B) CD148 and (C) LCK. X denotes mean fluorescence levels of reconstituted cells.

Titration of expression levels

The functional properties of signalling networks are often dependent on the relative concentration of molecules. Thus we examined to what extent it is possible to experimentally vary the LCK and/or CD148 concentrations in our system.

Our transfection procedure without ZAP-70 used 24 μg/ml of plasmid DNA, with 8 μg each of LCK, CD148 and ζ-chain. We varied the relative amounts of LCK and CD148 as follows: (i) LCK: 14 μg, CD148: 2 μg; (ii) LCK: 11 μg, CD148: 5 μg; (iii) LCK: 8 μg, CD148: 8 μg; (iv) LCK: 5 μg, CD148: 11 μg and (v) LCK: 2 μg, CD148: 14 μg. We determined the relative expression levels through flow cytometry, and we present the results of this experiment in Fig 4.10.

There were no large differences in the proportion of cells that expressed all components across the different transfection regimes (Fig 4.10A: percent positive cells). However varying the relative transfection amounts changed the relative amounts of LCK and CD148 expressed (Fig 4.10B,C). We note that the expression of each modifying enzyme was demarcated into a relatively high and low regime, corresponding to the amount of plasmid transfected (Fig 4.10C: LCK and CD148 expression panels).

The ratio of LCK/CD148 expression levels followed a graded pattern, and coincided with the relative amounts of plasmid transfected (Fig 4.10C: normalized LCK/CD148 expression ratios). Finally, as was expected, we did not observe any differences in the amount of TCR ζ expression. These results collectively suggest that relative cellular expression levels of molecules are adjustable, and that relative expression levels may be systematically varied by altering the transfection procedure.

We pursued these molecular titration experiments to validate our cellular reconstitution procedure. We did not pursue these experiments further due to our finding that the correlation between the number of

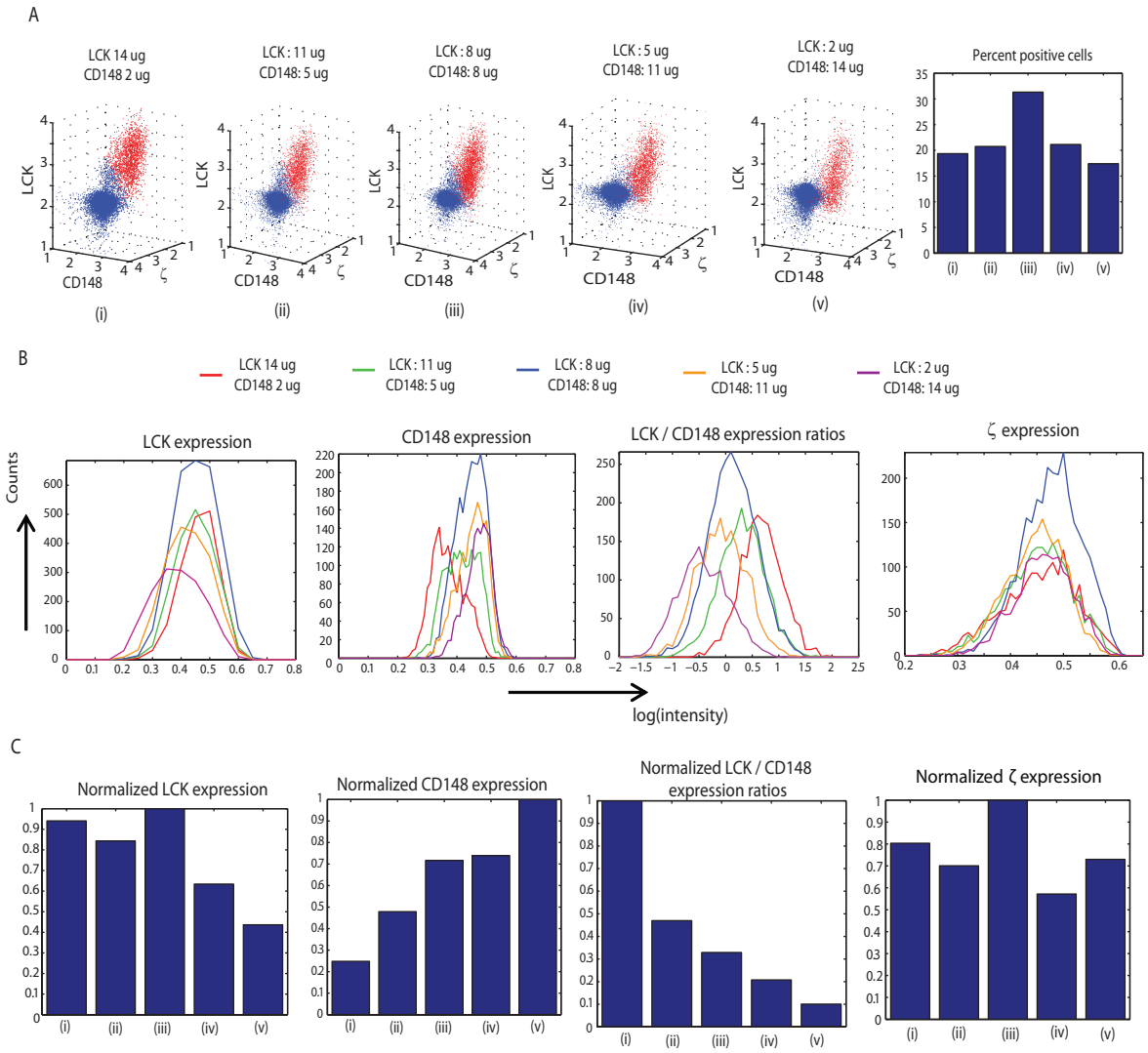

Fig 4.10: **Varying the relative expression levels of LCK and CD148 by titrating transfection amounts.** HEK cells were transfected with LCK, CD148 and the TCR ζ-chain. The procedure altered the relative amounts of LCK and CD148 transfected. (A) Three-component stains of LCK, CD148 and TCR ζ and proportion of expressing cells. Relative transfection amounts of modifying enzymes: (i) LCK: 14 μg, CD148: 2 μg; (ii) LCK: 11 μg, CD148: 5 μg; (iii) LCK: 8 μg, CD148: 8 μg; (iv) LCK: 5 μg, CD148: 11 μg; (v) LCK: 2 μg, CD148: 14 μg; (vi) percent positive cells in each transfection regime. (B) Expression histograms of LCK, CD148, the LCK/CD148 ratio and TCR ζ-chain for transfection regimes shown in part (A). (C) Quantification of relative expression levels for each transfection regime in panel (A) for LCK, CD148, the LCK/CD148 ratio and TCR ζ-chain.

ITAMs and the potency of phosphorylation is an intrinsic property of the ζ-chain. We note that a possible direction of further research would be to replicate our main results in this chapter under different kinase-to-phosphatase transfection regimes.

Discussion

Mathematical modelling of TCR proximal signalling (Chapter 3) predicted that multiple TCR ζ ITAMs enhance the potency and sensitivity of receptor phosphorylation. This enhancement depends on a sequential mechanism of ITAM modification, and ZAP-70 binding affinities increasing in the direction of phosphorylation. We sought to investigate the validity of our model predictions through experimental studies of TCR proximal signalling.

Our data suggest that multiple ITAMs enhance the potency of TCR ζ phosphorylation, but do not alter the sensitivity of response profiles. The correlation between the number of ITAMs and response potency is observed both in the presence and absence of ZAP-70. The introduction of ZAP-70 enhances the potency of all ITAM variants by roughly equal amounts, while not altering the sensitivities. Thus the assumptions and predictions from our mathematical modelling must be refined, and we consider these in turn.

TCR ζ modification does not follow a sequential mechanism

The emergent ultrasensitivity that our mathematical modelling predicted relied on a sequential mechanism of ζ-chain phosphorylation. We assumed that modifications proceed from the membrane-distal to the membrane-proximal ITAM ((10), (8)), and we note that alternative sequences have also been previously reported (64).

Our finding that all three single ITAM mutants have similar levels of phosphorylation is inconsistent with a strictly sequential mechanism of phosphorylation. One possible explanation to reconcile our data with previous observations is that there exists a dominant structure of phosphorylation, however modifications are not strictly sequential. Thus if a preceding ITAM in the purported sequence is mutated, modifications can still proceed. We also note that our experiments were performed in reconstituted HEK cells, while reports of structured schemes of TCR ζ modification were reported in T cells.

Potency does not correlate with reported ZAP-70 ITAM binding affinities

An additional assumption of our systems model was that ZAP-70 binds phosphorylated ITAMs with differential binding affinities. In accordance with previously published reports, we assumed affinities to increase in the direction of phosphorylation, from the membrane-distal to membrane-proximal ITAMs ((55), (56), (57), (58)).

We do not find significant differences in potency with different functional individual ITAMs, and we observe roughly equal enhancements in potency of all ITAM variants in the presence of ZAP-70. This is in agreement with unpublished data from our laboratory, where surface plasmon resonance experiments of ZAP-70 to individual TCR ζ ITAMs were performed at 37°C, and no significant differences in binding affinities were detected (not shown). Thus we conclude that while ZAP70 binding to all ITAMs enhances the potency of TCR proximal signaling, differential binding does not contribute to sensitivity.

Multiple ITAMs enhance the potency of TCR ζ phosphorylation

Reconstitution of the TCR ζ variants, LCK and CD148 revealed that multiple ITAMs enhance the potency (decrease the EC_{50}) of ζ-chain phosphorylation. This enhancement was directly correlated with the number of ITAMs, such that the wild type ζ-chain exhibited the most potent response, the single ITAM mutants displayed intermediate potencies, and the double mutants had the least potent response. The single mutants displayed similar potencies as a group, and the same held true for the double mutants. Such a correlation between the number of phosphorylation sites and response potency was independent of the SH2 domain of LCK, which is in agreement with data from in vitro reconstitution of TCR proximal signalling (73).

Reconstitution of the TCR ζ variants with LCK, CD148 and ZAP-70 revealed that ZAP-70 enhances the response potency for all TCR ζ mutants. However ZAP-70 reconstitution maintained a similar difference between the ITAM mutants. Thus the direct correlation between the number of ITAMs and response potency exists with and without ZAP-70.

Multiple ITAMs do not enhance the sensitivity of TCR ζ phosphorylation

We found similar sensitivities of phosphorylation for all our TCR ζ variants, both in the presence and absence of ZAP-70. Also we did not observe any change in sensitivity upon the introduction of ZAP-70 in our reconstitution system. Thus we conclude that multiple ITAMs do not enhance the sensitivity of TCR proximal signalling. The observation that ZAP-70 does not alter the sensitivity of response profiles is in agreement with results from in vitro reconstitution of TCR proximal signalling (73).

Numbers of molecules and titration of molecular amounts

We quantified the numbers of molecules expressed in our reconstitution system, and we detected approximately a million molecules of LCK, CD148 and TCR ζ. This suggests that our experiments were not performed in the zero-order regime of enzyme saturation. We also showed that the relative amounts of molecular expression can be adjusted by altering the transfection protocol.

Reconciling experimental data with mathematical models of TCR proximal signalling

Cellular reconstitution of TCR proximal signalling has revealed that we must refine our mathematical models. Our revised models must assume an unstructured random mechanism of TCR ζ phosphorylation and explain (i) the direct relation between the number of phosphorylation sites and the potency of phosphorylation and (ii) the similar sensitivities of phosphorylation regardless of the number of ITAMs.

Based on the correlation between the number of ITAMs and response potency we hypothesize that the efficiencies of enzymatic modification are modulated by the phosphorylation state of the TCR ζ-chain. In the subsequent chapter we consider how this hypothesis may be incorporated within a minimal model of multisite phosphorylation.

Chapter 5

Reconciling mathematical frameworks with experimental data: A phosphorylation-dependent modulation of enzymatic efficiencies is sufficient to explain the enhanced potency of TCR ζ phosphorylation

Introduction

Mathematical models of natural phenomena encapsulate relations between variables and processes. Such theoretical frameworks provide a language to articulate the relationships that underlie a system, and thus enable us to gain insights into the design principles that are inherent in nature. The realm of possiblities that constitute the theoretical design space is vast and infinite, and biological processes represent a specific realization of this design space. In this chapter we aim to reconcile mathematical models of T cell receptor (TCR) proximal signalling with our experimental results.

Mathematical modelling of TCR proximal signalling (Chapter 3) suggested the conditions that elicit ultrasensitive responses of receptor phosphorylation. These included a sequential mechanism of TCR ζ ITAM phosphorylation, coupled to the binding of ZAP-70 to phosphorylated ITAMs with affinities increasing in the direction of phosphorylation. We predicted that under such a design architecture, multiple ITAMs would enhance the potency and sensitivity of TCR ζ phosphorylation. We complemented these theoretical studies with experimental investigations of TCR proximal signalling.

Cellular reconstitution of TCR proximal signalling (Chapter 4) revealed that our original model assumptions must be revised and refined. Indeed, our data suggest that TCR ζ phosphorylation does not follow any defined sequence, and ZAP-70 does not bind different ITAMs with very different affinities. Our results suggest instead that multiple ITAMs enhance the potency of TCR ζ phosphorylation, and this enhancement is

an intrinsic property of the TCR ζ-chain. Contrary to our original predictions, we do not find any difference in the sensitivity of receptor phosphorylation with increasing numbers of ITAMs. In this chapter we aim to refine our original models of TCR proximal signalling to explain our experimental results.

Our data reveal a direct correlation between the number of ITAMs and the potency of TCR ζ phosphorylation. Thus the wild type ζ-chain exhibits the most potent response, followed by the single ITAM mutants, and the double ITAM mutants display the least potent response. Moreover we did not find any significant differences in potency between the single ITAM mutants, nor between the double ITAM mutants. However the juxtaposition of the three ITAMs into the wild type configuration gives rise to a cooperative effect of TCR ζ phosphorylation.

These findings led us to hypothesize that the phosphorylation state of the TCR ζ-chain modulates the efficiencies of enzymatic modification. Since we observe an increase in response potency with increasing numbers of ITAMs, we posit that phosphorylation enhances the efficiency of subsequent modifications.

There exist several possible molecular mechanisms that could mediate such a phosphorylation-dependent enhancement. The first involves the presence of clusters of positive charge between ITAMs, referred to as basic residue rich (BRR) motifs (8). These positively charged residues have been shown to mediate an association of the TCR ζ-chain with the cell membrane. Such membrane association could sequester ITAMs, and thus prevent enzymatic modifications. Triggering of the TCR abrogates this membrane association, and possibly exposes ITAMs for enzymatic modification. Thus an initial phosphorylation reaction would enhance the efficacy of subsequent modifications.

The second possible mechanism is based on changes in molecular entropy, and the functional consequences of intrinsically disordered regions in cellular signal transduction ((78), (79)). The cytoplasmic domain of the TCR ζ chain exhibits intrinsic disorder, in that it does not adopt a defined three-dimensional configuration (72). We hypothesize that ITAM phosphorylation mediates a transition from disorder to a more defined three-dimensional configuration, thus reducing the entropy of the TCR ζ-chain. This reduction in entropy would enhance the efficiency of subsequent enzymatic modifications, thus eliciting the trends we observe.

We envisage that the tuning of molecular entropy by multisite phosphorylation is a widespread mechanism in cellular signal transduction (78). The tuning of molecular entropy by multisite phosphorylation was recently proposed in the context of neuronal translation initiation (80). Cooperative interactions between phosphorylation sites within disordered regions has also been observed in the actin-binding protein ACTN4 (81).

We begin this chapter by revisiting canonical models of multisite phosphorylation, and we derive the key parameters that give rise to the steady-state properties of such modification systems. We subsequently consider how these parameters must be varied in order to explain our experimental results. Our analysis suggests that a phosphorylation-dependent enhancement of enzymatic efficiencies gives rise to the enhanced

potency of TCR ζ phosphorylation. We conclude the chapter with a discussion of the design principles of TCR proximal signalling that have been revealed through mathematical modelling and experimentation.

Steady state properties of multisite phosphorylation and the efficiency of enzymatic modifications

Our experimental results revealed that multiple ITAMs enhance the potency of TCR ζ phosphorylation. This enhancement was observed both in the presence and absence of ZAP-70. Thus we revisit our theoretical frameworks of multisite phosphorylation, and consider how our mathematical models should be refined to explain our experimental data.

Phosphorylation of the TCR ζ-chain is regulated according to the following modification scheme (Fig 5.1A):

$$\begin{aligned} E + S_j &\underset{ek_{\text{off}}}{\overset{ek_{\text{on}}}{\rightleftharpoons}} ES_j \overset{ek_{\text{cat}}}{\rightarrow} E + S_{j+1} \\ F + S_{j+1} &\underset{fk_{\text{off}}}{\overset{fk_{\text{on}}}{\rightleftharpoons}} FS_{j+1} \overset{fk_{\text{cat}}}{\rightarrow} F + S_j \end{aligned} \tag{5.1}$$

where E denotes the concentration of the kinase LCK, and F represents the concentration of the phosphatase CD148. The ζ-chain corresponds to the substrate, and is represented as S. The subscript j is the number of phosphorylated sites, and the substrate has a total of $N = 6$ sites. The parameters ek_{on} and fk_{on} denote rates of binding for the kinase and phosphatase, respectively. Similarly ek_{off} and fk_{off} are off-rates of dissociation for LCK and CD148, respectively. Finally, ek_{cat} is the rate constant of kinase-mediated phosphorylation, while fk_{cat} denotes the rate of phosphatase-mediated catalysis. For simplicity we set the rate constants of modification to be the same for the kinase and phosphatase. Also, we assume that individual sites are modified with equal on-, off-, and catalytic rates.

All our experimental dose-response profiles in Chapter 4 exhibited non-zero maxima, and thus we concluded that ζ-chain phosphorylation follows a random unstructured mechanism. Thus we attribute a random mechanism of substrate phosphorylation to model 5.1. We assume mass action kinetics and derive a system of ordinary differential equations to describe the time evolution of each chemical species in the system. For the substrate species we have:

$$\frac{d[S_j]}{dt} = k_{off}[ES_j] - k_{on}[E][S_j] + k_{cat}[FS_{j+1}] \tag{5.2}$$

$$\frac{d[S_{j+1}]}{dt} = k_{off}[FS_{j+1}] - k_{on}[F][S_{j+1}] + k_{cat}[ES_j] \tag{5.3}$$

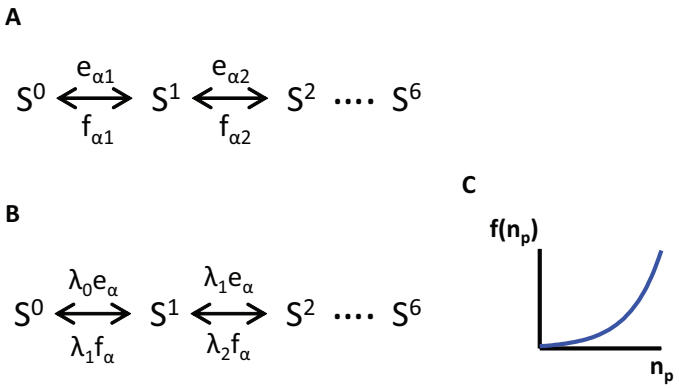

Fig 5.1: **Generic frameworks of multisite phosphorylation.** (A) Phosphorylation of a substrate with six sites from the fully dephosphorylated state S^0 to the fully phosphorylated state S^6. Each state shown is a combination of all states with the relevant number of phosphorylated sites. The steady state properties of such a system are defined by the relative efficiencies of enzymatic modification α. The efficiency of the kinase is denoted as e_α while that of the phosphatase is f_α. (B) Enzymatic efficiencies are modulated by the phosphorylation state of the substrate, and the weighting factor is denoted as λ_j, where j corresponds to the number of phosphorylated sites. (C) The algebraic form of the enhancement factor versus the phosphorylation state of the substrate, n_p.

and for the complex species we have:

$$\frac{d[ES_j]}{dt} = k_{on}[E][S_j] - (k_{off} + k_{cat})[ES_j] \tag{5.4}$$

$$\frac{d[FS_{j+1}]}{dt} = k_{on}[F][S_{j+1}] - (k_{off} + k_{cat})[FS_{j+1}] \tag{5.5}$$

Upon solving these equations at steady state, we obtain the following relations:

$$k_{cat}[FS_{j+1}] = k_{cat}[ES_j] \tag{5.6}$$

$$[ES_j] = \frac{[E][S_j]}{K_m} \tag{5.7}$$

$$[FS_{j+1}] = \frac{[F][S_{j+1}]}{K_m} \tag{5.8}$$

where $K_m = \frac{k_{off}+k_{cat}}{k_{on}}$ refers to the Michaelis-Menten constant. Therefore, the steady state properties of multisite phosphorylation are determined by the rate of catalysis and the Michaelis-Menten constant of enzymatic modification. We define a new parameter α as:

$$\alpha = \frac{k_{cat}}{K_m} \tag{5.9}$$

and we refer to α as the efficiency of enzymatic modification.

We aim to derive the simplest mathematical model that can explain our experimental results. Thus our first approach will be to vary α in isolation, and to obtain steady state dose-response profiles of TCR ζ phosphorylation. We shall compute the potency and sensitivity of these response profiles, and compare these metrics to our experimental data.

Varying the efficiency of enzymatic modifications alone is not sufficient to explain experimental results

In the previous section we derived the key parameter that defines the steady state properties of multisite phosphorylation, and we defined it as α (equation 5.9), or the ratio between the rate of enzyme catalysis and the Michaelis-Menten constant. We aim to understand how dose-response profiles of substrate phosphorylation change as α and the number of modification sites are varied. Thus in Fig 5.2 we vary α and compute dose-response characteristics for a substrate with different numbers of modification sites. We change the number of substrate phosphorylation sites in a manner that resembles the different TCR ζ ITAMs that we reconstituted, such that the substrate has six sites (wild type), four sites (single ITAM mutants) and two sites (double ITAM mutants). For each of these cases we depict the normalized maxima (Fig 5.2A) and minima (Fig 5.2B), as well as the potencies (Fig 5.2C) and sensitivities (Fig 5.2D) of phosphorylation.

ITAM mutations result in reductions in the maximal level of phosphorylation (Fig 5.2A), but do not impact the response minima (Fig 5.2B). However, beyond a certain threshold value of α, the E_{min} becomes greater than zero. The non-zero minima are due to the large binding affinity of the phosphatase, relative to the catalytic rate. Under such a parameter regime, the phosphatase binds a phosphorylated site, but does not mediate dephosphorylation. Similarly, at large values of α, we observe a decrease in the maxima. This occurs due to the kinase binding a dephosphorylated site, but failing to mediate phosphorylation due to the high affinity binding interaction.

In all our experiments, we did not detect any ζ-chain phosphorylation at zero pervanadate treatment concentration. Thus we constrain α such that it is less than the threshold value that elicits non-zero E_{mins}s, and from Fig 5.2B we constrain $\alpha \leq 1 * 10^{-3}$molecules^{-1}s^{-1}.

Given this maximum threshold constraint on α, we evaluate the potencies (Fig 5.2C) and sensitivities (Fig 5.2D) of phosphorylation for the different ITAM variants. The potencies and sensitivities of phosphorylation are the same for the ITAM variants within the allowed range of α (ie $\alpha \leq 1 * 10^{-3}$). This is in contrast to our experimental results, where response potencies are correlated to the number of ITAMs. Thus we conclude that varying the efficiency of enzymatic modifications, α, is not sufficient to explain our experimental results.

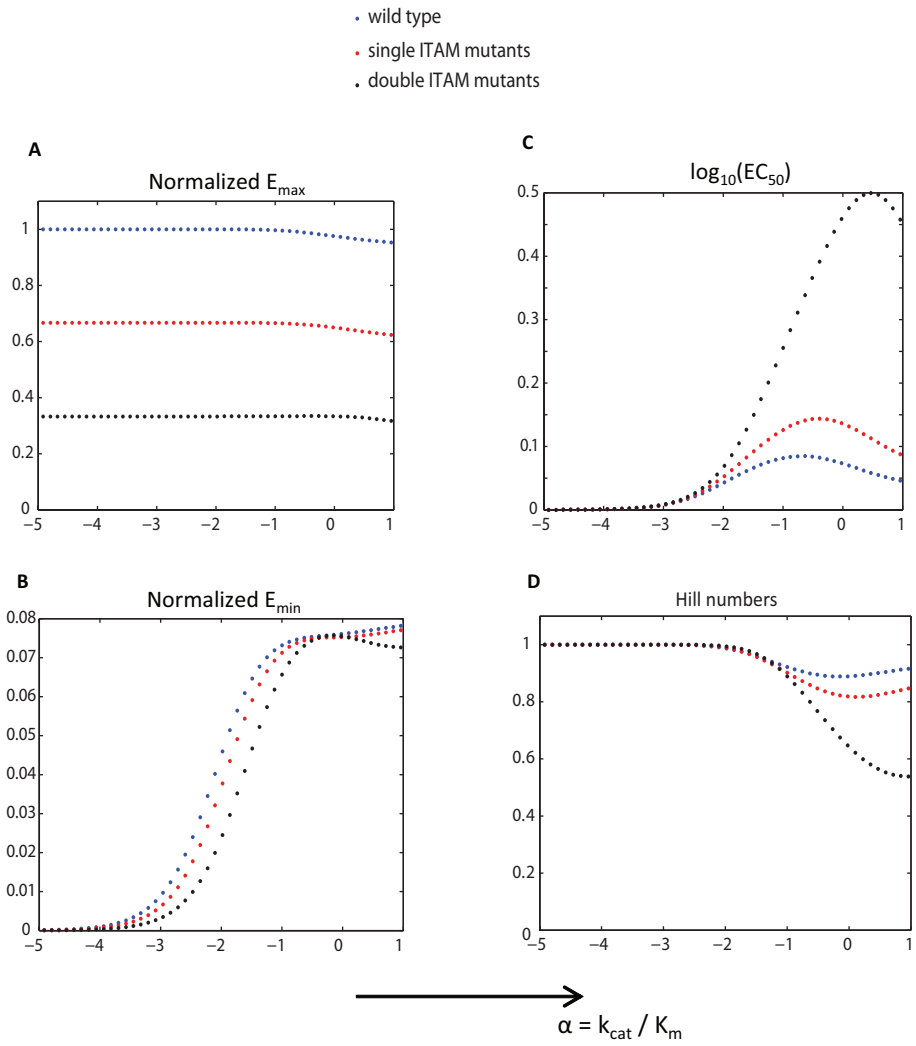

Fig 5.2: **Varying the efficiency of enzymatic modifications, α, is not sufficient to explain the experimental results.** The efficiency of enzymatic modifications, α, is varied on the x-axis, and dose-response profiles are evaluated for the wild type, single ITAM mutant and double ITAM mutant ζ-chains. Dose response metrics are computed for each value of α and presented as: (A) maxima and (B) minima normalized to wild type. A threshold minimum of 0.01 is implemented to constrain $\alpha \leq 1 * 10^{-3}$. (C) Response potencies presented as EC_{50}s ($\log_{10}$ scale) and (D) response sensitivities presented as Hill numbers.

A phosphorylation-dependent enhancement of enzymatic efficiencies is sufficient to explain experimental results

The correlation between response potency and the number of ITAMs led us to hypothesize that the efficiencies of enzymatic modification are regulated by the phosphorylation state of the TCR ζ-chain. The cytoplasmic domain of the TCR ζ-chain is intrinsically disordered (72), and there is an entropic penalty associated with a catalytic domain binding a disordered protein. This is because binding reduces the number of conformations that the disordered protein is capable of exploring, thus reducing molecular entropy. Phos-

phorylation has been posited to reduce molecular entropy (82), which decreases the entropic penalty when the catalytic domain binds. We model such an entropic mechanism by implementing a phosphorylation-dependent enhancement of enzymatic efficiencies.

Under such a framework, the efficiency of enzymatic modification, α, is weighted by an enhancement factor that we refer to as λ, and the magnitude of λ depends on the phosphorylation state of the ζ-chain (Fig 5.1B). In this section we show that such a phosphorylation-dependent enhancement of enzymatic efficiencies is sufficient to explain our experimental results.

The algebraic form of the phosphorylation-dependent enhancement

The direct correlation between response potency and the number of ITAMs suggests that the modulation factor, λ, increases with the phosphorylation state of the TCR ζ-chain. The simplest algebraic implementation of λ is to attribute equal enhancements in the efficiency of enzymatic modifications between substrate phosphoforms (Fig 5.1B), thus yielding the relations:

$$\frac{\lambda_1}{\lambda_0} = \frac{\lambda_2}{\lambda_1} = \frac{\lambda_3}{\lambda_2} ... = \frac{\lambda_N}{\lambda_{N-1}} \tag{5.10}$$

where the subscript i in λ_i indicates the number of sites that the substrate is phosphorylated on, and we set $\lambda_0 = 1$ and $\lambda = \lambda_1$. Thus we have:

$$f(n_p) = \lambda^{n_p} \tag{5.11}$$

where n_p corresponds to the number of phosphorylated sites, and $f(n_p)$ is the factor by which the efficiency of enzymatic modifications, α, is weighted (Fig 5.1C).

Dose-response profiles as a function of enzymatic efficiencies and phosphorylation-dependent modulation

In the previous sections we defined two key parameters. The first is the efficiency of enzymatic modifications (equation 5.9), α, which determines steady-state profiles of substrate phosphorylation. The second is a modulation factor, λ, which is scaled by the phosphorylation state of the substrate according to equation 5.11. In this section we evaluate dose-response profiles as functions of α and λ, and compute response potencies and sensitivities as the number of phosphorylation sites is varied.

In Fig 5.3 we depict heat maps of the EC_{50}s and Hill numbers as functions of α and λ as the number of phosphorylation sites is varied. The wild type substrate models the wild type ζ-chain with six phosphorylation sites, the single ITAM mutants correspond to four modification sites, and the double ITAM mutants are comprised of two sites. We note a certain threshold regime in α-λ space beyond which response profiles becomes less potent (ie EC_{50}s increase). The threshold region occurs at greater α values as the number of ITAMs is decreased (Fig 5.3A-C).

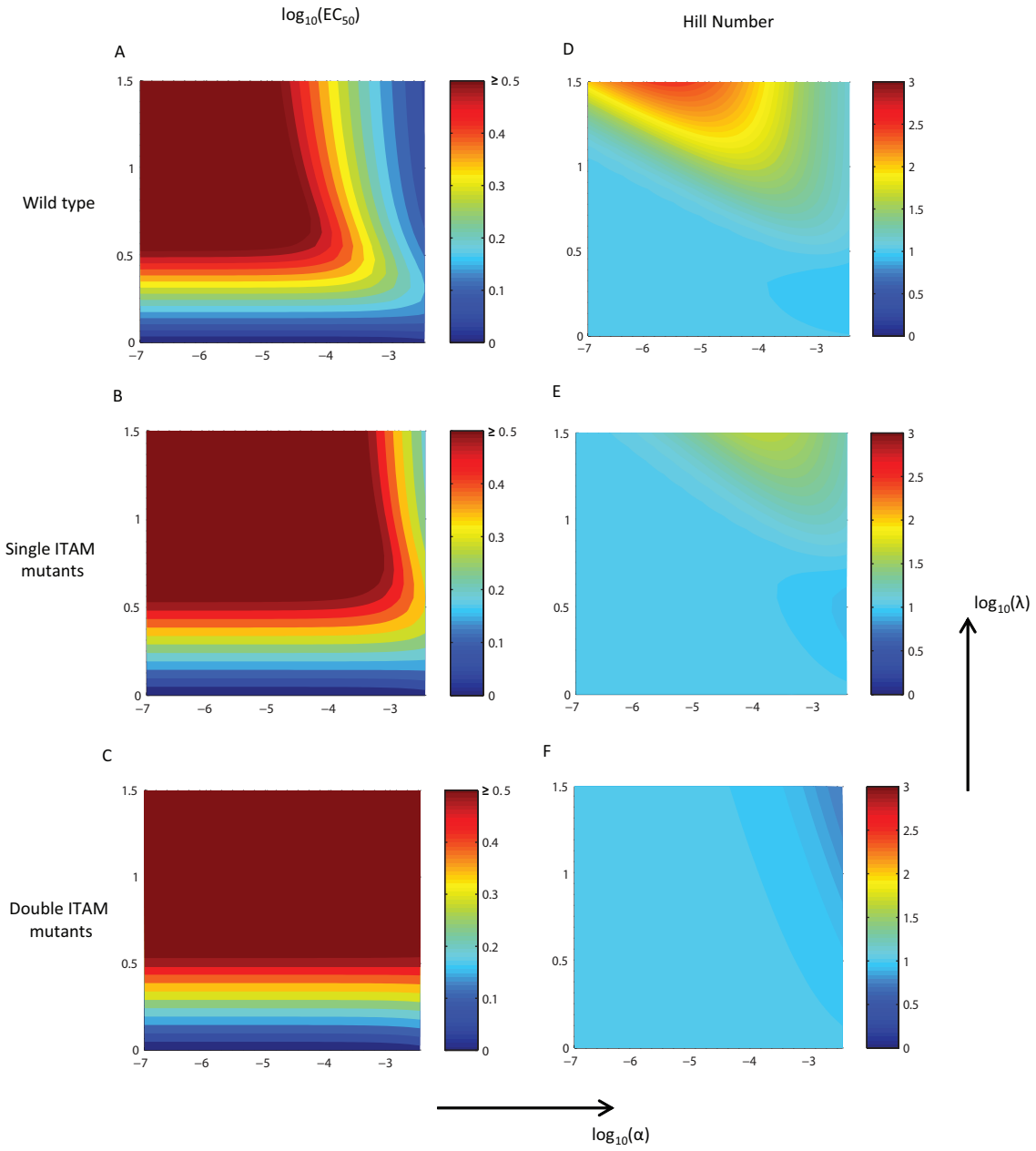

Fig 5.3: **Dose-response metrics of multisite phosphorylation as a function of enzymatic efficiencies and phosphorylation-dependent modulation.** The efficiency of enzymatic modifications, α, is varied on the x-axis and the y-axis varies the magnitude of the phosphorylation-dependent modulation factor λ. Dose-response profiles are evaluated in α-λ space, and the EC_{50}s ($\log_{10}$ scale) and Hill numbers of response profiles are depicted as heat maps. Left panels show $\log_{10}EC_{50}$s for (A) wild type, (B) single ITAM mutants and (C) double ITAM mutants. Right panels show Hill numbers for (D) wild type, (E) single ITAM mutants and (F) double ITAM mutants.

Response sensitivity profiles also change as the number of phosphorylation sites is altered (Fig 5.3D-F). We observe hyperbolic responses in the majority of α-λ space for all ITAM variants. However we note a threshold value of λ beyond which response profiles become ultrasensitive, and this threshold value

decreases with increasing numbers of phosphorylation sites.

Normalized dose-response metrics

Our experiments investigated relative differences in the potencies and sensitivities of phosphorylation as the number of TCR ζ ITAMs was varied. Thus we compute differences in response potencies, and ratios of response sensitivities, and present these as heat maps in Fig 5.4.

We compute the differences in EC_{50}s (on a $\log_{10}$ scale) between (i) wild type and single ITAM mutants (Fig 5.4A), (ii) wild type and double ITAM mutants (Fig 5.4B) and (iii) single and double ITAM mutants (Fig 5.4C) and depict these normalized EC_{50}s as heat maps in α-λ space. As we expect from our computations of the raw potencies and sensitivities in Fig 5.3, there exists a threshold region beyond which the relative differences in potencies begins to increase (Fig 5.4A-C).

We also compute the ratio of Hill numbers between (i) wild type and single ITAM mutants (Fig 5.4D), (ii) wild type and double ITAM mutants (Fig 5.4E) and (iii) single and double ITAM mutants (Fig 5.4F). We observe similar sensitivities for the majority of α-λ space. However for large values of λ, the wild type substrate exhibits more ultrasensitive responses than the single and double ITAM mutants (Fig 5.4D,E). Moreover, the single ITAM mutants exhibit more ultrasensitive response profiles than the double ITAM mutants for large values of λ and α (Fig 5.4F).

Region of parameter space where experimental results are satisfied

Our experimental results revealed a direct correlation between the number of TCR ζ ITAMs and the potency of phosphorylation. We did not find any significant differences in the sensitivities of phosphorylation across the ITAM variants. We use the dose-response metrics that we computed as functions of α and λ to determine the region of parameter space where our experimental results are satisfied.

We compare response potencies across the ITAM variants (Figs 5.3 and 5.4 panels A-C) and determine the region in parameter space where the wild type ζ-chain exhibits the most potent response, the single ITAM mutants display intermediate potencies, and the double ITAM mutants show the least potent response. We specify that the differences in EC_{50}s between ITAM variants be greater than a threshold value, and we set this threshold to be the standard error of the mean (sem) from our experimental data. These conditions yield the region of parameter space that satisfies the trends in response potencies in our experimental data (Fig 5.5A).

In a similar manner we compare response sensitivities across ITAM variants (Figs 5.3 and 5.4 panels A-C), and evaluate the region of parameter space where all ITAM variants display similar Hill numbers. We specify that the ratio of Hill numbers across ITAM variants be equal within a certain threshold value, and this threshold is again the sem of our experimental data. We evaluate the region of paramater space where these conditions are satisfied, and this yields the set of α and λ values that satisfy the trends in sensitivities in our experimental data (Fig 5.5B).

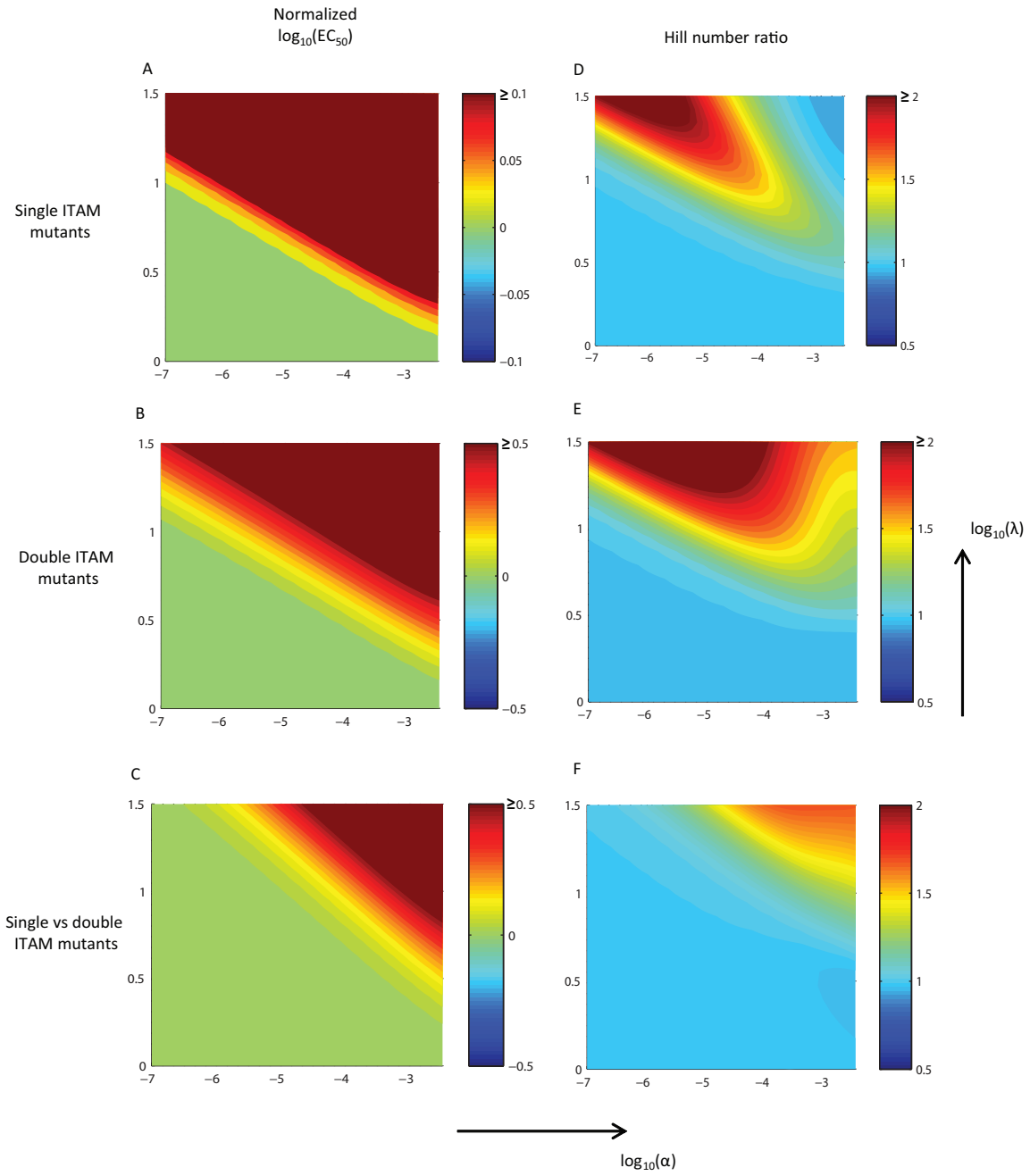

Fig 5.4: **Normalized dose-response metrics of multisite phosphorylation as a function of enzymatic efficiencies and phosphorylation-dependent modulation.** The efficiency of enzymatic modifications, α, is varied on the x-axis and the y-axis varies the magnitude of the phosphorylation-dependent modulation factor λ. Dose-response profiles are evaluated in α-λ space, and normalized EC_{50}s ($\log_{10}$ scale) and Hill number ratios are depicted as heat maps. Left panels show differences in $\log_{10}EC_{50}$s between: (A) single ITAM mutants and wild type, (B) double ITAM mutants and wild type and (C) double and single ITAM mutants. Right panels show Hill number ratios for (D) wild type to single ITAM mutants, (E) wild type to double ITAM mutants and (F) single versus double ITAM mutants.

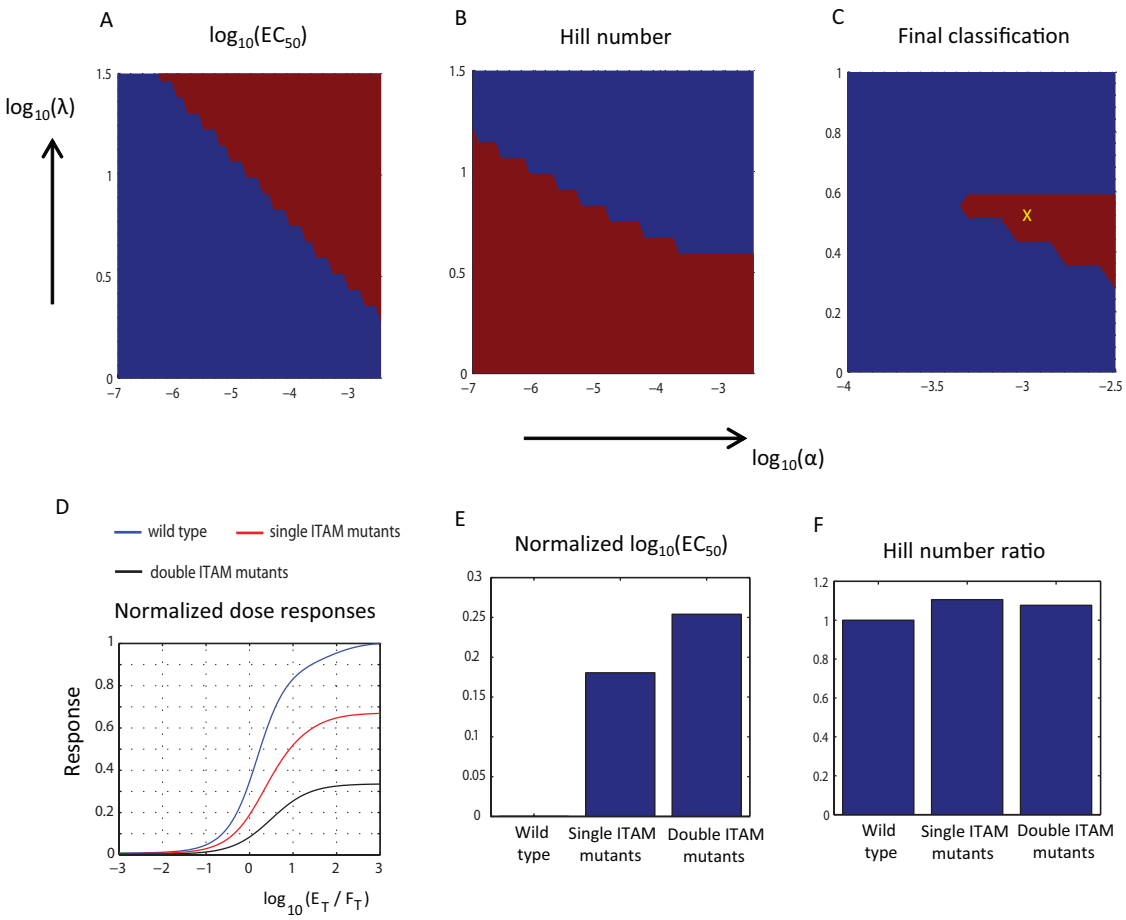

Fig 5.5: **Region of parameter space where experimental results are satisfied.** (A)-(C) The efficiency of enzymatic modifications, α, is varied on the x-axis and the y-axis varies the magnitude of the phosphorylation-dependent modulation factor λ. Each panel is a binary classification where red indicates the region of parameter space that satisfies experimental results. Binary maps of: (A) EC_{50} ($\log_{10}$ scale), (B) Hill numbers and (C) final classification obtained by multiplying maps in panels (A) and (B). X denotes parameter values for simulation results in panels (D)-(F) (D) Normalized dose-response profiles, (E) normalized $\log_{10}EC_{50}$s and (F) Hill number ratios across different ζ-chain constructs.

We combine our potency and sensitivity decision matrices to obtain the region of parameter space where our experimental results are satisfied (Fig 5.5C). We note that the set of values we obtain for the efficiency of enzymatic modification, α, is in good agreement with in vitro reconstitution studies of TCR proximal signalling (73). We choose a representative point in this space, and simulate sample dose-response profiles (Fig 5.5D). We find that the relative potencies (Fig 5.5E) and sensitivities (Fig 5.5F) of these simulated dose-responses agree with our experimental data. The magnitude of the differences in potencies across the ITAM variants are similar across the entire region of paramater space that satisfies the data. The same holds true for the sensitivities, in that all the ITAM variants exhibit similar Hill numbers across the final classification region.

Discussion

Cellular reconstitution of TCR proximal signalling (Chapter 4) revealed that multiple ITAMs enhance the potency of TCR ζ phosphorylation, but do not alter the sensitivity of response profiles. In this chapter we sought to reconcile our experimental results with mathematical models of multisite phosphorylation.

We find that a phosphorylation-dependent enhancement of enzymatic efficiencies is sufficient to explain our experimental results. It is likely that there are multiple molecular mechanisms that could mediate such an enhancement, and we consider each of these in turn.

Electrostatic interactions

A central question in receptor mediated signal transduction concerns the interplay between the membrane environment and the design of individual receptors. The TCR ζ-chain has a highly conserved architecture, whereby individual ITAM sequences are conserved across species, and clusters of positive charge are interspersed between these ITAMs. Several studies have suggested a functional role of electrostatic interactions in TCR ζ signal transduction, and such interactions represent one mechanism that could underlie the phosphorylation-dependent enhancement of enzymatic efficiencies that we modelled in this chapter.

Circular dichroism (CD) based studies revealed that the TCR ζ-chain is unstructured in aqueous solution, and it undergoes a folding transition in the presence of acidic phospholipids (11). In this lipid-bound conformation, the ζ-chain was found to be refractory to SRC-kinase mediated phosphorylation, while it was readily phosphorylated in the aqueous unstructured form. Phosphorylation was also reported to abrogate structure induction and lipid association. Thus these early in vitro experiments established a role of the membrane environment, as well as ITAM phosphorylation, in mediating transitions from unstructured-to-structured states.

Association of the TCR ζ-chain with the cell membrane has also been reported in resting T cells (8). Membrane association relies on the presence of positively charged residues interspersed between ITAMs, and these clusters of positive charge were termed basic residue rich (BRR) motifs. Mutagenesis of these residues, as well as receptor triggering, were found to abrogate membrane association. Indeed, the presence of charged residues and lipid binding segments has been proposed to regulate phosphorylation mechanisms in other receptors as well ((14), (15)), and could represent a general principle in receptor mediated signal transduction.

These studies collectively suggest that under resting conditions, the TCR ζ-chain associates with the cell membrane. A possible consequence of this association is a sequestration of ITAMs, such that only a subset of ITAMs are available for modification. Upon receptor triggering, an initial phosphorylation event abrogates membrane association, and enhances subsequent ITAM phosphorylations. Thus the phosphorylation-dependent enhancement in enzymatic efficiencies that we have modelled in this chapter could be mediated

by BRR motif-mediated membrane association of the TCR ζ-chain, and a phosphorylation-mediated abrogation of this association.

Entropic mechanisms

The TCR ζ-chain belongs to a family of molecules referred to as non-catalytic tyrosine phosphorylated receptors (NTRs) (72). A defining feature of these receptors is the presence of intrinsically disordered cytoplasmic domains. A further mechanism that could underlie the phosphorylation-dependent enhancement of enzymatic efficiencies is a disorder-to-order transition mediated by ITAM phosphorylation.

The functional consequences of intrinsically disordered regions in cellular signal transduction are only beginning to be appreciated (78). Post-translational modification sites are often enriched within, or in close proximity to, disordered regions. Since phosphorylation significantly alters the charge profile of molecules, it is possible that multisite phosphorylation is a mechanism to tune molecular entropy. In reconciling our experimental data with mathematical models, we assumed that ITAM phosphorylation mediates an ordering of the ζ-chain, and such a disorder-to-order transition enhances efficiencies of enzyme modification.

The rationale for such an enhancement comes from theoretical work that attributed multisite phosphorylation as a means to enhance the rate of binding between a disordered protein and a binding partner (82). Such an enhancement was posited to generate ultrasensitive binding profiles. We do not observe an enhancement in sensitivities in our system, however we do observe an enhancement in response potencies. A recent experimental study that demonstrates the role of multisite phosphorylation in tuning molecular entropy arises in the context of neuronal translation initiation (80). The authours use NMR to show that multisite phosphorylation mediates the folding of an intrinsically disordered region in 4E-BP2, and these modifications abrogate binding to the translation initiation factor eIF4E.

We envisage that the modulation of molecular entropy by multisite phosphorylation is a widspread phenomenon in cellular signal transduction. Indeed, many of the molecules that comprise TCR signalling, such as SH2 domain containing proteins, are comprised of intrinsically disordered regions (78). Thus transitions between disorder and order are likely to be a pervasive theme throughout TCR signalling.

Methods

Multisite phosphorylation model

The model includes the TCR ζ-chain with 6 phosphorylation sites that are randomly phosphorylated by LCK and dephosphorylated by CD148. We assume that LCK and CD148 cannot simultaneously bind the TCR ζ-chain. We take k_{on}, k_{off}, and k_{cat} to be identical for both enzymes.

The system of ODEs representing the biochemical reaction network based on this scheme was generated in BioNetGen (52) and integrated in Matlab (Mathworks, MA). A phosphorylation-dependent enhancement

of enzymatic efficiencies was implemented by weighting the modification on-rate k_{on} according to equation 5.11.

The concentration of total TCR ζ phosphorylation was calculated at steady-state by varying the concentration of phosphatase (identical results can be obtained by varying the concentration of the kinase). Total ζ-chain phosphorylation is the multiplicative product of 1) the concentration of a particular TCR ζ isoform (regardless of whether it is bound to an enzyme) and 2) the number of phosphate groups attached to the isoform.

Curve fitting

Response profiles of total TCR ζ-chain phosphorylation were fitted to logarithmic Hill functions using lsqcurvefit in Matlab (Mathworks, MA),

$$y = E_{min} + \frac{E_{max} - E_{min}}{1 + 10^{(\log(EC_{50} - x))n}}$$

where y corresponds to total TCR ζ-chain phosphorylation and x the kinase-to-phosphatase ratio on a logarithmic (base 10) scale. The fitted parameter values include: E_{min} and E_{max}, which correspond to the minimum and maximum values, respectively, $\log(EC_{50})$, which is the logarithmic value of the kinase-to-phosphatase ratio that yields half of the maximal response (otherwise known as potency), and n, which is the Hill number that determines the steepness of the response (otherwise known as the sensitivity).

Chapter 6

Discussion and future work

We have investigated the functional consequences of multiple ITAMs in the regulation of TCR ζ phosphorylation. We have shown that multiple ITAMs enhance the potency of TCR ζ phosphorylation, but do not alter the sensitivity of response profiles. These results are consistent with a phosphorylation-dependent enhancement of enzymatic efficiencies. We conclude this thesis with a discussion of our pertinent findings and possible future directions of research.

Mathematical modelling of TCR proximal signalling

Mathematical modelling of TCR proximal signalling (Chapter 3) revealed the conditions that generate ultrasensitive responses. These include a sequential mechanism of TCR ζ ITAM modification ((10), (8)), and the binding of ZAP-70 to fully phosphorylated ITAMs with affinities increasing in the direction of phosphorylation ((55), (56), (58), (57)). Under these model assumptions, we predicted that multiple ITAMs enhance the potency as well as sensitivity of TCR ζ phosphorylation.

Cellular reconstitution of TCR proximal signalling

We sought to evaluate our model assumptions and predictions through cellular reconstitution of the TCR proximal signalling network (Chapter 4). Our experimental results suggest that TCR ζ modification follows a random mechanism of phosphorylation, and that ZAP-70 does not bind the three different phosphorylated TCR ζ ITAMs with significantly different affinities.

Our reconstitution studies revealed that multiple ITAMs enhance the potency of TCR ζ phosphorylation, but do not alter the sensitivity of response profiles. The correlation between the number of ITAMs and response potency was observed both in the presence and absence of ZAP-70.

The main effect of ZAP-70 is to further enhance the potency of TCR ζ phosphorylation, and this enhancement is approximately equal across all ITAM variants. We did not find any change in response sensitivities in the presence of ZAP-70, and this is in agreement with liposomal reconstitution of TCR proximal signalling (73).

Reconciling mathematical models with experimental data

Our experimental results suggested that our original model assumptions must be revised. Thus we revisited mathematical models of multisite phosphorylation, and investigated minimal models that are sufficient to explain our experimental data (Chapter 5).

A central revision to our original model assumptions concerns the underlying structure of ζ-chain phosphorylation. Our data in Chapter 4 suggests a random mechanism of ζ-chain phosphorylation, while previous studies have suggested that the membrane distal ITAMs are phosphorylated before the membrane proximal ITAM ((10), (8)). One possible explanation is that ζ-chain modifications can proceed under an unstructured and random mechanism, however there exists a preferential sequence of ITAM modifications in vivo. In reconciling our experimental data with mathematical models, we assumed a random mechanism of ITAM modifications.

The observed correlation between the number of ITAMs and response potency led us to hypothesize that the phosphorylation state of the TCR ζ-chain modulates enzymatic efficiencies of ITAM modification. We modelled a phosphorylation-dependent enhancement of enzymatic efficiencies, and found that this minimal model of multisite phosphorylation is sufficient to explain our experimental data.

Possible molecular mechanisms that underlie phosphorylation-dependent enhancement of enzymatic efficiencies

We envision that multiple molecular mechanisms could mediate a phosphorylation-dependent enhancement of enzymatic efficiencies. The first involves the presence of positively charged residues between ITAMs that mediate an association of the TCR ζ-chain with the cell membrane (8). ITAM phosphorylation is posited to abrogate this membrane association, and expose sequestered ITAMs so that they become available for enzymatic modification.

The second mechanism involves the modulation of TCR ζ-chain entropy by ITAM phosphorylation. The cytoplasmic domain of the TCR ζ-chain exhibits intrinsic disorder (72), and ITAM phosphorylation could mediate a disorder-to-order transition. Such a reduction in molecular entropy would enhance the binding affinity of the modifying enzymes (82), thus eliciting an enhancement of enzymatic efficiencies of modification. We envisage that the modulation of molecular entropy by multisite phosphorylation represents a ubiquitous theme throughout cellular signal transduction ((78), (80), (81)).

Future work

There are multiple possible future directions of research that emanate from our work. These can be largely divided into cellular reconstitution studies similar to the ones we have pursued, as well as in vitro structural

studies. The combination of these approaches should be combined towards inspiring rational strategies for designing chimeric antigen receptors (CARs) for immunotherapy.

Cellular reconstitution studies

We have found that multiple ITAMs enhance the potency of TCR ζ phosphorylation. A challenge will be to investigate how this effect could be abrogated. One possible strategy is to mutate the clusters of positive charge that are juxtaposed between ITAMs, and to pursue the cellular reconstitution and treatment experiments that we have performed. Alternatively, one could introduce phosphomimetic residues in place of ITAM mutations, and study the effects of the introduction of negative charge within ITAMs. We predict that both these approaches will abrogate the graded regulation of response potencies that we observe.

In vitro structural studies

We have postulated that the correlation between the number of ITAMs and response potencies is mediated by a phosphorylation-dependent enhancement of enzymatic efficiencies. A possible direction of future research is a direct demonstration of this effect through surface plasmon resonance. These experiments would entail measuring the enzymatic efficiencies of ITAM phosphorylation on TCR ζ-chain variants with different numbers of ITAMs.

We have also speculated that the phosphorylation-dependent enhancement of enzymatic efficiencies is partly mediated by a disorder-to-order transition of the TCR ζ-chain. The entropic profile of molecules can be studied using techniques such as nuclear magnetic resonance (NMR) spectroscopy. Thus we propose to peform NMR experiments on TCR ζ-chain variants that alter the phosphorylation state, as well as the charge profile of molecules.

Inspiring the design of novel CARs

One of our objectives is to use our experimental system to inspire the design of novel CARs for immunotherapy. The optimal CAR response is one that exhibits high affinity to target antigens, low antigen potency, and large maximum responses. However our results suggest that there exists an inevitable trade-off between maximal responses and response potencies, such that large maxima also exhibit high potencies. Thus we propose to exploit our experimental system in conjunction with in vitro structural studies to investigate the design of CARs that exhibit large maxima as well as low potencies.

Appendix A

BioNetGen program code

```
# Mathematical model in Chapter 3

begin parameters

#Kinase-substrate on rates
ek_on1 1e-4
ek_on2 1e-4
ek_on3 1e-4
ek_on4 1e-4
ek_on5 1e-4
ek_on6 1e-4

#Kinase-substrate off rates
ek_off1 10.0
ek_off2 10.0
ek_off3 10.0
ek_off4 10.0
ek_off5 10.0
ek_off6 10.0

#Kinase catalysis rates
ek_cat1 10.0
ek_cat2 10.0
ek_cat3 10.0
ek_cat4 10.0
ek_cat5 10.0
ek_cat6 10.0

#Phosphatase-substrate on rates
fk_on1 1e-4
fk_on2 1e-4
fk_on3 1e-4
fk_on4 1e-4
fk_on5 1e-4
fk_on6 1e-4

#Phosphatase-substrate off rates
fk_off1 10.0
```

```
fk_off2 10.0
fk_off3 10.0
fk_off4 10.0
fk_off5 10.0
fk_off6 10.0

#Phosphatase catalysis rates
fk_cat1 10.0
fk_cat2 10.0
fk_cat3 10.0
fk_cat4 10.0
fk_cat5 10.0
fk_cat6 10.0

#Binding parameters for ZAP-70 binding
zap_on1 1.0
zap_on2 1.0
zap_on3 1.0

zap_off1 0.1
zap_off2 0.1
zap_off3 0.1

#Total substrate (S_T), kinase (E_T), phosphatase (F_T),
#and ZAP-70 (Z_T) concentrations
E_T 100
F_T 100
S_T 100
Z_T 100

end parameters

begin molecule types

#Substrate
#Attribute b~1 indicates that an enzyme is bound to substrate,
#and b~0 indicates no enzyme is bound
#Attributes Y1, Y2, and Y3 each refer to individual ITAMs.
#Each ITAM can be unphosphorylated (Y~U),
#phosphorylated on one tyrosine (Y~P), or doubly phosphorylated (Y~2P)

S(b~0~1,Y1~U~P~2P,Y2~U~P~2P,Y3~U~P~2P)

#Kinase
E(b)

#Phosphatase
F(b)

#ZAP-70
Z(b)

end molecule types
```

```
begin seed species

S(b~0,Y1~U,Y2~U,Y3~U) S_T
E(b) E_T
F(b) F_T
Z(b) Z_T

end seed species

begin reaction rules

#ITAM1 MODIFICATIONS

E(b)+S(b~0,Y1~U,Y2~U,Y3~U)<->E(b!1).S(b~1,Y1~U!1,Y2~U,Y3~U) ek_on1,ek_off1
E(b!1).S(b~1,Y1~U!1,Y2~U,Y3~U)->E(b)+S(b~0,Y1~P,Y2~U,Y3~U) ek_cat1

F(b)+S(b~0,Y1~P,Y2~U,Y3~U)<->F(b!1).S(b~1,Y1~P!1,Y2~U,Y3~U) fk_on1,fk_off1
F(b!1).S(b~1,Y1~P!1,Y2~U,Y3~U)->F(b)+S(b~0,Y1~U,Y2~U,Y3~U) fk_cat1

E(b)+S(b~0,Y1~P,Y2~U,Y3~U)<->E(b!1).S(b~1,Y1~P!1,Y2~U,Y3~U) ek_on2, ek_off2
E(b!1).S(b~1,Y1~P!1,Y2~U,Y3~U)->E(b)+S(b~0,Y1~2P,Y2~U,Y3~U) ek_cat2

F(b)+S(b~0,Y1~2P,Y2~U,Y3~U)<->F(b!1).S(b~1,Y1~2P!1,Y2~U,Y3~U) fk_on2, fk_off2
F(b!1).S(b~1,Y1~2P!1,Y2~U,Y3~U)->F(b)+S(b~0,Y1~P,Y2~U,Y3~U)   fk_cat2

#ITAM2 MODIFICATIONS

E(b)+S(b~0,Y1~2P!?,Y2~U,Y3~U)<->E(b!1).S(b~1,Y1~2P!?,Y2~U!1,Y3~U)  ek_on3, ek_off3
E(b!1).S(b~1,Y1~2P!?,Y2~U!1,Y3~U)->E(b) + S(b~0,Y1~2P!?,Y2~P,Y3~U) ek_cat3

F(b)+S(b~0,Y1~2P!?,Y2~P,Y3~U)<->F(b!1).S(b~1,Y1~2P!?,Y2~P!1,Y3~U)  fk_on3, fk_off3
F(b!1).S(b~1,Y1~2P!?,Y2~P!1,Y3~U)->F(b)+S(b~0,Y1~2P!?,Y2~U,Y3~U)   fk_cat3

E(b)+S(b~0,Y1~2P!?,Y2~P,Y3~U)<->E(b!1).S(b~1,Y1~2P!?,Y2~P!1,Y3~U) ek_on4, ek_off4
E(b!1).S(b~1,Y1~2P!?,Y2~P!1,Y3~U)->E(b)+S(b~0,Y1~2P!?,Y2~2P,Y3~U) ek_cat4

F(b)+S(b~0,Y1~2P!?,Y2~2P,Y3~U)<->F(b!1).S(b~1,Y1~2P!?,Y2~2P!1,Y3~U)  fk_on4, fk_off4
F(b!1).S(b~1,Y1~2P!?,Y2~2P!1,Y3~U)->F(b)+S(b~0,Y1~2P!?,Y2~P,Y3~U) fk_cat4

#ITAM3 MODIFICATIONS

E(b)+S(b~0,Y1~2P!?,Y2~2P!?,Y3~U)<->E(b!1).S(b~1,Y1~2P!?,Y2~2P!?,Y3~U!1) ek_on5, ek_off5
E(b!1).S(b~1,Y1~2P!?,Y2~2P!?,Y3~U!1)->E(b)+S(b~0,Y1~2P!?,Y2~2P!?,Y3~P)  ek_cat5

F(b)+S(b~0,Y1~2P!?,Y2~2P!?,Y3~P)<->F(b!1).S(b~1,Y1~2P!?,Y2~2P!?,Y3~P!1) fk_on5, fk_off5
F(b!1).S(b~1,Y1~2P!?,Y2~2P!?,Y3~P!1)->F(b)+S(b~0,Y1~2P!?,Y2~2P!?,Y3~U) fk_cat5

E(b)+S(b~0,Y1~2P!?,Y2~2P!?,Y3~P)<->E(b!1).S(b~1,Y1~2P!?,Y2~2P!?,Y3~P!1) ek_on6, ek_off6
E(b!1).S(b~1,Y1~2P!?,Y2~2P!?,Y3~P!1)->E(b)+S(b~0,Y1~2P!?,Y2~2P!?,Y3~2P) ek_cat6

F(b)+S(b~0,Y1~2P!?,Y2~2P!?,Y3~2P)<->F(b!1).S(b~1,Y1~2P!?,Y2~2P!?,Y3~2P!1) fk_on6, fk_off6
F(b!1).S(b~1,Y1~2P!?,Y2~2P!?,Y3~2P!1)->F(b)+S(b~0,Y1~2P!?,Y2~2P!?,Y3~P)  fk_cat6

#ZAP70 BINDING
```

```
Z(b) + S(Y1~2P) <-> Z(b!1).S(Y1~2P!1) zap_on1, zap_off1

Z(b) + S(Y2~2P) <-> Z(b!1).S(Y2~2P!1) zap_on2, zap_off2

Z(b) + S(Y3~2P) <-> Z(b!1).S(Y3~2P!1) zap_on3, zap_off3

end reaction rules

begin observables

1 Molecules Bound_ZAP Z(b!+)

2 Molecules Szero S(b~?,Y1~U!?,Y2~U!?,Y3~U!?)

3 Molecules Sone S(b~?,Y1~P!?,Y2~U!?,Y3~U!?)

4 Molecules Stwo S(b~?,Y1~2P!?,Y2~U!?,Y3~U!?)

5 Molecules Sthree S(b~?,Y1~2P!?,Y2~P!?,Y3~U!?)

6 Molecules Sfour S(b~?,Y1~2P!?,Y2~2P!?,Y3~U!?)

7 Molecules Sfive S(b~?,Y1~2P!?,Y2~2P!?,Y3~P!?)

8 Molecules Ssix S(b~?,Y1~2P!?,Y2~2P!?,Y3~2P!?)

end observables

generate_network({overwrite=>1});

writeMfile({});

# Mathematical model in Chapter 5

begin parameters

ek_on1 1
ek_on2 1
ek_on3 1
ek_on4 1
ek_on5 1
ek_on6 1

fk_on1 1
fk_on2 1
fk_on3 1
fk_on4 1
fk_on5 1
fk_on6 1

ek_off1 1
ek_off2 1
ek_off3 1
```

```
ek_off4 1
ek_off5 1
ek_off6 1

fk_off1 1
fk_off2 1
fk_off3 1
fk_off4 1
fk_off5 1
fk_off6 1

ek_cat1 1
ek_cat2 1
ek_cat3 1
ek_cat4 1
ek_cat5 1
ek_cat6 1

fk_cat1 1
fk_cat2 1
fk_cat3 1
fk_cat4 1
fk_cat5 1
fk_cat6 1

S_T 100
E_T 1e3
F_T 1e3

end parameters


begin molecule types

S(Y~U~P~2P~3P~4P~5P~6P)
E(ecat)
F(fcat)

end molecule types


begin seed species

S(Y~U) S_T
E(ecat) E_T
F(fcat) F_T

end seed species


begin reaction rules

# 0 <-> 1
```

```
E(ecat) + S(Y~U) <-> E(ecat!1).S(Y~U!1) ek_on1, ek_off1
E(ecat!1).S(Y~U!1) -> E(ecat) + S(Y~P) ek_cat1

F(fcat) + S(Y~P) <-> F(fcat!1).S(Y~P!1) fk_on1, fk_off1
F(fcat!1).S(Y~P!1) -> F(fcat) + S(Y~U) fk_cat1

# 1 <-> 2

E(ecat) + S(Y~P) <-> E(ecat!1).S(Y~P!1) ek_on2, ek_off2
E(ecat!1).S(Y~P!1) -> E(ecat) + S(Y~2P) ek_cat2

F(fcat) + S(Y~2P) <-> F(fcat!1).S(Y~2P!1) fk_on2, fk_off2
F(fcat!1).S(Y~2P!1) -> F(fcat) + S(Y~P) fk_cat2

# 2 <-> 3

E(ecat) + S(Y~2P) <-> E(ecat!1).S(Y~2P!1) ek_on3, ek_off3
E(ecat!1).S(Y~2P!1) -> E(ecat) + S(Y~3P) ek_cat3

F(fcat) + S(Y~3P) <-> F(fcat!1).S(Y~3P!1) fk_on3, fk_off3
F(fcat!1).S(Y~3P!1) -> F(fcat) + S(Y~2P) fk_cat3

# 3 <-> 4

E(ecat) + S(Y~3P) <-> E(ecat!1).S(Y~3P!1) ek_on4, ek_off4
E(ecat!1).S(Y~3P!1) -> E(ecat) + S(Y~4P) ek_cat4

F(fcat) + S(Y~4P) <-> F(fcat!1).S(Y~4P!1) fk_on4, fk_off4
F(fcat!1).S(Y~4P!1) -> F(fcat) + S(Y~3P) fk_cat4

# 4 <-> 5

E(ecat) + S(Y~4P) <-> E(ecat!1).S(Y~4P!1) ek_on5, ek_off5
E(ecat!1).S(Y~4P!1) -> E(ecat) + S(Y~5P) ek_cat5

F(fcat) + S(Y~5P) <-> F(fcat!1).S(Y~5P!1) fk_on5, fk_off5
F(fcat!1).S(Y~5P!1) -> F(fcat) + S(Y~4P) fk_cat5

# 5 <-> 6

E(ecat) + S(Y~5P) <-> E(ecat!1).S(Y~5P!1) ek_on6, ek_off6
E(ecat!1).S(Y~5P!1) -> E(ecat) + S(Y~6P) ek_cat6

F(fcat) + S(Y~6P) <-> F(fcat!1).S(Y~6P!1) fk_on6, fk_off6
F(fcat!1).S(Y~6P!1) -> F(fcat) + S(Y~5P) fk_cat6


end reaction rules


begin observables

1 Molecules Szero S(Y~U!?)
2 Molecules Sone S(Y~P!?)
```

```
3 Molecules Stwo S(Y~2P!?)
4 Molecules Sthree S(Y~3P!?)
5 Molecules Sfour S(Y~4P!?)
6 Molecules Sfive S(Y~5P!?)
7 Molecules Ssix S(Y~6P!?)

end observables


generate_network({overwrite=>1});

writeMfile({});
```

Bibliography

1. Murphy K (2012) *Janeway's Immunobiology, 8th Edition* (Garland Science, Taylor & Francis Group, LLC).
2. Smith-Garvin JE, Koretzky GA, Jordan MS (2009) T cell activation. *Annu Rev Immunol* 27:591–619.
3. Love PE, Hayes SM (2010) ITAM-mediated signaling by the T-cell antigen receptor. *Cold Spring Harb Perspect Biol* 2:a002485.
4. Acuto O, Bartolo VD, Michel F (2008) Tailoring T-cell receptor signals by proximal negative feedback mechanisms. *Nat Rev Immunol* 8:699–712.
5. Hermiston ML, Zikherman J, Zhu JW (2009) CD45, CD148, and Lyp/Pep: critical phosphatases regulating Src family kinase signaling networks in immune cells. *Immunol Rev* 228:288–311.
6. Lorenz U (2009) SHP-1 and SHP-2 in t cells: two phosphatases functioning at many levels. *Immunol Rev* 228:342–359.
7. Stefanova I, et al. (2003) TCR ligand discrimination is enforced by competing ERK positive and SHP-1 negative feedback pathways. *Nat Immunol* 4:248–254.
8. Zhang H, Cordoba SP, Dushek O, van der Merwe PA (2011) Basic residues in the T-cell receptor zeta cytoplasmic domain mediate membrane association and modulate signaling. *Proc Natl Acad Sci U S A* 108:19323–19328.
9. Love PE, Shores EW (2000) ITAM multiplicity and thymocyte selection: how long can you go? *Immunity* 12:591–597.
10. van Oers NS, et al. (2000) The 21- and 23-kD forms of tcr zeta are generated by specific ITAM phosphorylations. *Nat Immunol* 1:322–328.
11. Aivazian D, Stern LJ (2000) Phosphorylation of T cell receptor zeta is regulated by a lipid dependent folding transition. *Nat Struct Biol* 7:1023–1026.
12. Sigalov AB, Aivazian DA, Uversky VN, Stern LJ (2006) Lipid-binding activity of intrinsically unstructured cytoplasmic domains of multichain immune recognition receptor signaling subunits. *Biochemistry* 45:15731–15739.
13. Sigalov AB, Hendricks GM (2009) Membrane binding mode of intrinsically disordered cytoplasmic domains of T cell receptor signaling subunits depends on lipid composition. *Biochem Biophys Res Commun* 389:388–393.
14. Xu C, et al. (2008) Regulation of T cell receptor activation by dynamic membrane binding of the cd3epsilon cytoplasmic tyrosine-based motif. *Cell* 135:702–713.
15. Paddock C, et al. (2011) Residues within a lipid-associated segment of the PECAM-1 cytoplasmic domain are susceptible to inducible, sequential phosphorylation. *Blood* 117:6012–6023.
16. Salmond RJ, Filby A, Qureshi I, Caserta S, Zamoyska R (2009) T-cell receptor proximal signaling via the Src-family kinases, Lck and Fyn, influences T-cell activation, differentiation, and tolerance. *Immunol Rev* 228:9–22.

17. Kabouridis PS, Magee AI, Ley SC (1997) S-acylation of LCK protein tyrosine kinase is essential for its signalling function in T lymphocytes. *EMBO J* 16:4983–4998.

18. Turner JM, et al. (1990) Interaction of the unique N-terminal region of tyrosine kinase p56lck with cytoplasmic domains of CD4 and CD8 is mediated by cysteine motifs. *Cell* 60:755–765.

19. Kim PW, Sun ZYJ, Blacklow SC, Wagner G, Eck MJ (2003) A zinc clasp structure tethers Lck to T cell coreceptors CD4 and CD8. *Science* 301:1725–1728.

20. Harder T, Engelhardt KR (2004) Membrane domains in lymphocytes - from lipid rafts to protein scaffolds. *Traffic* 5:265–275.

21. Sicheri F, Kuriyan J (1997) Structures of Src-family tyrosine kinases. *Curr Opin Struct Biol* 7:777–785.

22. Nika K, et al. (2010) Constitutively active Lck kinase in T cells drives antigen receptor signal transduction. *Immunity* 32:766–777.

23. van der Merwe PA, Dushek O (2011) Mechanisms for T cell receptor triggering. *Nat Rev Immunol* 11:47–55.

24. Imbert V, et al. (1994) Induction of tyrosine phosphorylation and T-cell activation by vanadate peroxide, an inhibitor of protein tyrosine phosphatases. *Biochem J* 297 (Pt 1):163–173.

25. Secrist JP, Burns LA, Karnitz L, Koretzky GA, Abraham RT (1993) Stimulatory effects of the protein tyrosine phosphatase inhibitor, pervanadate, on T-cell activation events. *J Biol Chem* 268:5886–5893.

26. O'Shea JJ, McVicar DW, Bailey TL, Burns C, Smyth MJ (1992) Activation of human peripheral blood T lymphocytes by pharmacological induction of protein-tyrosine phosphorylation. *Proc Natl Acad Sci U S A* 89:10306–10310.

27. Zamoyska R (2007) Why is there so much CD45 on T cells? *Immunity* 27:421–423.

28. Desai DM, Sap J, Silvennoinen O, Schlessinger J, Weiss A (1994) The catalytic activity of the CD45 membrane-proximal phosphatase domain is required for TCR signaling and regulation. *EMBO J* 13:4002–4010.

29. Folmer RHA, Geschwindner S, Xue Y (2002) Crystal structure and NMR studies of the apo SH2 domains of ZAP-70: two bikes rather than a tandem. *Biochemistry* 41:14176–14184.

30. Hatada MH, et al. (1995) Molecular basis for interaction of the protein tyrosine kinase ZAP-70 with the T-cell receptor. *Nature* 377:32–38.

31. Wang H, et al. (2010) ZAP-70: an essential kinase in T-cell signaling. *Cold Spring Harb Perspect Biol* 2:a002279.

32. Deindl S, et al. (2007) Structural basis for the inhibition of tyrosine kinase activity of ZAP-70. *Cell* 129:735–746.

33. Deindl S, Kadlecek TA, Cao X, Kuriyan J, Weiss A (2009) Stability of an autoinhibitory interface in the structure of the tyrosine kinase ZAP-70 impacts T cell receptor response. *Proc Natl Acad Sci U S A* 106:20699–20704.

34. Okamura H, et al. (2000) Concerted dephosphorylation of the transcription factor NFAT1 induces a conformational switch that regulates transcriptional activity. *Mol Cell* 6:539–550.

35. Komeili A, O'Shea EK (1999) Roles of phosphorylation sites in regulating activity of the transcription factor Pho4. *Science* 284:977–980.

36. Nash P, et al. (2001) Multisite phosphorylation of a CDK inhibitor sets a threshold for the onset of DNA replication. *Nature* 414:514–521.

37. Ferrell JE, Machleder EM (1998) The biochemical basis of an all-or-none cell fate switch in xenopus oocytes. *Science* 280:895–898.

38. Cohen P (2000) The regulation of protein function by multisite phosphorylation–a 25 year update. *Trends Biochem Sci* 25:596–601.

39. Yang XJ (2005) Multisite protein modification and intramolecular signaling. *Oncogene* 24:1653–1662.

40. Michaelis L, Menten M (1913) Die kinetik der invertinwirkung. *Biochem. Z.* 49:333–369.

41. Murray J (2002) *Mathematical Biology, 3rd Ed.* (Springer-Verlag).

42. Berg JM, Tymoczko JL, Stryer L (2007) *Biochemistry* (New York: W.H. Freeman).

43. Goldbeter A, Koshland DE (1981) An amplified sensitivity arising from covalent modification in biological systems. *Proc Natl Acad Sci U S A* 78:6840–6844.

44. Dushek O, van der Merwe PA, Shahrezaei V (2011) Ultrasensitivity in multisite phosphorylation of membrane-anchored proteins. *Biophys J* 100:1189–1197.

45. Gunawardena J (2005) Multisite protein phosphorylation makes a good threshold but can be a poor switch. *Proc Natl Acad Sci U S A* 102:14617–14622.

46. Wang L, Nie Q, Enciso G (2010) Nonessential sites improve phosphorylation switch. *Biophys J* 99:L41–L43.

47. Salazar C, Hfer T (2009) Multisite protein phosphorylation–from molecular mechanisms to kinetic models. *FEBS J* 276:3177–3198.

48. Liu X, Bardwell L, Nie Q (2010) A combination of multisite phosphorylation and substrate sequestration produces switchlike responses. *Biophys J* 98:1396–1407.

49. Strogatz SH (2000) *Nonlinear dynamics and chaos : with applications to physics, biology, chemistry, and engineering* (Westview Press).

50. Thomson M, Gunawardena J (2009) Unlimited multistability in multisite phosphorylation systems. *Nature* 460:274–277.

51. Markevich NI, Hoek JB, Kholodenko BN (2004) Signaling switches and bistability arising from multisite phosphorylation in protein kinase cascades. *J Cell Biol* 164:353–359.

52. Faeder JR, Blinov ML, Hlavacek WS (2009) Rule-based modeling of biochemical systems with BioNetGen. *Methods Mol Biol* 500:113–167.

53. Restifo NP, Dudley ME, Rosenberg SA (2012) Adoptive immunotherapy for cancer: harnessing the T cell response. *Nat Rev Immunol* 12:269–281.

54. Guy CS, Vignali DAA (2009) Organization of proximal signal initiation at the TCR:CD3 complex. *Immunol Rev* 232:7–21.

55. Isakov N, et al. (1995) ZAP-70 binding specificity to T cell receptor tyrosine-based activation motifs: the tandem SH2 domains of ZAP-70 bind distinct tyrosine-based activation motifs with varying affinity. *J Exp Med* 181:375–380.

56. Bu JY, Shaw AS, Chan AC (1995) Analysis of the interaction of ZAP-70 and syk protein-tyrosine kinases with the T-cell antigen receptor by plasmon resonance. *Proc Natl Acad Sci U S A* 92:5106–5110.

57. Zenner G, Vorherr T, Mustelin T, Burn P (1996) Differential and multiple binding of signal transducing molecules to the ITAMs of the TCR-zeta chain. *J Cell Biochem* 63:94–103.

58. Vely F, Nuns JA, Malissen B, Hedgecock CJ (1997) Analysis of immunoreceptor tyrosine-based activation motif (ITAM) binding to ZAP-70 by surface plasmon resonance. *Eur J Immunol* 27:3010–3014.

59. Ottinger EA, Botfield MC, Shoelson SE (1998) Tandem SH2 domains confer high specificity in tyrosine kinase signaling. *J Biol Chem* 273:729–735.

60. Sadelain M, Brentjens R, Rivire I (2009) The promise and potential pitfalls of chimeric antigen receptors. *Curr Opin Immunol* 21:215–223.

61. Roberts MR, et al. (1998) Antigen-specific cytolysis by neutrophils and NK cells expressing chimeric immune receptors bearing zeta or gamma signaling domains. *J Immunol* 161:375–384.

62. Haynes NM, et al. (2001) Redirecting mouse CTL against colon carcinoma: superior signaling efficacy of single-chain variable domain chimeras containing TCR-zeta vs Fc epsilon RI-gamma. *J Immunol* 166:182–187.

63. Osman N, Turner H, Lucas S, Reif K, Cantrell DA (1996) The protein interactions of the immunoglobulin receptor family tyrosine-based activation motifs present in the T cell receptor zeta subunits and the CD3 gamma, delta and epsilon chains. *Eur J Immunol* 26:1063–1068.

64. Kersh EN, Shaw AS, Allen PM (1998) Fidelity of T cell activation through multistep T cell receptor zeta phosphorylation. *Science* 281:572–575.

65. Rotin D, et al. (1992) SH2 domains prevent tyrosine dephosphorylation of the EGF receptor: identification of Tyr992 as the high-affinity binding site for SH2 domains of phospholipase C gamma. *EMBO J* 11:559–567.

66. Faeder JR, et al. (2003) Investigation of early events in Fc epsilon RI-mediated signaling using a detailed mathematical model. *J Immunol* 170:3769–3781.

67. Kleiman LB, Maiwald T, Conzelmann H, Lauffenburger DA, Sorger PK (2011) Rapid phospho-turnover by receptor tyrosine kinases impacts downstream signaling and drug binding. *Mol Cell* 43:723–737.

68. Altan-Bonnet G, Germain RN (2005) Modeling T cell antigen discrimination based on feedback control of digital ERK responses. *PLoS Biol* 3:e356.

69. Das J, et al. (2009) Digital signaling and hysteresis characterize ras activation in lymphoid cells. *Cell* 136:337–351.

70. Fuss H, Dubitzky W, Downes CS, Kurth MJ (2008) Src family kinases and receptors: analysis of three activation mechanisms by dynamic systems modeling. *Biophys J* 94:1995–2006.

71. Kim HR, et al. (2011) IGSF4 is a novel TCR zeta-chain-interacting protein that enhances TCR-mediated signaling. *J Exp Med* 208:2545–2560.

72. Dushek O, Goyette J, van der Merwe PA (2012) Non-catalytic tyrosine-phosphorylated receptors. *Immunol Rev* 250:258–276.

73. Hui E, Vale RD (2014) In vitro membrane reconstitution of the T-cell receptor proximal signaling network. *Nat Struct Mol Biol* 21:133–142.

74. Furlan G, Minowa T, Hanagata N, Kataoka-Hamai C, Kaizuka Y (2014) Phosphatase CD45 both positively and negatively regulates T cell receptor phosphorylation in reconstituted membrane protein clusters. *J Biol Chem* 289:28514–28525.

75. James JR, Vale RD (2012) Biophysical mechanism of t-cell receptor triggering in a reconstituted system. *Nature* 487:64–69.

76. Stepanek O, et al. (2011) Regulation of Src family kinases involved in T cell receptor signaling by protein-tyrosine phosphatase CD148. *J Biol Chem* 286:22101–22112.

77. Bibbins KB, Boeuf H, Varmus HE (1993) Binding of the Src SH2 domain to phosphopeptides is determined by residues in both the SH2 domain and the phosphopeptides. *Mol Cell Biol* 13:7278–7287.

78. van der Lee R, et al. (2014) Classification of intrinsically disordered regions and proteins. *Chem Rev* 114:6589–6631.

79. Flock T, Weatheritt RJ, Latysheva NS, Babu MM (2014) Controlling entropy to tune the functions of intrinsically disordered regions. *Curr Opin Struct Biol* 26:62–72.

80. Bah A, et al. (2015) Folding of an intrinsically disordered protein by phosphorylation as a regulatory switch. *Nature* 519:106–109.

81. Travers T, et al. (2015) Tandem phosphorylation within an intrinsically disordered region regulates ACTN4 function. *Sci Signal* 8:ra51.

82. Lenz P, Swain PS (2006) An entropic mechanism to generate highly cooperative and specific binding from protein phosphorylations. *Curr Biol* 16:2150–2155.